Master's thesis

NTNU
Norwegian University of Science and Technology
Faculty of Medicine and Health Sciences
Department of Clinical and Molecular Medicine

Mina Heggedal

The functional role of NEIL3 DNA glycosylase in the hippocampus

Master's thesis in Molecular Medicine
Supervisor: Jing Ye
Co-supervisor: Magnar Bjørås
May 2022

NTNU
Kunnskap for en bedre verden

Mina Heggedal

The functional role of NEIL3 DNA glycosylase in the hippocampus

Master's thesis in Molecular Medicine
Supervisor: Jing Ye
Co-supervisor: Magnar Bjørås
May 2022

Norwegian University of Science and Technology
Faculty of Medicine and Health Sciences
Department of Clinical and Molecular Medicine

NTNU
Norwegian University of
Science and Technology

Abstract

Emerging evidence suggests novel functions of NEIL3 in the brain. Studies with rodents have revealed a discrete expression pattern of NEIL3 in the subgranular zone of the dentate gyrus and in the subventricular zone of the lateral ventricles during embryonic development, suggesting a role of NEIL3 in neurogenesis and embryonic brain development. A low level NEIL3 expression have been detected in the adult hippocampus, and NEIL3 is shown to play a role in adult neurogenesis. In addition, NEIL3-depleted mice display impaired spatial learning and memory in the Morris Water Maze (MWM), suggesting a role of NEIL3 in hippocampus-dependent memory.

This project aimed to investigate the functional role of NEIL3 associated with hippocampal-dependent spatial learning and memory, with a special focus on the dentate gyrus. This was achieved by investigating the role of NEIL3 in learning-induced adult neurogenesis, expression of immediate early genes, activation of inhibitory interneurons and the volume changes in infrapyramidal mossy fiber bundles. Immunohistochemistry studies with detection of different cellular markers were performed using sagittal brain sections from naïve wildtype (WT) and *Neil3-/-* mice as well as the ones after spatial training. The samples were visualized with confocal imaging and analyzed in the 3D software Imaris. In addition, mouse embryos at different developmental stages were collected to study the function of NEIL3 in embryonic hippocampal development. However, due to limited time, only a trial experiment to test the methodology was performed.

My results suggest that: (1) Spatial experience-associated adult neurogenesis is increased in wildtype mice but displays a tendency to be reduced in mice lacking NEIL3. (2) Spatial experience-induced expression of immediate early genes in the hippocampal dentate gyrus is impaired in NEIL3-deficient mice. (3) Inhibitory GABAergic interneurons in the dentate gyrus are activated in response to spatial training in wildtype mice, but such activation is impaired in NEIL3-depleted mice. (4) NEIL3 has no effect on regulation of the infrapyramidal mossy fiber volume after spatial training. (5) I obtained wildtype and *Neil3-/-* embryos (E13.5 and E18.5) from a heterozygous breeder and immunohistochemistry with paraffin embedded brain sections is tested in a pilot experiment.

In summary, my results indicate that NEIL3 plays an important role in the dentate gyrus associated with spatial learning and memory.

Sammendrag

Tiltagende bevis tyder på at NEIL3 har viktige funksjoner i hjernen. Studier med gnagere har avslørt et diskret ekspresjonsmønster av NEIL3 i den subgranulære sonen av dentate gyrus og i den subventrikulære sonen av de laterale ventriklene under embryonal utvikling, noe som antyder at NEIL3 har en rolle i nevrogenese og embryonal utvikling av hjernen. Videre har lave nivåer av NEIL3 blitt påvist i hippocampus hos ferdigutviklede individer, og studier har vist at NEIL3 ser ut til å ha en funksjon i nevrogenese hos voksne. I tillegg har det blitt vist at mus som mangler NEIL3 har svekket romlig læring og hukommelse i Morris Water Maze (MWM), noe som antyder at NEIL3 har en rolle i hippocampus-avhengig hukommelse og læring.

Dette prosjektet hadde som mål å undersøke den funksjonelle rollen til NEIL3 assosiert med hippocampus-avhengig romlig læring og hukommelse, med spesielt fokus på den dentate gyrus. Dette ble oppnådd ved å undersøke rollen til NEIL3 i læringsindusert nevrogenese hos voksne mus, uttrykk av umiddelbare tidlige gener, aktivering av inhibitoriske internevroner og volumendringer i de infrapyramidale mossy fibrene. Immunhistokjemistudier med påvisning av forskjellige cellulære markører ble utført ved bruk av sagittale hjerneseksjoner fra villtype (WT) og *Neil3-/-* mus, så vel som de samme etter romlig trening. Prøvene ble visualisert med konfokal avbildning og analysert i 3D-programvaren Imaris. I tillegg ble museembryoer på forskjellige utviklingsstadier samlet for å studere funksjonen til NEIL3 i embryonal utvikling av hippocampus. På grunn av begrenset tid ble det imidlertid kun utført et prøveeksperiment for å teste metodikken.

Resultatene mine tyder på at: (1) Romlig erfaring-indusert voksen nevrogenese er økt hos villtypemus, men viser en tendens til å være svekket hos mus som mangler NEIL3. (2) Romlig erfarings-indusert ekspresjon av umiddelbare tidlige gener i den dentate gyrus er svekket i NEIL3-manglende mus. (3) Inhibitoriske GABAergiske internevroner aktiveres som respons på romlig trening i villtypemus, men slik aktivering er svekket i mus som mangler NEIL3. (4) NEIL3 har mulig ingen effekt på regulering av det infrapyramidale mossy fiber volumet etter romlig trening. (5) Jeg etablerte villtype og *Neil3-/-* embryoer (E13.5 og E18.5) fra en heterozygot oppdretter og immunhistokjemi med parafininnstøpte hjerneseksjoner ble testet i et piloteksperiment.

Oppsummert indikerer resultatene mine at NEIL3 spiller en viktig rolle i funksjoner i den dentate gyrus assosiert med romlig læring og hukommelse.

Acknowledgements

First, I would like to thank my main supervisor Jing Ye for always being available for questions and discussions and giving me constant guidance from the start to the end of this master project. Secondly, I would like to thank Magnar Bjørås for making this project possible. Special thanks to Marion Silvana Fernandez Berrocal, for being really generous with your time and for always helping me in the lab and with procedures at the animal facility as well as answering all my questions and advising me in the writing process. I would also like to thank Anna Maria Bugaj for helping me with statistics and teaching me brain sectioning in the start-up phase. Furthermore, I would like to thank my family and friends for always supporting me. Finally, a special thanks to Natalie Sagnes for always being there for me and cheering me on.

Table of contents

List of figures and tables

Abbreviations

Arc	Activity-dependent cytoskeleton associated protein
Aga	Aspartylglucosaminidase
Ascl1	Achaete-scute homolog 1
BER	Base excision repair
BrdU	Bromodeoxyuridine
c-fos	Cellular feline osteosarcoma
CA	Cornu Ammonis
DCX	Doublecortin
DG	Dentate gyrus
DISH	Double in situ hybridization
DNE	Dentate neuroepithelium
DNMT	DNA methyl transferase
EC	Entorhinal cortex
EC	Entorhinal cortex
GABA	Gamma aminobutyric acid
GAD67	Glutamic acid decarboxylase
GCL	Granular cell layer
GCL	Granular cell layer
Gsx2	GS Homeobox 2
HF	Hippocampal formation
HNE	Hippocampal neuroepithelium
IHC	Immunohistochemistry
IMF	Infrapyramidal mossy fibers
LEC	Lateral entorhinal cortex
LOCI	Laboratory for Optical and Computational Instrumentation
MCL	Molecular cell layer

MEC	Medial entorhinal cortex
MF	Mossy fibers
NEIL1	Nei endonuclease VIII-like protein 1
NEIL2	Nei endonuclease VIII-like protein 2
NEIL3	Nei endonuclease VIII-like protein 3
NeuN	Neuronal nuclear antigen
NeuroD1	Neurogenic differentiation 1
NHI	National Institutes of Health
NOL	Novel object location
NR2D1	Nuclear receptor subfamily 1 group D member 2
NSC	Neural stem cell
NSPC	Neural stem progenitor cell
PaS	Parasubiculum
Pax6	Paired box protein Pax-6
PCL	Pyramidal cell layer
PER	Perirhinal cortex
PHR	Parahippocamal region
POR	Postrhinal cortex
Prox1	Prospero homeobox protein 1
PrS	Presubuculum
PSA-NCAM	Polysialylated neuronal cell adhesion molecule
PV	Parvalbumin
RGL	Radial Glial-like
RGLs	Radial glial-like cells
RMS	Rostal migratory stream
ROS	Reactive oxygen species
SGZ	Subgranular zone
SL	Stratum lucidum
SLM	Stratum lacunosum-moleculare

SMF	Suprapyramidal mossy fibers
SO	Stratum oriens
Sox2	Sex determining region Y-box 2
Sp8	Specificity protein 8
SR	Stratum radiatum
ssDNA	Single stranded DNA
SVZ	Subventricular zone
TDG	Thymine DNA glycosylase
TET	Ten-eleven translocation methylcytosine dioxygenases
TOAD64	Turned-on-after-division 64-kD protein
Vegfc	Vascular Endothelial Growth Factor C
VZ	Ventricular zone
WT	Wild type
5caC	5-carboxsylcytosine
5fC	5-formylcytosine
5hmC	5-hydroxymethylcytosine
5mC	5-methylcytosine

1 Introduction

1.1 DNA repair

An organism is not only dependent on the accurate DNA replication mechanism, it also requires DNA repairing mechanisms for mending the high number of lesions that DNA continually suffers.[1] Most of the spontaneous DNA changes are immediately fixed by DNA repair mechanisms.[1] Dysfunction or absence of a DNA repair gene can increase the genomic instability and mutagenesis, which are linked to several pathological conditions like cancer and neurodegenerative disorders.[2, 3]

1.1.1 DNA damage and repair in the brain

Oxidative DNA damage is particularly prevalent in the brain, arising primarily from endogenous sources like reactive oxygen species (ROS).[4] ROS are byproducts of the electron transport chain during cellular respiration.[2, 5] Although they are produced naturally during cellular metabolism, they have the ability to cause DNA damage such as oxidized bases, abasic sites and strand breaks.[6-8] DNA damage response systems are therefore important to repair the damage caused by ROS and maintain genomic stability. The main repair mechanism for oxidative damage in the brain is base excision repair (BER).[4]

The brain has a high energy demand because of the continuous electrochemical signaling between its cells, which explains the high prevalence of ROS in brain tissue.[4] Following, more DNA repair activity is required which also requires energy.[4] The consequence is a permanent state of oxidative stress. Thus, the brain is especially vulnerable to oxidative damage.[4] Post-mitotic neurons do not divide since they are terminally differentiated and lack the replication-associated damage detection and repair machinery of DNA, resulting in a high reliance on the BER mechanism in the brain.[4, 5]

1.1.2 Base Excision Repair (BER) in the brain

Neurons in the brain are mainly in a post-mitotic stage, with only a few regions producing new neurons through adulthood.[9] DNA repair in the brain is thus crucial for neuronal survival and maintenance of brain homeostasis.[3] Defects in the repair machinery are associated with increased mutation load which can lead to neuronal dysfunction and neuronal degeneration.[10] As earlier established, the main DNA repair mechanism for oxidative damage in the brain is BER.

The BER pathway involves several steps (Figure 1). The initiating step is base recognition by a DNA glycosylase specific for the altered base.[11] Currently, 11 human DNA glycosylases have been identified, including NEIL3.[12] The DNA glycosylase identifies the damaged base and cleaves the N-glycosidic bond, leaving an abasic site. Subsequently, AP endonuclease (APE1) generates a single strand break by incising the abasic site on the 5'-side. The gap is then filled by a DNA polymerase and a DNA ligase joins the DNA ends and the correct base is restored.[1, 11, 13]

Two mechanisms of BER can take place depending on the type of DNA glycosylase and the physiological state of the cell (Figure 1). They differ in the enzymes participating and repair gap size.[11] In short-patch BER, a DNA glycosylase removes a single nucleotide followed by single strand break by APE1. DNA Pol-β fills the gap by resynthesizing the correct base and a DNA ligase (I or III) ligates the DNA strand. The proteins that this mechanism depends on do not participate in replication, and are hence equally efficient in both proliferating and non-proliferating cells.[11, 14] Long-patch BER on the other hand, involves removal of 2-10 nucleotides. After the base identification and removal by a DNA glycosylase, followed by cleavage by APE1, several replication proteins like DNA polymerase δ/ε, PCNA, RFC, FEN1, and LIG1 are involved in the following steps. Due to the presence of replication proteins, this mechanism mostly takes place in proliferating cells.[11, 14]

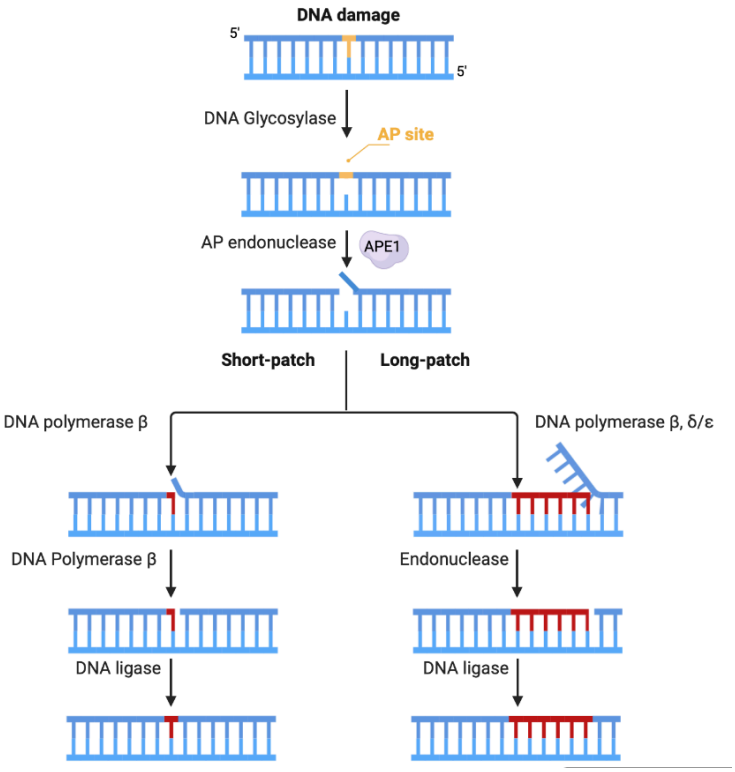

Figure 1: *BER. Mechanisms of short-patch and long-patch BER. In short patch BER, a DNA glycosylase recognizes the damaged base and cleaves the N-glycosidic bond leaving an abasic site. AP endonuclease generates a single strand break and the gap is filled by DNA polymerase β and the ends are joined by DNA ligase. Long patch BER follows the same mechanism, but removes 2-10 nucleotides, and utilizes replication proteins for gap-filling and ligation. The figure is made in BioRender with inspiration from [11].*

1.1.3 BER in DNA demethylation

Besides its role in DNA repair, BER is also known to participate in active DNA demethylation.[15] DNA demethylation along with DNA methylation are epigenetic mechanisms for regulation of gene expression, without alteration of the DNA sequence.[16] It has been observed that genome-wide demethylation occurs only at specific points during embryonic development, while gene-specific demethylation occurs in cells responding to specific signals. In addition, active DNA demethylation has been found to be important for expression of neurogenesis genes and it has been observed in post-mitotic neurons.[17]

DNA demethylation can take place passively or actively. Passive DNA demethylation is replication dependent, which contrasts with active DNA demethylation. Active DNA demethylation is an enzymatic process that removes or modifies the methyl group in 5-methylcytosine (5mC) by oxidation facilitated by BER to replace the modified base (Figure 2).[17]

DNA methyltransferases (DNMTs) are active in DNA methylation and methylate the fifth carbon in cytosine which results in 5mC.[18] The cytosine can be restored to its original state through active DNA demethylation.[18] The methyl group can be removed by TET-mediated oxidation to 5-hydroxymethylcytosine (5hmC), 5-formylcytosine (5fC) and 5-carboxsylcytosine (5caC).[18] Thymine DNA glycosylase (TDG) coupled with BER excise 5fC or 5caC, resulting in an unmethylated cytosine.[18] However, growing evidence suggest that active DNA demethylation may be achieved by multiple mechanisms with different enzymes participating.[17, 19]

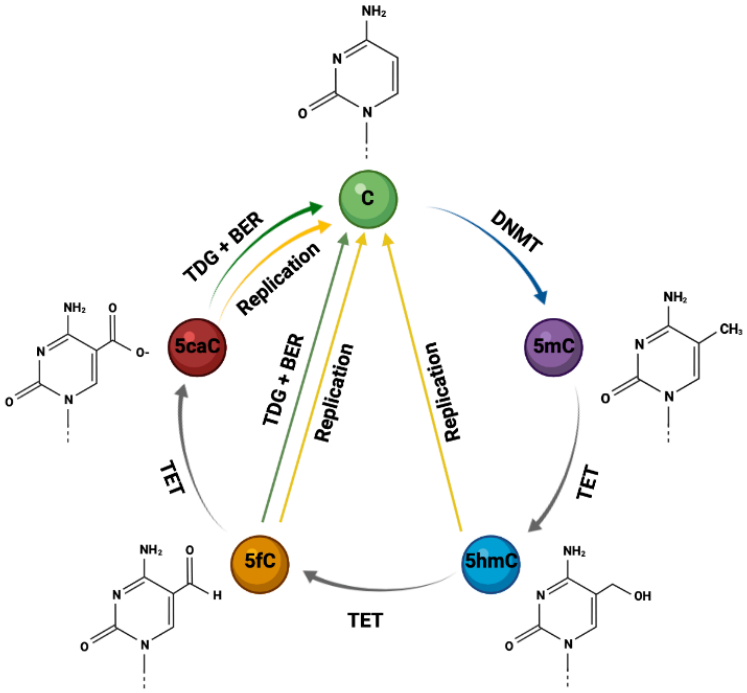

Figure 2: *Active DNA demethylation. DNMT methylate cytosine to 5mC. The methyl group is removed by TET-mediated oxidation to 5hmC, 5fC and 5caC. TDG coupled with BER restore the C. Replication-dependent (passive) DNA demethylation pathways are also marked in yellow in the figure. The figure is a modified version of* [18].

1.2 Nei Like DNA glycosylase 3 (NEIL3)

NEIL3, short for Nei endonuclease VIII-like protein 3, is a mammalian DNA glycosylase.[20] NEIL1 and NEIL2 DNA glycosylases belongs to the same family, but NEIL3 differs in expression pattern, structure and substrate specificity.[21] In mice, the *Neil3* gene is located on chromosome 8 B1.3. The minus strand encodes the gene and it is flanked by Vegfc (Vascular Endothelial Growth Factor C) and Aga (Aspartylglucosaminidase) on the telomeric end and centromeric side respectively. The mouse NEIL3 protein is comprised of 606 amino acids, and nine potential variants of the protein are predicted from alternative splicing.[21]

As mentioned above, NEIL3 is structurally different from the other NEIL glycosylases. It has a valine residue at the N-terminus in contrast to the two others that have a catalytic proline in this position.[22] In addition to this, NEIL3 has a long extension at the C-terminus providing an extra C-domain with different structural features including a putative nuclear localization signal (NLS), a RAN-binding protein-like zinc finger motif and two tandem GRF zinc finger motifs.[22, 23] Furthermore, NEIL3 exhibits glycosylase activity and participate in the BER pathway.[20, 22, 24]

NEIL3 has the ability to process a broad specter of different substrates due to its structural organization, and has a base excision activity with a preference for lesions in ssDNA.[21, 25] NEIL3 primarily excise DNA lesions by beta-elimination,[24] some of them which are hydantoin lesions, including guanidinohydantoin (Gh) and spiroiminodihydantoin (Sp),[24] and mutagenic lesions such as 5-hydroxy-2'-deoxyuridine (5OHU) and 5-hydroxy-2'-deoxycytidine (5OHC).[22]

In addition to this, recent studies implicate that NEIL3 has a functional role in epigenetic gene regulation.[26, 27]

1.2.1 NEIL3 expression in the mouse brain

Studies with rodents have revealed that there is a discrete expression pattern of *Neil3* in the subgranular zone (SGZ) of the dentate gyrus (DG) and subventricular zone (SVZ) of the lateral ventricles during the embryonic development and perinatal stages.[28] This expression pattern indicates that NEIL3 is present in neural stem progenitor cells (NSPCs), suggesting a role of NEIL3 in neurogenesis.[29] Furthermore, NEIL3 is found to be highly expressed at E12.5 in mice, which is the same time as neurogenesis is initiated. The NEIL3 expression decreases in line with the embryonic development[30, 31], and only a few cells in the DG and lateral ventricles are found to express NEIL3 at birth.[31] At P3, NEIL3 is found to be expressed in the SVZ, the DG, the rostral migratory stream (RMS) and in the Purkinje cells in the cerebellum. The expression decline with age, with only expression in the SGZ and entorhinal cortex (EC) layer V in later postnatal stages.[29] This tissue specific and age dependent expression strengthen the evidence that NEIL3 expression is dependent on the developmental stage and is important for neurodevelopment in mice.

However, although NEIL3 expression is shown to decline with age, low levels of NEIL3 has been found in the adult hippocampus in mice[27], suggesting that NEIL3 may have important roles in hippocampal functions such as spatial memory and learning and maintenance of adult neurogenesis.

1.2.2 NEIL3 function in the brain

As established before, NEIL3 is a mammalian DNA glycosylase that participates in the BER pathway by removing oxidized base lesions.[20] The repair of oxidative DNA damages is essential for keeping the brain functions intact.[10, 27] In addition to its role in DNA repair, BER is also known to participate in active DNA demethylation.[18] NEIL3 is one of the glycosylases that initiate the BER mechanism and is suggested to activate silenced genes by active DNA demethylation through an alternative BER pathway.[27] Studies have shown that NEIL glycosylases accompanies TDG in reactivation of epigenetically silenced genes, and NEIL1 and NEIL3 have been suggested to be potential binders for oxidized cytosine derivatives.[32] However, their exact function in TET dependent active DNA demethylation is yet to be elucidated. The same study provides evidence that NEIL3 in some way can compensate for the loss of TDG and initiate BER after TET oxidation, suggesting that NEIL glycosylases may constitute an alternative pathway for active DNA demethylation and have a role in epigenetic gene regulation.[32]

Neil3-depleted mice appear to be phenotypically normal, with normal fertility, no increase in mutagenesis or other pathological conditions.[33, 34] However, *Neil3-/-* mice have been showed to display decreased spatial performance in behavior studies using the Morris Water Maze (MWM).[20] Furthermore, NEIL3 have been shown to play a role in adult neurogenesis[20], which seems to be essential for maintaining the functions dependent on hippocampus in learning and memory.[35] This implicates that NEIL3 may be important for regulating different hippocampal-dependent functions and maintenance of adult neurogenesis.[20]

Subsequently, as earlier mentioned, *Neil3* also have a discrete expression pattern[28-31] in parts of the hippocampal formation (HF) and cells lacking NEIL3 have shown decreased proliferation and differentiation rates.[36] These findings suggest that NEIL3 may have a role in hippocampal development and neurogenesis.[27-29] Moreover, there is evidence that NEIL3 modulates the transcription essential for functional and structural development of the hippocampal circuitry. However, how NEIL3 interacts with epigenetic marks during development of the hippocampus is still unknown.[27] Finally, there are also indications of that pathways involved in active DNA demethylation during development also are operational in post-mitotic neurons.[15]

1.3 The hippocampal formation

1.3.1 Hippocampal formation anatomy and function

The hippocampal region is located in the medial temporal lobe and plays a pivotal role in spatial learning and episodic memory.[37-41] The region can be divided into two cortical sub-regions named the hippocampal formation (HF) and the parahippocampal region (PHR).[42] The HF is comprised of the DG, the hippocampus proper and the subiculum (Sub). The hippocampus proper can further be subdivided into CA1, CA2 and CA3. For convenience, the term hippocampus is used for hippocampus proper and DG.[42] The PHR consists of the perirhinal cortex (PER), the postrhinal cortex (POR), the entorhinal cortex (EC), the parasubiculum (PaS) and the presubiculum (PrS).[42] The structures in the hippocampal formation are all three-layered, which is in contrast to the parahippocampal structures that consist of more than three layers. The HF and the PHR together make up a functional system/neuronal network called the parahippocampal-hippocampal circuitry (Figure 3A-B).[42, 43] This circuitry provides connectional routes between all the hippocampal fields as well as pathways for information flow.[42]

The HF works in association with the PHR and together they play a key role in memory formation and spatial navigation.[44] Memory formation and recall require interactions between the structures in the hippocampal-parahippocampal network, which processes the multisensory inputs from the neocortex.[38, 39, 45, 46] In contrast to other regions in the neocortex, the connections in the hippocampal region are largely unidirectional.[42] Multisensory input from the neocortex is first received by the PHR.[47] There are two parallel projection routes, where the PER projects to the superficial layers (II, III) of the lateral entorhinal cortex (LEC) and conveys non-spatial information[48], and the POR projects to the superficial layers (II, III) of the medial entorhinal cortex (MEC) and conveys spatial information.[49, 50] The EC also receives input from the PaS. The EC is the main source of cortical input to the hippocampal formation.[42, 51] LEC (III) conveys non-spatial information directly to the CA1 and Sub, while MEC (III) transmit spatial information directly to the CA1 and Sub. Layer II of LEC and MEC are confined to transfer information to the DG and CA3.[42, 52] Multisensory inputs are received by the DG from the EC (II) via a connectional route called the perforant pathway (PP).[45] The DG projects this sensory input to CA3 via the granule cell axons, called mossy fibers (MF), which collateralize in the hilus before entering the CA3 where they form synapses on the dendrites of the pyramidal cells.[45] These pyramidal cells routes the sensory inputs to the pyramidal cells in CA1 via Schaffer collateral synapses. CA1 can further project the inputs to the Sub. However, both CA1 and the Sub send the processed memory output back to the deep layers of the EC (V, VI) as well as they can communicate with other brain structures.[42, 46] In addition to the interactions between the excitatory principal cells, interneurons exhibit inhibitory activity locally in the circuit and play an essential role in regulating and controlling these interactions.[53]

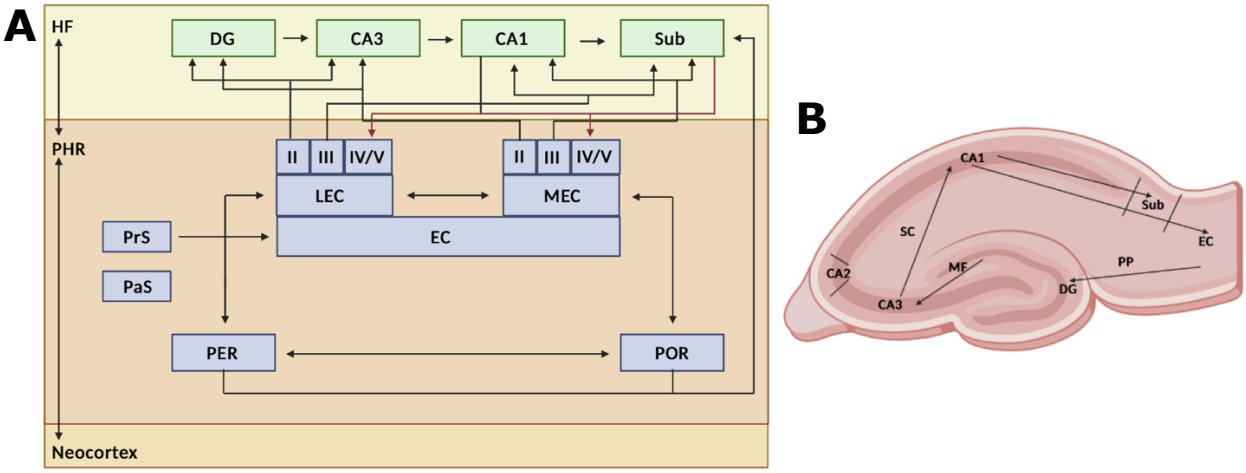

Figure 3: A. *The hippocampal-parahippocampal network. The parahippocampal region receives input from the neocortex. Two parallel projection routes are present in the parahippocampal region. The PER projects to the LEC and the POR projects to the MEC. The EC cortexes respond to the input and forwards it to the hippocampal region. In addition, EC receives input from the presubiculum (PrS). Layer II of LEC and MEC project to the DG and CA3, while layer III projects to CA1 and the subiculum (Sub).The unidirectional route that connects all the hippocampal regions, called the polysynaptic pathway, starts with EC projecting to DG via the perforant path, followed by DG projection to CA3 via mossy fibers. Schaffer collaterals in CA3 project to CA1, which further projects to the Sub. Output from the hippocampal formation is directed from both CA1 and Sub to the deep layers (IV/V) of the MEC and LEC in the parahippocampal region. The figure is a modified version of [42].* ***B.*** *A simplified illustration of figure A representing the connections within the hippocampal region. DG receives input from the EC (MEC/LEC) via the PP and projects the input to CA3 via MF. Following, SC in CA3 projects to CA1, which further projects to the Sub and back to the EC. The figure is made in BioRender.*

1.3.2 Hippocampus proper

The hippocampus proper can be divided into three distinct regions named CA1, CA2 and CA3. It is as the DG organized in a layered structure (Figure 4). Stratum oriens (SO), also called the infrapyramidal region, is the deepest layer and consists mainly of dendrites of the pyramidal cells and a variety of interneurons. The pyramidal cell layer (PCL) lies superficial to the SO and mainly harbors pyramidal neurons and interneurons.[42, 43] The molecular layer is the most superficial layer and can be further divided into sublayers named stratum radiatum (SR) and stratum lacunosum-moleculare (SLM). SR is often referred to as the suprapyramidal region and is where the Schaffer collaterals that connects the CA3 and CA1 are located. In addition to these two sublayers, CA3 contains a narrow acellular region called the stratum lucidum (SL) located right above the (PCL). This layer contains the MFs that connect the DG with the CA3 region.[42, 43]

It is worth mentioning that the CA regions seems to have important functions related to memory and learning. The CA regions harbor a type of pyramidal neurons called place cells, which are shown to be crucial for spatial navigation and memory.[54] These neurons fire when the animal is in a particular place and creates and internal map of the space, called a cognitive map.[39] However, this will not be touched deeply due to the focus on the DG in this thesis.

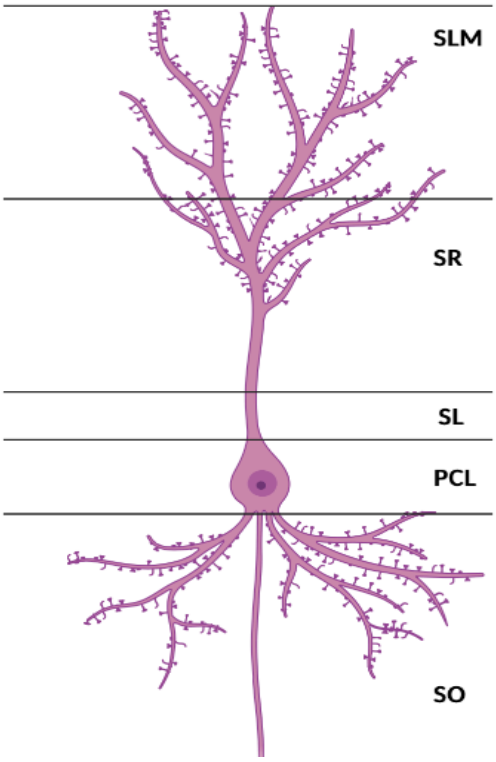

Figure 4: *A pyramidal neuron stretching through the CA layers. Illustration of a pyramidal neuron and its dendrites according to its location in the different layers. SO, stratum oriens; PCL, pyramidal cell layer; SL, stratum lucidum; SR, straum radiatum; SLM, stratum lacunosum-moleculare. The figure is made in BioRender.*

1.3.3 The dentate gyrus

The DG is comprised of three different layers named the molecular cell layer (MCL), the granular cell layer (GCL) and the polymorphic layer (hilus) (Figure 5A,C).[47] The MCL is the most superficial layer, closer to the hippocampal fissure, and is relatively cell-free, consisting mainly of dendrites of the granule cells, interneurons and polymorphic cells as well as some interneurons and axons from the EC and other sources.[47] The GCL is located deeper to the MCL and is comprised of densely packed granule cells which forms the characteristic V-shape in dorsal position, constituted of a suprapyrmidal (SPB) and infrapyramidal blade (IPB) (Figure 5B).[55] Granule cells are the main cell type in the DG, and their characteristic branched tree of dendrites are stretching from the granule cell layer to the hippocampal fissure in the MCL.[47] It is also worth mentioning that the granule cells is the only cell type that give rise to the MFs, used to innervate the CA3. The MFs are divided into two tracts, called the infrapyramidal (IMF) and suprapyramidal (SMF) mossy

fibers (Figure 5B).[47] In addition to granular neurons, a number of GABAergic interneurons are also found in the GCL which stretch their axons to the MCL and modulate granular cell activity (Figure 5C).[43] The hilus is enclosed by the GCL and contains a variety of cell types.[47] However, the main cell types in this layer are GABAergic interneurons and mossy cells.[47]

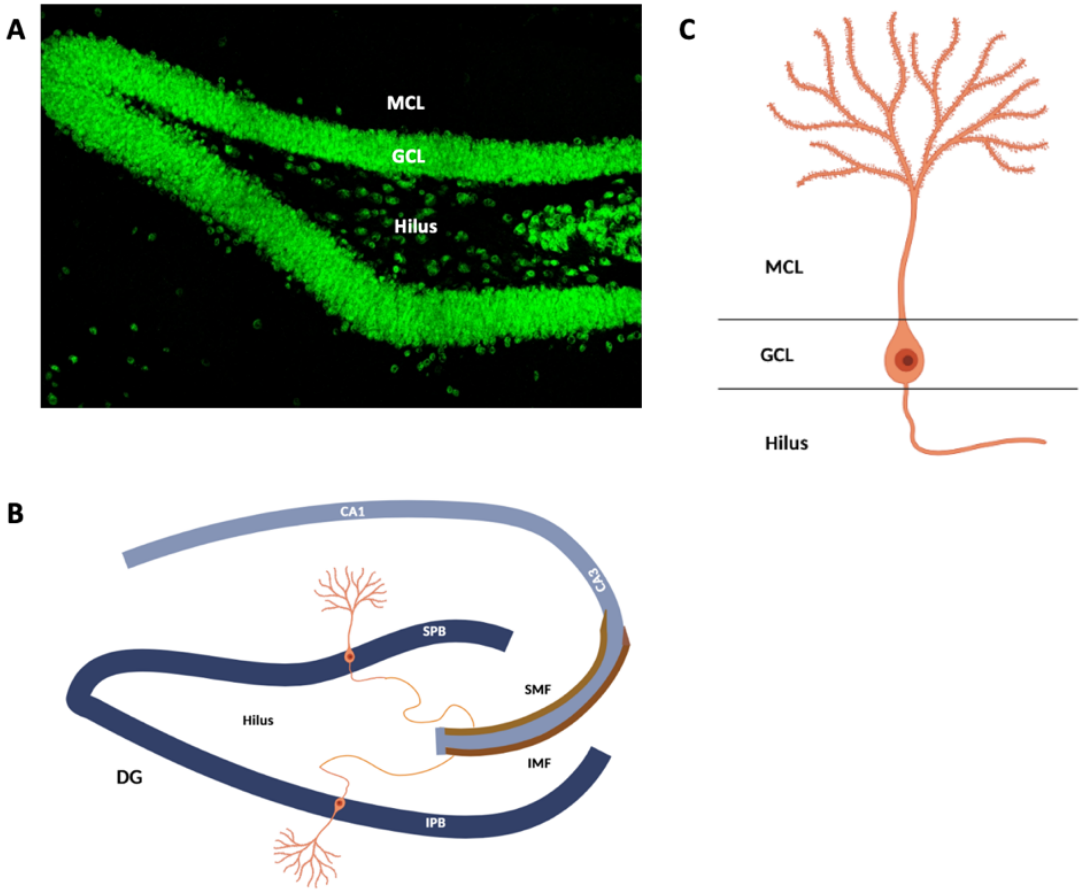

Figure 5: A. *A representative confocal image of the DG with the three layers marked.* ***B.*** *A schematic representation of the dentate gyrus with mature granule cells and mossy fiber tracts illustrated. SPB, suprapyramidal blade; IPB, infrapyramidal blade; IMF, infrapyramidal mossy fibers; SMF, suprapyramidal mossy fibers.* ***C.*** *A granular neuron. Illustration of a granular neuron with its dendrites located in the MCL and its axons located in the hilus, which connects the DG with the CA3 region. The figure is made in BioRender.*

1.3.4 DG and hippocampal function in learning and memory

Formation of long-term memory is a process with several steps including encoding the sensory input as a permanent memory trace (engram), storage of the memory, consolidation and memory recall.[56] As earlier established (section 1.3.1), the DG is a major input region to the hippocampus, and is thought to play an important role in hippocampal-dependent memory, including episodic and spatial memory functions.[57] Furthermore, several hippocampus-dependent memory functions are impaired in the presence of DG lesions.[56, 58, 59] However, the exact role and function of the DG in memory and learning have been a large matter of debate the recent years. Despite this, a

lot of theorized mnemonic functions of the DG exists and many of them are supported by empirical evidence. Computational models[60] of the DG and behavioral studies[61-63] based on dysfunction of the DG have revealed that it appears that the DG have mnemonic functions related to spatial information. Evidence exists for a DG-role in processing and representing spatial information, including encoding of inputs[64], pattern separation[65] and encoding of spatial information in cooperation with CA3.[60, 65] Furthermore, studies have suggested that the granular neurons in the DG are required for memory encoding and consolidation, but dispensable for memory recall.[56, 59]

The SGZ of the DG is one of the sites where adult neurogenesis occurs (section 1.4.2). Mice with reduced adult neurogenesis in the DG have been shown to have impaired performance in spatial pattern separation tasks, and have been proved to affect long-term memory retention in the MWM.[57] However, how the adult neurogenesis enhance DG function is still unknown.[57]

In a clinical context, spatial memory in particular have been shown to decline during age-related neurodegenerative diseases as well as during normal aging.[66] Various functional changes within the hippocampal-parahippocampal network associated with the DG are observed in several types of cognitive deficits, including reduced input to the DG via the PP[67], reduced adult neurogenesis[68, 69], impaired pattern separation[70] and altered synaptic plasticity.[71] Therefore, an understanding of the DGs exact role and the underlying mechanisms associated with spatial memory and learning will be of both clinical and neurobiological relevance.

1.4 Neurodevelopment in mice

Neural stem cells (NSCs) are the precursors for neurons in the brain. The process where NSCs transition to differentiated neurons is called neurogenesis, and they are generated from early stages in the embryonic development until early postnatal stages. However, a few regions in the brain continue neuronal production throughout life. The SVZ of the lateral ventricles and the SGZ of the DG have been shown to be active sites for generation of neurons in the adult brain.[72]

1.4.1 Hippocampal development in mice

1.4.1.1 CA development

The origin of hippocampal neurons is the hippocampal neuroepithelium (HNE) (Figure 6).[73] Neuroepithelial cells undergo mitosis and generate neurons in the ventricular zone before they migrate along radial glial fibers and settle in their destined hippocampal field.[74] Findings also suggest that multipolar cells in the SVZ and IMZ transdifferentiate into pyramidal neurons during non-radial migration to CA1 and CA3.[74] As earlier established, the pyramidal layer is present in all the hippocampal fields, but the pyramidal neurons have different genetic and morphological properties, which divides them into CA1, CA2 and CA3.[75] The peak and termination of neurogenesis is different for the various

hippocampal fields. Interneurons for the CA fields are generated before the principal cells and peak between E12-13.[76-78] Formation of pyramidal neurons for CA2 as well as neurons and interneurons in the infrapyramidal and suprapyramidal layers are completed at E16. However, the generation of pyramidal neurons and interneurons of CA1 and CA3 is not complete at this time. The peak of pyramidal neuron formation for CA1 and CA3 is E15 and E14 respectively, but continues until E18.[79] After final mitosis, the post-mitotic neurons migrates for several days before they differentiate into pyramidal neurons and settle in the pyramidal cell layer.[75] The generation of pyramidal neurons to the pyramidal layer of the CA regions follow an inside-out gradient where neurons first are generated to the deepest zone of the layer, closest to striatum oriens, and subsequently builds to the more superficial zone.[79] In addition, in CA3, neurons in the region closest to CA1 are generated first, and the neurons closest to the DG are generated last.[73] The formation of the neurons for the hippocampal pyramidal layer is completed at E18.[74, 79]

1.4.1.2 DG development

In contrast to the pyramidal neurons of the CA fields that is produced exclusively during embryonic development, the granule cells of the DG are generated over a period that starts during embryonic development and continues postnatally (Figure 6).[55] The dentate neuroepithelium (DNE), from here referred to as the primary matrix, is a part of the ventricular zone of the medial pallium and the origin of the DG. At E12.5 the DNE is located between the HNE and the cortical hem.[72] The cortical hem produces Cajal-Retzius cells, which functions as "organizers" during embryonic development and influences the organization of the brain by signaling that affects the neurons.[80, 81] The primary matrix contains neural progenitor cells which start to migrate out of the DNE to the pial side of the cortex at E14.5.[72] These neural progenitor cells are a mixture of stem cells and neuronal precursors at different differentiation stages, which still exhibits proliferative activity.[72, 73] At E14.5, they start glial scaffold-directed migration to the pial surface of the cortex where they form the secondary matrix.[72, 74] The hippocampal fissure is formed at E17.5, which divides the boundary between the CA fields and DG.[82] The glial scaffolds extends from the cortical hem to the hippocampal fissure and directs the neuronal progenitors from the secondary matrix to the hippocampal fissure and form the tertiary matrix.[72]

The neurons in the MCL and the hilus of DG are completed around E15. However, the GCL of the DG starts to form at P0 and is not complete before postnatal week 3.[83] Granular cells generated by the precursors from all the matrices form the GCL. Cajal-Retzius cells facilitates the organization of the granule cells resulting in the characteristic V-shaped blade.[72] In contrast to the CA regions, the GCL of DG is constructed with an outside-in gradient, starting with the most superficial zone that borders the MCL and at last the deepest zone of the GCL.[74, 84] The gross structure of the SPB is apparent at birth[85], and the structure of the IPB appear within postnatal week 1 where the generation of granule cells reaches its maximum.[55] The source of granule cells gets more restricted at this stage, and they are here only generated by the tertiary matrix.[72] Dendrites of the granule cells starts to form after their generation, and they develop branches covered with dendritic spines stretching through the MCL and axons stretching towards the CA3 in the weeks after their birth. The foundation of the GCL is completed in the early postnatal period due to the massive generation of granule cells. Although the neurogenesis peaks in the

early postnatal period, it continues through adulthood.[55] However, the source of the granule cells gets even more restricted after the early postnatal period and the source is confined to the SGZ where they reside throughout life.[72, 86]

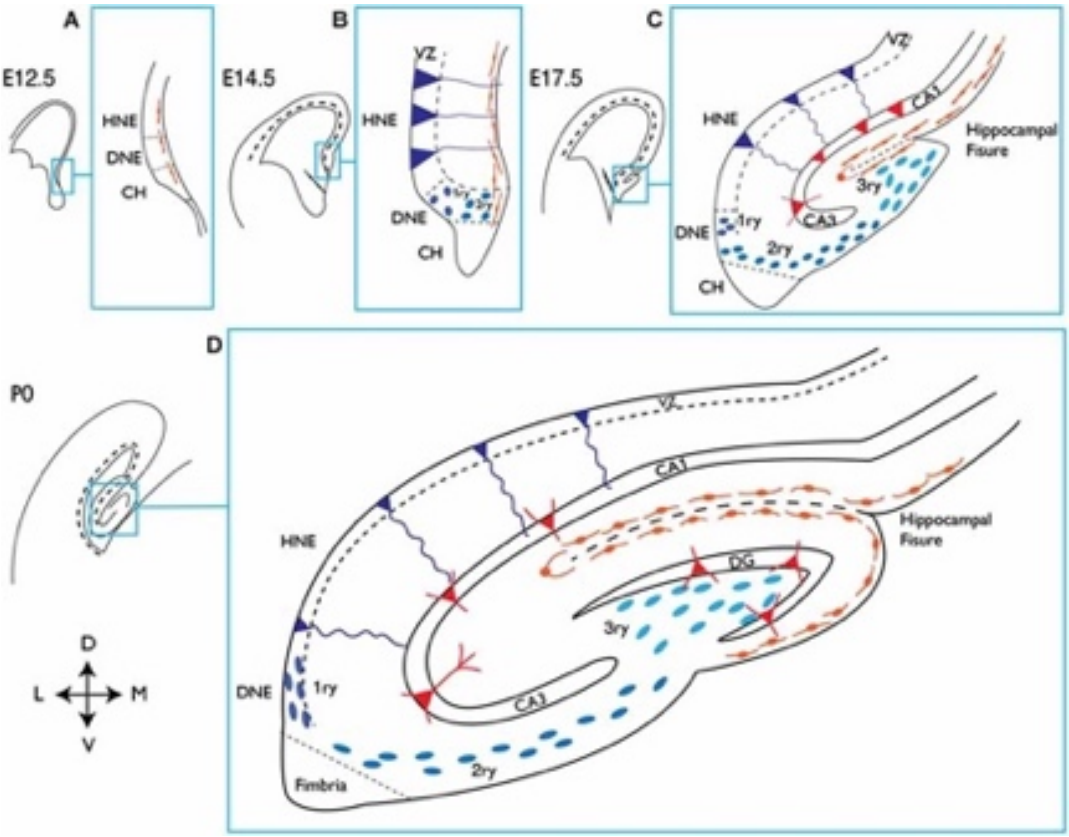

Figure 6: *Hippocampal development in mice.* ***A.****E12.5. The DNE is located between the CH and the HNE.* ***B.*** *E14.5. The cells in the primary matrix (dark blue circles) are located in the ventricular zone and migrates toward the pial surface where they form the secondary matrix. RGL cells in the ventricular zone in the HNE (blue triangles) give rise to CA-neurons.* ***C.*** *E17.5. The hippocampal fissure is created and secondary matrix cells migrate to form the tertiary matrix (light blue circles). Cajal-Retzius cells produced by the CH lines the hippocampal fissure. RGL precursors from the HNE (red triangles) starts radial-glial-directed migration to their destined field where they become CA-neurons (red triangles)* ***D.*** *P0. Initiation of DG blade formation starts. Granule neurons (red triangles in DG) starts to build in the IPB and further Cajal-Retzius cells promotes formation of the SPB. DNE, dentate neuroepithelium; HNE, hippocampal neuroepithelium; RGL, radial-glial-like; CH, cortical hem; DG, dentate gyrus; VZ, ventricular zone. This figure is made by Urbán et al.[72].*

1.4.2 Adult neurogenesis

Adult neurogenesis was first reported in the late 1960's where Altman et al. observed that the brain is capable of generating new neurons. This changed the dogma that the mammalian brain is incapable of producing new neurons.[87] However, it was not before 1990s that the attention was turning away from questioning whether generation of new neurons in the adult brain occurred, toward the attempt to unravel the molecular mechanisms behind adult neurogenesis. The interest of this phenomena further increased when studies suggested that adult neurogenesis plays a role in memory and learning.[88]

After early postnatal period, generation of new neurons are confined to two distinct areas in the brain, namely the SGZ of the DG and the SVZ of the lateral ventricles.[89] The neurons produced in the SVZ migrate through the RMS to the olfactory bulb, while the subgranular neurons migrate to the GCL of the DG and become granule cells.[89, 90]

Adult neurogenesis is a process composed of several steps including proliferation, differentiation, migration and integration into the neural network.[90] In the SGZ, NSCs divide and give rise to radial glial-like cells (RGL)/type 1 cells which are neural progenitors.[91] Activation of the RGL cells results in generation of non-radial proliferating cells named type 2 cells.[91] These type 2 cells undergo further differentiation to immature neurons, called type 3 cells. Subsequently, the immature neurons migrate to the GCL where they mature to dentate granule cells and integrate in the pre-existing neural network by projecting their dendrites to the molecular cell layer and mossy fiber axons to the CA3.[16, 91]

Each step of the lineage progression is controlled by intrinsic regulators like epigenetic mechanisms and transcriptional regulators that ensure appropriate levels of proliferation and accurate differentiation as well as the migration and integration of the newly born neurons.[91] Some of the important transcriptional regulators of adult neurogenesis in the DG include NR2E1, NeuroD1, Sox2, Pax6, Prox1, Sp8, Gsx2 and Ascl1. In addition, growth factors, neurotransmitters and cytokines have been connected to control of neuronal differentiation.[91]

The granular neurons have distinct properties that enable them to contribute to particular functions in learning and memory.[16] Adult neurogenesis in the DG is enhanced following experience and learning[89, 92, 93], and deficits in adult neurogenesis may reduce the hippocampal function, leading to impaired learning and memory.[35, 92] Although the adult-born neurons are small in number compared to the total neural population in the DG, the generation of adult-neurons is continuous and high enough to potentially increase hippocampal plasticity.[94] Evidence suggest that adult neurogenesis is important for brain functions dependent on the hippocampus and contributes to structural and functional plasticity.[94] Further, impaired adult neurogenesis is linked to several neurodegenerative disorders.[87] In addition, ageing of the brain is associated with a major decrease in the adult neurogenesis.[95]

2 Project aims

NEIL3 is a DNA glycosylase that participates in the base excision repair (BER) pathway.[20] BER is engaged in active DNA demethylation, which is a mechanism that epigenetically regulates gene expression,[18] and recent studies implicate that NEIL3 has a functional role in epigenetic gene regulation.[26, 27]

Neil3 depleted mice appear to be phenotypically normal, with normal fertility, no increase in mutagenesis or other pathological conditions.[33, 34] However, emerging evidence suggests novel functions of NEIL3 in the brain.[20, 27, 28, 31] Studies with rodents have revealed a discrete expression pattern of NEIL3 in the subgranular zone of the DG and in the SVZ zone of the lateral ventricles during embryonic development, suggesting a role of NEIL3 in neurogenesis and embryonic development.[28]

A low level NEIL3 expression is detected in the adult hippocampus[27], and NEIL3 is shown to play a role in adult neurogenesis.[20, 28] In addition, NEIL3-depleted mice display impaired spatial learning and memory in the Morris Water Maze (MWM)[20], suggesting a role of NEIL3 in hippocampus-dependent memory. It is known that spatial learning is associated with enhanced adult neurogenesis.[93, 96], elevated expression of immediate early genes[97, 98] and activation inhibitory interneurons in the hippocampal region.[99]However, the role of NEIL3 in these processes remains to be elusive.

The primary objective of the project is to unravel new knowledge about how NEIL3 impacts hippocampal development and function, with a special focus on the dentate gyrus. This master project aims to elucidate:

1. Whether NEIL3 impacts adult neurogenesis associated with spatial learning and memory.
2. Whether NEIL3 impacts spatial learning-induced expression of immediate early genes
3. Whether NEIL3 impacts spatial learning-induced activation of inhibitory GABAergic interneurons
4. Whether NEIL3 impacts spatial experience induced synaptic changes.
5. Whether NEIL3 impacts embryonic brain development.

3 Methods

All experiments performed for this thesis were approved by the Norwegian Animal Research Authority (FOTS28340) and conducted in accordance with the Norwegian Animal Welfare Act.

3.1 Mouse model

Male *Neil3-/-* C57BL/6N knockout mice and male wild type C57BL/6N control mice were bred in the transgenic unit of Comparative Medicine Core Facility at NTNU. The animals had *ad libitum* access to food and water and were kept at a 12:12-hour light dark cycle. The temperature in the room housing the mice was 25 °C. The adult animals that were studied in association with spatial learning were collected at three months. The animals participating in the hippocampal development study were collected at E13.5, E18.5 and P2.

3.2 Heterozygous breeding

Neil3+/- mice was established to obtain WT and *Neil3-/-* mice. They were checked daily to ensure time of pregnancy and collected at different timepoints; E13.5, E18.5 and P2.

3.3 Embryo retrieval and brain dissection

The female mouse carrying the embryos was anesthetized using isoflurane (Baxter, Cat.No. 1001936060) in a closed chamber. Subsequently, she was euthanized by an overdose of pentobarbital (2g/kg bodyweight) injected intraperitoneally. The embryos were collected and separated in petri dishes filled with PBS. A surgery microscope (Zeiss-Opmi pro Ergo) was used to further dissect the embryos, extract the heads and cut the tails. The dissected embryos' heads were transferred to tubes filled with 4% paraformaldehyde (PFA) in PBSx1 and stored in minimum 48 hours at 4°C for fixation. The tails were collected in separate tubes for genotyping. After genotyping the desired-genotype embryo heads were dissected and the brains were extracted by using fine tools to first extract the cervical bones, followed by occipital bones and parietal bones and finally scooped out into a well of a 24 well plate filled with more 4% PFA. They were stored there at 4°C until paraffin embedding.

3.4 Brain perfusion

The animal was first anesthetized using isoflurane (1 mL, Baxter, Cat.No. 1001936060) in a chamber in order for the mouse to lose its consciousness. Subsequently, the animal was further anesthetized by an overdose of pentobarbital (2 g/kg bodyweight) injected intraperitoneally. Pain reflexes (pedal reflex, spinal reflex) were tested to ensure that the animal was properly anesthetized. First, a cut was made to expose the thorax and then another cut around the ribs through the diaphragm was made in order to expose the heart. A 20G needle was used to puncture the left ventricle, the right atrium was nicked, and 60 ml of 0.9% Saline Solution was slowly injected to clear the blood from the body. After the perfusion, the head was cut. Following, the skin covering the skull was cut to expose it, and the occipital and parietal bones were removed with forceps. Finally, the brain was extracted and stored in 4 % PFA and the tail was collected in a separate tube for genotyping.

3.5 Genotyping

3.5.1 DNA preparation

The tail samples were lysed in lysis buffer (100 μl, 10mM Tris, 1M KCl, 0.4 % NP-40/Igepal CA630 Sigma, 0.1 % Tween 20) with Protein kinase K (2 μl) for 12-16 hours, incubating at 60°C. After incubation, the samples were heated at 95°C for 30 min, followed by a full speed centrifugation (14.000 rpm) for 20min.

3.5.2 PCR

The DNA was collected from the supernatant and diluted 1:1. The diluted DNA (1 μl) was added to a PCR-mix (2,75μl ddH2O, 5μl Taq Master Mix (10XPCR Buffer, 2.5/10 mM dNTPs, 5U/μl paq5000, 50 mM $MgCl_2$), 0,5μl Neil3 forward primer, 0,5μl N3 reverse primer and 0,25μl of Primer KO for N3) (Table 3.5). The tubes were vortexed and spinned down before the following PCR-program was initiated; 3min at 95°C + 38x (30s at 95°C+30s at 58°C+60s at 72°C) + 5min at 72°C + ∞ at 4°C.

3.5.3 Gel electrophoresis

An agarose gel was made by dissolving 2 % agarose (LE Agarose, BioNordica, Cat. #BN50004) in TAE-buffer (Tris Base, Glacial Acetic Acid, 0.5M EDTA) with 0.001 % SYBR safe stain (ThermoFisher/Invitrogen, Cat. #S33102). The solution was then poured into a plastic gel holder with a suitable well-comb (BioRad) and any bubble in the gel was removed using a pipet tip. When the gel was hardened it was transferred to the electrophoresis machine with the top of the gel pointing towards the black electrode, and

the plastic bath was filled with TAE-buffer. The gel was loaded with 5 μl in each well in the following order: 100 bp DNA ladder (New England Biolabs), samples and controls (Neil3 standard, WT standard, negative control). The gel ran for 40min at 120V. After the run, the gel was placed in a ChemiDoc Imaging System (BIORAD) to capture the image of the gel.

Table 3.5: *List of primers for PCR. KO, knock-out.*

Gene	Sequence
Neil3	Forward: CTTGTTTTCCCACCACAATCTG
Neil3	Reverse: GTGGGCTGAAATTACACAAACAAT
Neil3 KO	Forward: GCCTCTGTTCCACATACACTTCAT
Neil3 KO	Reverse: GTGGGCTGAAATTACACAAACAAT

3.6 Frozen sectioning

The adult brains were sectioned using a cryomicrotome (CryoStar NX70, Thermo Fisher). The chamber temperature and section thickness were set to -20 °C and 30 μm respectively. A scalpel was used to make a sagittal cut through the brain, separating the right and left hemisphere. The right hemisphere was used for sectioning. The right hemisphere was mounted on a cryostat metal chip with a suitable amount of mounting medium (OCT). The brain was quickly freezed by using a quick freezing spray (PRF) at -55 °C to avoid crystallization and to shorten the freezing time. The metal chip was then placed on the cryobar in the cryostat to completely freeze. The glass and the cutting blade were adjusted into correct position and the metal chip was placed in the cutting position. Sagittal sections of the brain were cut in rounds with 20 sections per round. The sections were individually picked up with a bent glass pipet and distributed over one row per sample (6 wells) in a 24 welled plate filled with PBSx1 and 0.03 % ProClin 300 (Sigma Aldrich, Cat. #48912-U). The plate was stored at 4°C.

3.7 Immunohistochemistry, frozen section staining

Immunohistochemistry (IHC) was performed with the adult brain samples in order to analyze proliferating cells (Ki67), immature neurons (DCX) and immediate early genes (Arc, c-fos) in the DG granular zone, interneurons (GAD67, PV) in the DG granular zone and hilus, and the mossy fiber volume (Calbindin) in the CA3. Three naïve animals were used from each genotype (WT/*Neil3-/-*) and five trained animals were used from each genotype (WT/*Neil3-/-*). Two sections from each animal were used for analysis. The antibodies are listed in table 3.7. The solutions are listed in APPENDIX.

3.7.1 Sorting of slices

A bent glass pipet was used to gently transfer the slices (30 μm) from a 24 welled storage-plate to a large petri dish filled with PBSx1. Two medial sections (Figure 7) from the right hemisphere were sorted out for each sample and placed in a 12 welled plate filled with PBSx1. Similar sections were chosen for all the samples.

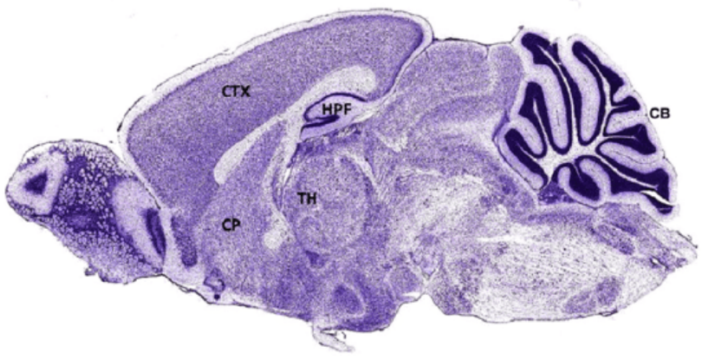

Figure 7: *Medial, sagittal section of a mouse brain. HPF, hippocampal formation; TH, thalamus; CB, cerebellum; CTX, cortex. The figure is made by Honigman et al. [100].*

3.7.2 Antigen retrieval

Use of formaldehyde for tissue-fixation causes chemical modifications in the tissue. Antigen retrieval was done in order to unmask the antigens and allow antibodies to bind.[101] 1 mL of a 40 mM trisodium citrate (Trisodium citrate 5,5 hydrate, Merck Millipore 1.06431.100) solution with pH 6 was filled in 1.5 mL Eppendorf tubes, with one tube for each sample. The tubes were preheated to 99°C using a heating block before the samples was added and allowed to incubate for 3 min. After incubation, the samples were cooled to room temperature (27 min) followed by washing 3 times for 5 min in PBSx1.

3.7.3 Blocking of unspecific binding

Blocking was done in order to prevent unspecific binding of antibodies or other reagents. The sections were transferred directly from PBSx1 to a 24 welled plate filled with 200 μL blocking buffer (5 % NGS/5 % BSA/0.1 % Triton X-100 in PBS). The plate was placed on a shaker (15/min) in room temperature for 2 hours.

3.7.4 Primary antibodies

Primary antibodies (table 3.7) were vortexed and diluted in a dilution buffer (1 % NGS/1 % BSA/0.1 % Triton X-100 in PBS). 200 μL of the primary antibody solution was filled in each well and the sections were transferred directly from the blocking solution to the primary antibody solution before the plate was placed on a shaker (15/min) in 4°C overnight.

3.7.5 Secondary antibodies

After primary antibody incubation, the sections were washed three times (10-20-30 min) in PBS-Tx1 (PBSx1 + 0.1 % Tween20) at room temperature. The secondary antibodies (table 3.7) were vortexed and diluted in a dilution buffer (1 % NGS/1 % BSA/0.1 % Triton X-100 in PBS). 200 μL of the secondary antibody solution was filled in each well and the sections were transferred from PBS-Tx1 to the secondary antibody solution. The plate was covered in aluminum foil in order to protect the sections from light and placed on a shaker (15/min) for 2 hours. After secondary antibody incubation, the sections were washed three times (10-20-30 min) in PBS-Tx1 (PBS + 0.1 % Tween20).

3.7.6 Mounting

The sections were transferred to a large petri dish filled with PBS, one well at a time. A bent glass pipet was used to twirl the sections in the same orientation, and a fine brush was used to mount them on coated slides (SuperFrost). The slides were left in a light protected container overnight to allow them to dry. The next day, the slides were stained with DAPI solution (DAPI + PBSx1, 1:1000, 1 min) followed by washing in PBSx1 (2x10s) and ddH_2O (1x10s) using a metal slide holder. The slides dried for 10 min before they were cover-slipped using mounting oil (ProLong Gold Antifade Mountant with DAPI, Invitrogen, Cat. #P36935). The samples were allowed to dry and then stored in a light-protected box at 4°C.

3.7.7 List of antibodies

Primary and secondary antibodies used for IHC are presented in table 3.7.

Table 3.7: *List of antibodies used for IHC. R, rabbit; m, mouse.*

Primary antibodies	Isotype	Dilution	Manufacturer	Catalog number	RRID
Anti-NeuN	mIgG1	1:500	Merck Millipore	MAB377	AB_2298772
Anti-DCX	rIgGs	1:1000	Abcam	AB18723	AB_732011
Anti-Calbindin	rIgG	1:1000	Swant	CB-38a	AB_10000340
Anti-c-fos	rIgG	1:1000	Synaptic Systems	226 003	AB_2231974
Anti-PV	rIgG	1:1000	Swant	PV25	AB_10000344
Anti-GAD67	mIgG2a	1:2000	Merck Millipore	MAB5406	AB_2278725
Ki67	ratIgG2a	1:500	Thermo Fisher	14-5698-82	AB_10854564
Anti-Arc	rIgG	1:1000	Synaptic Systems	156 003	AB_887694
Anti-Sox2	rIgG	1:1000	Merck Millipore	AB5603	AB_2286686
Secondary antibodies					
A488	mIgG1	1:1000	Invitrogen	A-21121	AB_2535764
A555	rIgG	1:1000	Invitrogen	A-21431	AB_2535852
A647	mIgG2a	1:1000	Invitrogen	A-21241	AB_2535810
A647	ratIgG	1:1000	Invitrogen	A-21247	AB_141778
A647	ratIgG2a	1:1000	Invitrogen	51-4321-81	AB-2716967

3.8 Immunohistochemistry, paraffin section staining

The embryonic brains obtained from the dissected embryos were extremely fragile, and frozen sectioning was found to be an unsuited method. Therefore, the brains were embedded in paraffin wax before they were sectioned and mounted on glass slides. The paraffin-embedding was done by the technicians at the Histology Core, NTNU. IHC with the paraffin-embedded sections was done in order to study NSCs (Sox2), proliferating cells (Ki67) and mature neurons (NeuN) in the developing hippocampus in mice. The antibodies are listed in table 3.7.

3.8.1 Deparaffinization and rehydration

First, the samples were incubated at 58°C for 15 min before they were transferred directly to glass jars containing different solutions, and incubated in the following order; Xylene (Sigma-Aldrich, 247642) 2x for 5min; 100% Ethanol (VWR, 20821.296) 2x for 3min; 96% Ethanol (VWR, 20824.296) for 1min; 70% Ethanol (VWR) for 1min; PBSx1.

3.8.2 Antigen retrieval

Antigen retrieval buffer (40 mM Trisodium citrate 5,5 hydrate (Merck Millipore 1.06431.100), pH 6, 1L) were boiled on a hot plate in a pressure cooker. The sections were transferred to the boiling buffer and the sections were allowed to incubate in the boiling buffer for 3 min. The sections were cooled by placing the cooker under cold running water for 10 min before the sections were transferred to a glass jar with PBS-Tx1 (PBSx1 + 0.1 % Tween20). The slides were carefully dried using a dust-free paper cloth and hydrophobic circle was drawn around the tissue using a Dako Pen. PBS-Tx1 + 0,25 % triton was added in the circle using a pipet before they were left at 4 °C for 15 minutes.

3.8.3 Staining

The solution was removed from the slides by carefully drying them one by one using a dust-free paper cloth without touching the tissue. The hydrophobic circle was re-marked using a Dako Pen. The sections were blocked for 1 hour at room temperature by pipetting 200µl of blocking buffer (PBS + 5% NGS + 5% BSA + 0,1% Triton X-100) in the hydrophobic circle. After blocking, they were washed in PBS-Tx1 3x for 10 min. Again, the solution was removed from the slides and the hydrophobic circle was re-marked. The primary antibodies (table 3.7) were diluted in dilution buffer (PBS + 0,5%NGS + 0,5% BSA + 0,1% Triton X-100) and added it in the hydrophobic circle. Subsequently, they were incubated overnight at 4°C.

The next day, the sections were washed 3x (5-10-20min) in PBS-Tx1 at room temperature in a glass jar. The solution was removed from the slides and the hydrophobic circle was re-marked. Secondary antibodies (table 3.7) were diluted in dilution buffer (PBS + 0,5%NGS + 0,5% BSA + 0,1% Triton X-100) and added it in the hydrophobic circle. The

slides were allowed to incubate for 1 hour. The sections were washed 3x (5-10-20min) in PBS-T at room temperature and then dipped in DAPI (1:1000 in PBS) for 1-2 min at room temperature. They were then washed 2x in PBSx1 (2min each) and 1x in ddH2O (2min). The sections were allowed to dry for 10 minutes before they were cover-slipped using mounting oil (ProLong Gold Antifade Mountant with DAPI, Invitrogen, Cat. #P36935). Nail polish was used to seal the cover glass.

3.9 Confocal Microscopy

A Zeiss LSM880 confocal fluorescence microscope (Carl Zeiss) with a Plan-Apochromat 40x/1.4 Oil DIC M27 objective (Carl Zeiss, Jena, Germany) and ZEN software (Carl Zeiss) was used to image the samples from the immunohistochemical stainings. The DAPI channel with a 365 nm laser was used to visualize the section and to localize the dorsal DG. A live image of the DG was obtained using the NeuN channel with a 690 nm laser. The settings were adjusted and optimized for each laser channel, which corresponds to the different antibodies used in the immunostainings. Intensity and gain were adjusted individually for each channel, while the pinhole value was set the same for all channels for each batch. The z-stack interval was selected using the NeuN channel in order to capture all the cell layers in the tissue. Further, the z-stack interval was optimized for each batch using the "optimize stacks" function. The NeuN channel was used with the "tile scan" function to adjust number of tiles to fit the dorsal DG in the image. Finally, all the channels were turned on and the image was captured. For each batch, the settings were kept the same.

3.10 Imaris Image Analysis

The samples imaged by confocal fluorescence microscopy were analyzed using the 3D software Imaris 9.4 (Oxford Instruments).

3.10.1 Ki67

First, a 3D surface through all the stack images containing only the DG, was drawn using the surface-tool in the software. The surface was then masked for the Ki67 channel. Subsequently, the number of Ki67 positive cells in the granular zone were counted manually using the slice-view in order to eliminate artifacts the was found to be detected by the spots-tool in the software. The number of Ki67-positive cells per mm^3 were calculated using the formula presented below.

$$\frac{\text{Positive stained cells}}{\text{mm}^3} = \frac{\text{Number of positive stained cells}}{\text{DG surface volume [mm}^3\text{]}} \qquad (3.10.1)$$

3.10.2 DCX

A 3D surface containing only the DG was made and masked for the DCX channel. A second surface was then constructed like the first one, but with a threshold 3.5x the mean intensity volume of the DCX channel, allowing the software to only detect the voxels of the DCX positive cells in the DG surface. The DCX expression level in the DG was presented as a voxel ratio, calculated using the formula below.

$$\text{DCX expression} = \frac{\text{Number of DCX voxels}}{\text{DG surface volume}} * 100\ \mu m^3 \qquad (3.10.2)$$

3.10.3 Calbindin

Three different 3D surfaces were made for the mossy fiber (MF) analysis. First, a surface containing only the CA3 was made using the surface tool. Similarly, as described for the CA3 surface, a surface of the infrapyramidal mossy fibers (IMF) and a surface of both the infrapyramidal and the suprapyramidal mossy fibers (SMF). Three values were calculated using the volumes obtained in the analysis; IMF/CA3, IMF/MF and MF/CA3 given as percentage. How the IMF was defined is presented in figure 8.

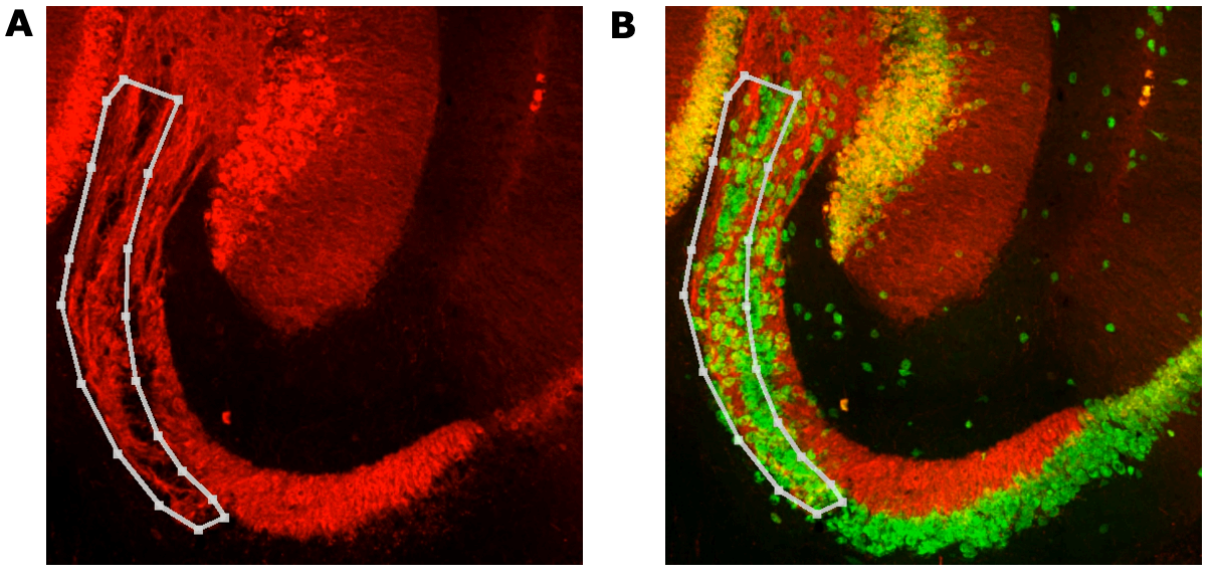

Figure 8: *Illustration of how the infrapyramidal mossy fiber bundle was defined in Imaris 9.4.*

3.10.4 Arc and c-fos

A 3D surface of the DG was drawn using the surface-tool in the software. Following, the surface was first masked for the c-fos channel and then for the Arc channel. Subsequently, the number of c-fos-positive cells and Arc-positive cells in the granular zone were counted manually using the slice-view in order to eliminate artifacts that was found to be detected by the spots-tool. Formula 3.10.1 was used to calculate the number of positive cells per mm^3.

3.10.5 GAD67 and PV

A 3D surface through all the layers was drawn loosely around the dentate gyrus including a small part of the molecular layer and excluding the first part of the CA3 that can be seen in the dentate gyrus (Figure 9). Subsequently, the surface was first masked for the GAD67 channel and then for the PV channel. Furthermore, the number of GAD67 positive cells and PV positive cells in the granular zone and in the hilus were counted manually using the slice-view in order to eliminate artifacts. Formula 3.10.1 was used to calculate the number of positive cells per mm^3.

The number of co-stained cells were counted manually by counting the cells that overlapped from the abovementioned analysis. This was done in order to quantify the number the PV-positive cells that were GABAergic, and was calculated using the presented formula:

$$\text{GABAergic PV cells} = \frac{\text{Number of co} - \text{stained cells}}{\text{Volume } [\text{mm}^3]} \qquad (3.10.3)$$

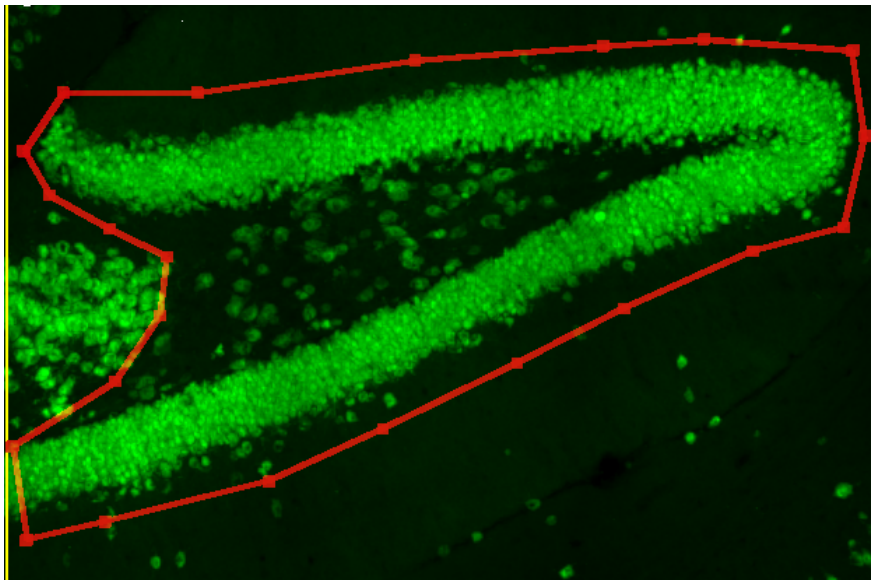

Figure 9: *Illustration of the 3D surface used in analysis of GAD67-positive and PV-positive cells.*

3.11 ImageJ

The software ImageJ (Fiji v1.53, NHI and LOCI Wisconsin) was used to make representative images from the IHC stainings. A maximum intensity z-stack projection, with equal number of stacks for each channel, was made. Subsequently, the image from each channel was merged in order to obtain an image with both channels represented.

3.12 Statistical Analysis

The software GraphPad Prism 9.3.1 was used to perform the statistical analyses. The two samples from each animal was averaged before the analysis, giving one value per animal (n(naïve WT/*Neil3-/-*) = 3, n(trained WT/*Neil3-/-*) = 3-5). The ROUT-analysis was used to identify outliers in each group. A two-way ANOVA was used, subsequently, a Tukey multiple comparison test was performed to compare the data between the groups; baseline WT; trained WT; baseline *Neil3-/-* and trained *Neil3-/-.*

4 Results

To address the questions for this thesis, behavioral studies were performed in order to investigate the impact of NEIL3 on spatial memory. WT mice were used as controls. Naïve WT and *Neil3-/-* were compared to trained WT and *Neil3-/-* mice to investigate whether NEIL3 has an impact on (1) adult neurogenesis associated with spatial learning, (2) activation of immediate early genes (IEGs) associated with spatial learning, (3) activation of inhibitory interneurons associated with spatial learning, and (4) spatial experience induced synaptic changes by measuring the IMF volume.

The mice were exposed to an open field test to measure their anxiety and general activity levels. A modified protocol of Seibenhener et al.[102] was used. Following, novel object location (NOL) test (after 3 days habituation) and Y-maze test (after 6 days habituation) were performed with 24-hour intertrial interval in order to test their hippocampal-dependent spatial memory. Modified protocols of Denninger et al.[103] and Sanderson et al.[104] were used respectively. The animals were sacrificed 24 hours after training. The behavior studies and the extraction of the mouse brains were performed by Marion Silvana Fernandez Berrocal.

4.1 Exploring the impact of NEIL3 on adult neurogenesis associated with spatial learning and memory

It is known that NEIL3 plays a role in neurogenesis [20, 28] and NEIL3-deficient mice show impaired spatial learning in the Morris Water Maze.[20] Furthermore, spatial experience is involved in and associated with enhanced adult neurogenesis.[93, 96] As earlier established (section 1.4.2), adult neurogenesis occur in the SGZ of the DG, and the NSCs migrate to the DG granular zone where they reside, differentiate and mature to neurons. Here, I aimed to investigate whether NEIL3 affects adult neurogenesis associated with spatial learning. To achieve this, I used immunohistochemistry (IHC) with Ki67 and DCX as markers for proliferating and immature neurons respectively, to examine whether the number of these cells in the DG granular zone are affected in *Neil3-/-* mice after spatial training.

4.1.1 Number of Ki67-positive proliferating cells in DG granular zone

Ki67 is expressed during all the active phases of the cell cycle, but the expression varies in intensity through the different phases as well as its cellular location.[105] The expression of Ki67 is low in G1 and S phase and increases from S phase to mitosis where it reaches its maximum, followed by a quick decrease in anaphase and telophase. Therefore, Ki67 is often used as a marker for proliferating cells.[105]

Frozen brain sections of WT and *Neil3-/-* mice (3-months-old) with and without spatial training were analyzed by IHC using antibodies against Ki67. The hippocampal DG was imaged by confocal fluorescence microscopy (Zeiss LSM880, Z-stack (30), tile (2x3)) and the Ki67-positive proliferating cells in the DG granular zone were quantified using the 3D-image analysis software Imaris 9.4.

As expected, Ki67-positive cells were found in the DG granular zone (Figure 10A-B). In WT mice, the number of Ki67-positive proliferating cells increased after spatial learning (n(naïve WT) = 1224 cells/mm^3, n(trained WT) = 1607 cells/mm^3; p = 0.1507; two-way ANOVA, Tukey; n(naïve WT) = 3 , n(trained WT) = 4) (Figure 10C). However, this increase was not detected in mice lacking NEIL3 (n(naïve *Neil3-/-*) = 1185 cells/mm^3, n(trained *Neil3-/-*) = 1274 cells/mm^3; p = 0.9456; two-way ANOVA, Tukey; n(naïve *Neil3-/-*) = 3 , n(trained *Neil3-/-*) = 4) (Figure 10C). No significant difference between the genotypes (naïve mice, p = 0.9957; mice after spatial learning p = 0.1855; two-way ANOVA (Tukey)) was detected (Figure 10C). In summary, these results suggest that NEIL3-deficient mice show a tendency of impaired adult neurogenesis in DG after spatial training.

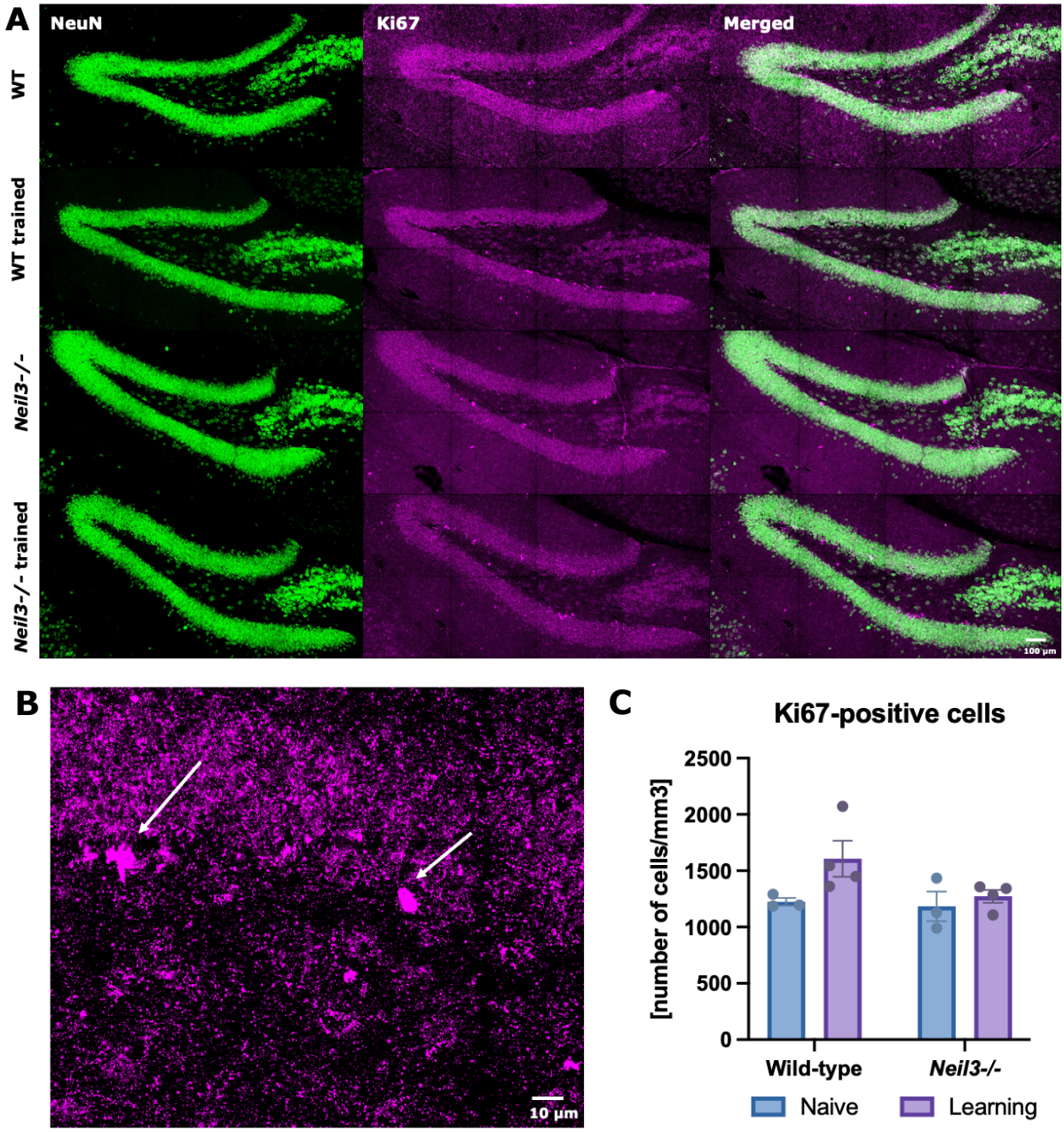

Figure 10: A. *Representative confocal images of immunostained DG samples from naïve WT (top), trained WT, naïve Neil3-/- and trained Neil3-/- (bottom). Each image is represented from left to right: NeuN (green), Ki67 (magenta) and both channels merged together. The samples were scanned with Zeiss LSM880 using a Plan-Achromat 40x/NA 1.3 oil immersion objective (Z stack (30), tile (2x3)). Each image is further processed with ImageJ (Fiji v1.53) to obtain a maximum intensity z-stack projection (n(z stacks) = 25). Scale bar 100 µm.* ***B.*** *A representative image of Ki67+ cells counted with Imaris 9.4. The image is obtained similar as described above. Scale bar 10 µm.* ***C.*** *Number of Ki67+ cells/mm^3 in the granular zone of the DG in naïve WT, trained WT, naïve Neil3-/- and trained Neil3-/- mice. The data was statistically analyzed in GraphPad Prism 9.3.1 using a two-way ANOVA (Tukey) (n(naïve WT/Neil3-/-) = 3, n(trained WT/Neil3-/-) = 4). The error bars indicate SEM and a p-value below p = 0.05 was considered as significant.*

4.1.2 DCX expression level in immature neurons in DG granular zone

DCX is a nervous-system specific microtubule-associated protein expressed in the brain during embryonic and postnatal development.[106] The expression of DCX is high during neuronal migration, early differentiation and during maturation.[107] DCX promotes cell migration and differentiation during neurogenesis and is highly expressed in the cell body and dendrites of immature neurons in the SGZ zone of the DG.[108, 109] Therefore, DCX is widely used as a marker for immature neurons and analysis of adult neurogenesis.[110]

Frozen brain sections of WT and *Neil3-/-* mice (3-months-old) with and without spatial training was analyzed by IHC using antibodies against DCX. The hippocampal DG was imaged by confocal fluorescence microscopy (Zeiss LSM880, Z-stack (30), tile (2x3)) and the voxel ratio as a measure for DCX expression level in the DG granular zone were obtained using the 3D-image analysis software Imaris 9.4.

As presumed, DCX-expressing immature neurons were detected in the DG, with a characteristic expression in the SGZ (Figure 11A). An insignificant decrease of the DCX expression level was observed in WT mice after spatial training (DCX expression; naïve WT = 185 voxels/1000μm^3, trained WT = 140 voxels/1000μm^3; p = 0.2104; two-way ANOVA, Tukey; n(naïve WT) = 3 , n(trained WT) = 4) (Figure 11B). Nonetheless, this decrease was not detected in NEIL3 deficient mice (DCX expression; naïve *Neil3-/-* = 220 voxels/1000μm^3, trained *Neil3-/-* = 201 voxels/1000μm^3; p = 0.8172; two-way ANOVA, Tukey; n(naïve *Neil3-/-*) = 3, n(trained *Neil3-/-*) = 4) (Figure 11B). Interestingly, a significant difference between the genotypes was detected after spatial learning (p = 0.0443; two-way ANOVA (Tukey)), with a notably lower expression level of DCX in WT mice (Figure 11C). No significant difference between the naïve genotypes (p = 0.4471, two-way ANOVA (Tukey) was detected. These results indicate that NEIL3-deficient mice show a tendency of increased DCX expression in DG immature neurons compared to WT, especially more after spatial training.

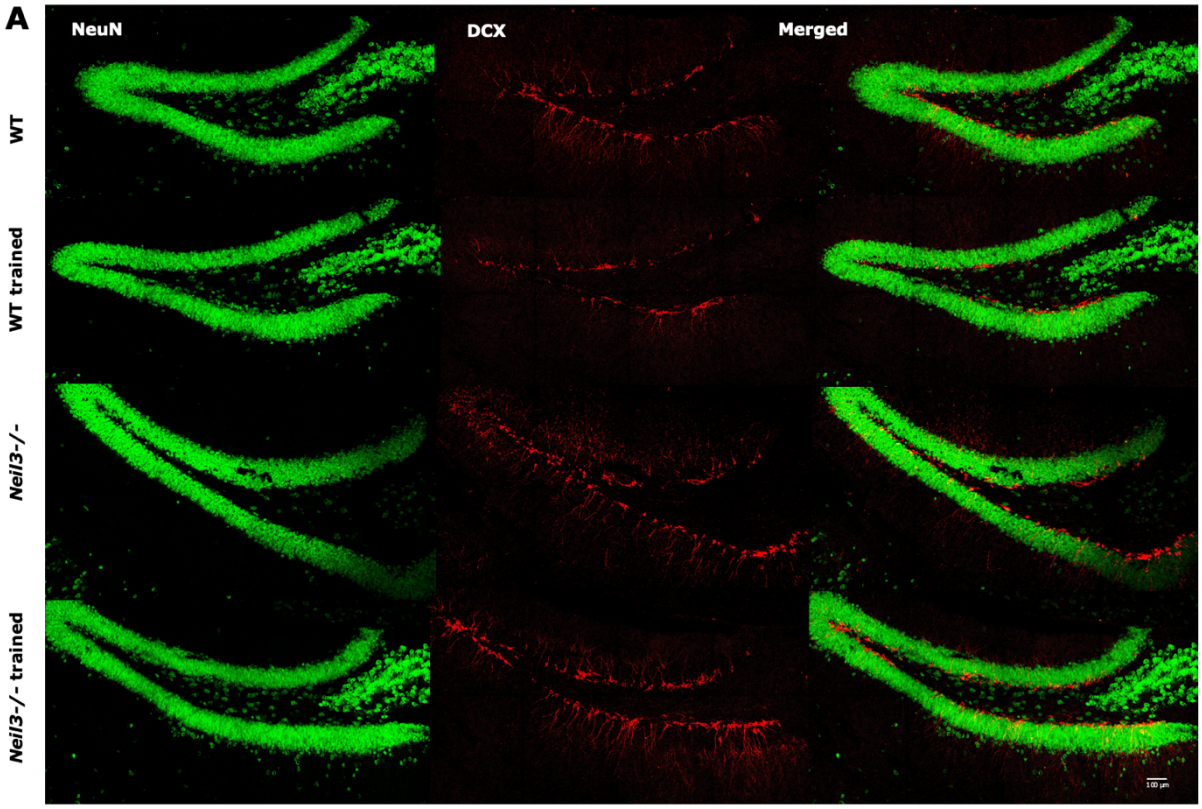

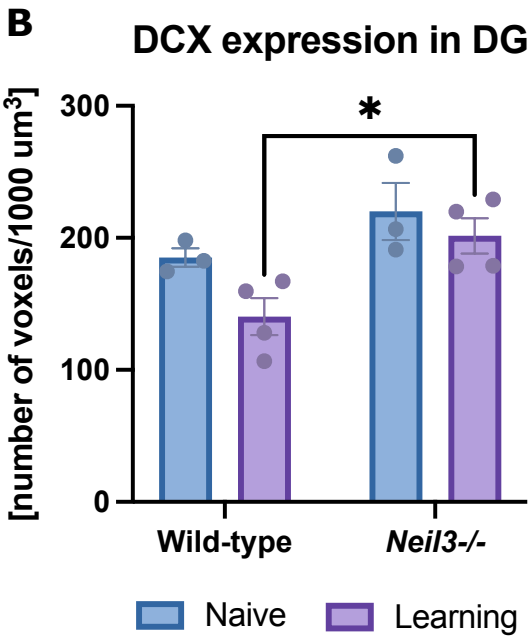

Figure 11: A. *Representative confocal images of immunostained DG samples from naïve WT (top), trained WT, naïve Neil3-/- and trained Neil3-/- (bottom). Each image is represented from left to right: NeuN (green), DCX (red) and both channels merged together. The samples were scanned with Zeiss LSM880 using a Plan-Achromat 40x/NA 1.3 oil immersion objective (Z stack (30), tile (2x3)). Each image is further processed with ImageJ (Fiji v1.53) to obtain a maximum intensity z-stack projection (n(z stacks) = 25). Scale bar 100 μm.* ***B.*** *DCX expression level represented as number of voxels/1000um^3 in the DG granular zone. The data was statistically analyzed in GraphPad Prism 9.3.1 using a two-way ANOVA (Tukey) (n(naïve WT/Neil3-/-) = 3, n(trained WT/Neil3-/-) = 4). The error bars indicate SEM and a p-value below p = 0.05 was considered as significant.*

4.2 Exploring the impact of NEIL3 in expression of immediate early genes in response to spatial experience in the DG

4.2.1 Number of c-fos and Arc-positive cells in the DG granular zone

Learning and behavioral experiences is associated with upregulated expression of immediate early genes (IEGs), such as c-fos[97] and Arc[98], in hippocampal neurons and play a critical role in regulating synaptic plasticity and formation of long term memory.[98, 111-113] Furthermore, suppression of the IEG proteins c-fos and Arc have been shown to impair long term memory consolidation.[98] Here, I aimed to investigate whether NEIL3 impacts the expression of IEGs in response to spatial experience. To accomplish this, I performed IHC with markers for the IEG proteins c-fos and Arc and quantified the number of these positive cells in order to see whether the expression of the IEGs is affected in NEIL3-deficient mice after spatial learning.

Generally, IEGs are expressed when neurons get activated.[114] *c-fos* and *Arc* are two IEGs that is expressed during neuronal activation.[97, 98] Their proteins can thus be used as markers for neuronal activation and expression of IEGs.

Frozen brain sections of WT and *Neil3-/-* mice (3-months-old) with and without spatial training was analyzed by IHC using antibodies against Arc and c-fos. The hippocampal DG was imaged by confocal fluorescence microscopy (Zeiss LSM880, Z-stack (28), tile (2x3)) and the Arc-positive and c-fos-positive neurons in the DG granular zone were quantified using the 3D-image analysis software Imaris 9.4.

C-fos- and Arc-positive cells were detected in the DG granular zone (Figure 12A-B, 13A-B). As expected in WT mice, the number of c-fos-positive cells in the DG granular zone increased significantly after spatial learning (n(naïve WT) = 241 cells/mm^3, n(trained WT) = 875 cells/mm^3; p = 0.0116; two-way ANOVA, Tukey; n(naïve WT) = 3, n(trained WT) = 3) (Figure 12C). However, this increase was not detected in mice lacking NEIL3 (n(naïve *Neil3-/-*) = 184 cells/mm^3, n(trained *Neil3-/-*) = 387 cells/mm^3; p = 0.5844; two-way ANOVA, Tukey; n(naïve *Neil3-/-*) = 3 , n(trained *Neil3-/-*) = 3) (Figure 12C). No significant difference between the naïve genotypes (p = 0.9878, two-way ANOVA (Tukey) was detected. Strikingly, there was a significant difference between the genotypes after spatial training (p = 0.0442, two-way ANOVA (Tukey)) (Figure 12C), suggesting that NEIL3 impacts the spatial-experience-induced expression of IEGs in the DG.

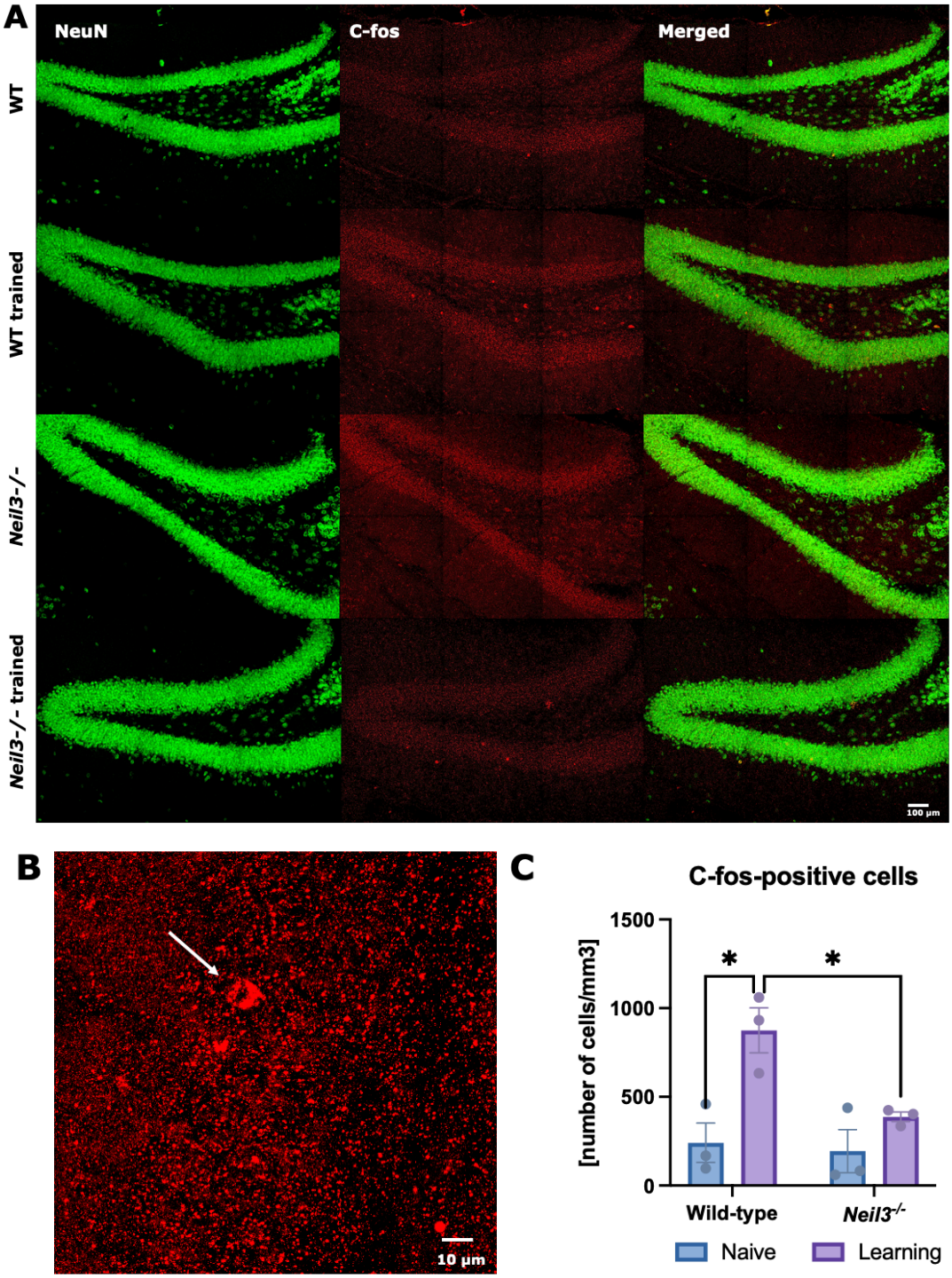

Figure 12: A. *Representative confocal images of immunostained DG samples from naïve WT (top), trained WT, naïve Neil3-/- and trained Neil3-/- (bottom). Each image is represented from left to right: NeuN (green), c-fos (red) and both channels merged together. The samples were scanned with Zeiss LSM880 using a Plan-Achromat 40x/NA 1.3 oil immersion objective (Z stack (28), tile (2x3)). Each image is further processed with ImageJ (Fiji v1.53) to obtain a maximum intensity z-stack projection (n(z stacks) = 25). Scale bar 100 µm.* ***B.*** *A representative image of c-fos+ cells counted with Imaris 9.4. The image is obtained similar as described above. Scale bar 10 µm.* ***C.*** *Number c-fos+ cells/mm^3 in the granular zone of the DG in naïve WT, trained WT, naïve Neil3-/- and trained Neil3-/- mice. The data was statistically analyzed in GraphPad Prism 9.3.1 using a two-way ANOVA (Tukey) (n(naïve WT/Neil3-/-) = 3, n(trained WT/Neil3-/-) = 3). The error bars indicate SEM and a p-value below p = 0.05 was considered as significant.*

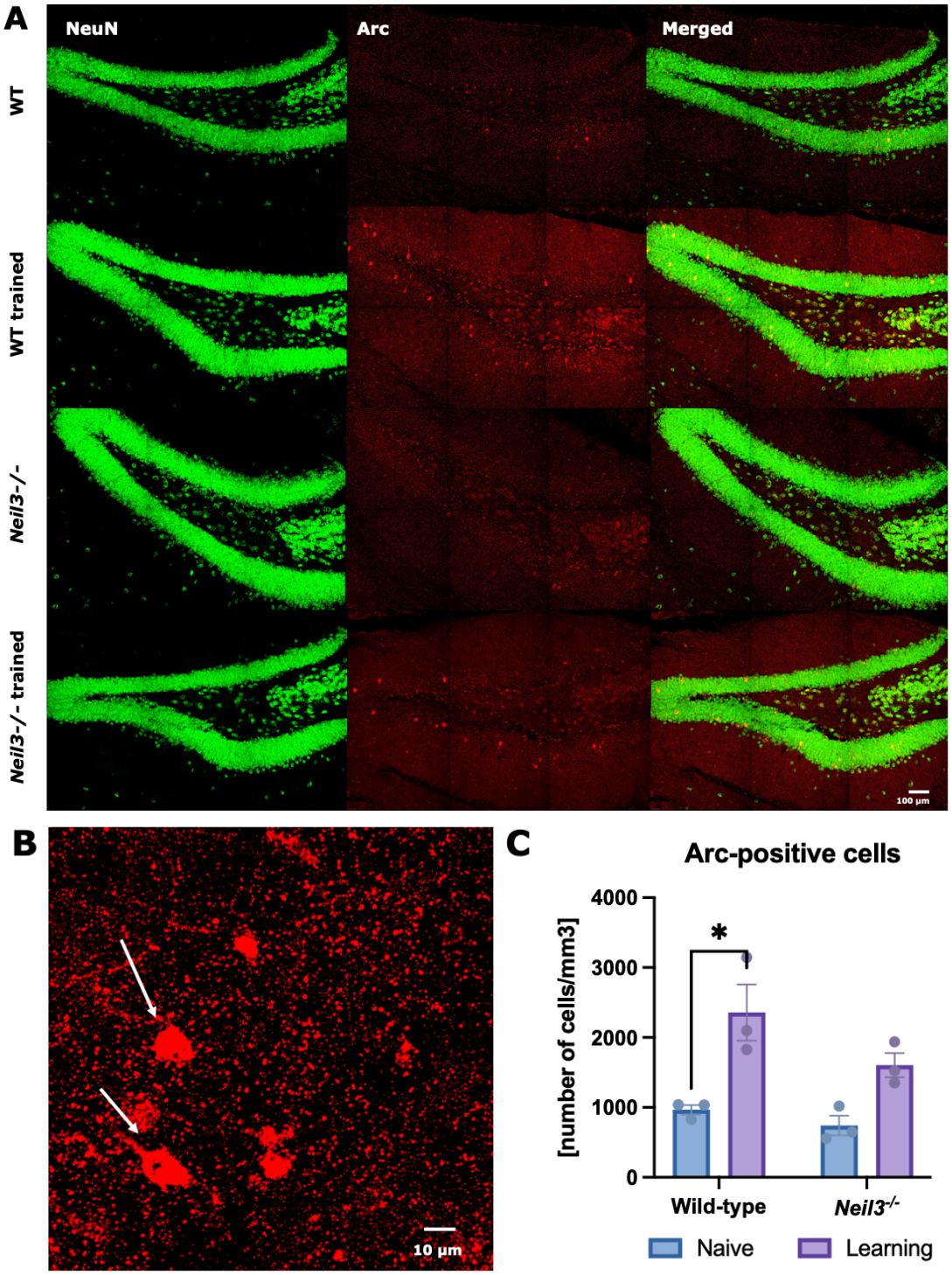

Figure 13: A. *Representative confocal images of immunostained DG samples from naïve WT (top), trained WT, naïve Neil3-/- and trained Neil3-/- (bottom). Each image is represented from left to right: NeuN (green), Arc (red) and both channels merged together. The samples were scanned with Zeiss LSM880 using a Plan-Achromat 40x/NA 1.3 oil immersion objective (Z stack (28), tile (2x3)). Each image is further processed with ImageJ (Fiji v1.53) to obtain a maximum intensity z-stack projection (n(z stacks) = 25). Scale bar 100 µm.* ***B.*** *A representative image of Arc+ cells counted with Imaris 9.4. The image is obtained similar as described above. Scale bar 10 µm.* ***C.*** *Number c-fos+ cells/mm^3 in the granular zone of the DG in naïve WT, trained WT, naïve Neil3-/- and trained Neil3-/- mice. The data was statistically analyzed in GraphPad Prism 9.3.1 using a two-way ANOVA (Tukey) (n(naïve WT/Neil3-/-) = 3, n(trained WT/Neil3-/-) = 3). The error bars indicate SEM and a p-value below p = 0.05 was considered as significant.*

Similarly, in WT mice, a significant increase in the number of Arc-positive cells was observed after spatial training (n(naïve WT) = 967 cells/mm^3, n(trained WT) = 2357 cells/mm^3; p = 0.0123; two-way ANOVA, Tukey; n(naïve WT) = 3 , n(trained WT) = 3) (Figure 13C). Nonetheless, this increase was not detected in NEIL3 deficient mice (n(naïve *Neil3-/-*) = 742 cells/mm^3, n(trained *Neil3-/-*) = 1646 cells/mm^3; p = 0.1127; wo-way ANOVA, Tukey; n(naïve *Neil3-/-*) = 3, n(trained *Neil3-/-*) = 3) (Figure 13C). No significant difference was observed between the genotypes ((naïve mice, p = 0.9000; mice after spatial learning p = 0.1809; two-way ANOVA (Tukey)). In essence, these results indicate that mice lacking NEIL3 show a tendency of impaired Arc expression in DG associated with spatial learning, which is in line with the results from the c-fos analysis.

In conclusion, these results suggest that NEIL3 plays a role in spatial-experience induced expression of IEGs in the DG.

4.3 Exploring the impact of NEIL3 in spatial experience-induced activation of GABAergic inhibitory interneurons in the DG

4.3.1 Number of GAD67 and PV-positive cells in the DG granular zone and hilus

The hippocampal circuitry consists of an interplay between excitatory hippocampal neurons and inhibitory hippocampal interneurons.[115] Although excitatory neurons account for the largest portion of the neuronal population in the hippocampus, inhibitory interneurons is crucial for maintaining the fine-tuned excitation-inhibition balance in the hippocampal circuitry.[116] They form connections between other types of neurons and modulate the hippocampal circuitry as well as regulating the circuit activity.[117] They do so by synaptically releasing GABA[117], which is the main inhibitory neurotransmitter in the cortex[118].

The excitation-inhibition balance of neuronal activity in the hippocampus is thought to be essential for normal memory and learning, and is associated with an increase in GABA release and inhibitory synaptic plasticity.[99] Furthermore, it is evidence that inhibition of GABAergic interneuron activity impairs spatial learning.[99] I aimed to see whether NEIL3 affects the activation of GABAergic interneurons associated with spatial learning.[99] In the DG, interneurons are mainly located in the granular cell layer and in the hilus.[119, 120] Therefore, to investigate this, I used IHC with GAD67 and PV antibodies as markers for GABAergic interneurons and PV-interneurons respectively, to see whether their activation is altered in *Neil3-/-* mice.

GAD67 is an enzyme which synthesizes GABA when it is activated[121], and is a widely used marker for GABAergic interneurons[122]. An increase in GAD67 support replenishing GABA released after stimulation.[123] Therefore, GAD67 can be used as a marker for recently activated GABAergic inhibitory interneurons. PV is a calcium-binding protein expressed in one type of interneurons and can be used as a PV-interneuron marker.[119] However, PV-inhibitory interneurons are also mainly GABAergic.[119]

Frozen brain sections of WT and *Neil3-/-* mice (3-months-old) with and without spatial training was analyzed by IHC using antibodies against GAD67 and PV. The hippocampal DG was imaged by confocal fluorescence microscopy (Zeiss LSM880, (Z stack (28), tile (2x3)) and the GAD67-positive and PV-positive neurons in the DG granular zone and in the hilus were quantified using the 3D-image analysis software Imaris 9.4.

In line with my assumptions, GAD67-positive cells were detected in both the DG granular zone and in the hilus (Figure 14A-B). A significant increase in GAD67-positive cells was observed in WT mice after spatial learning (n(naïve WT) = 986 cells/mm^3, n(trained WT) = 1584 cells/mm^3; p = 0.0204, two-way ANOVA (Tukey); n(naïve WT) = 3 , n(trained WT) = 3) (Figure 14C). Strikingly, this increase was not observed in NEIL3 deficient mice after spatial learning (n(naïve *Neil3-/-*) = 916 cells/mm^3, n(trained *Neil3-/-*) = 996 cells/mm^3; p = 0.9531, two-way ANOVA (Tukey); n(naïve *Neil3-/-*) = 3 , n(trained *Neil3-/-*) = 3) (Figure 14C). No significant difference between the naïve genotypes (p = 0.9675, two-way ANOVA (Tukey)) was detected. Interestingly, the number of GAD67-positive cells was significantly higher in WT mice than *Neil3-/-* mice after spatial training (p = 0.0223, two-way ANOVA (Tukey)) (Figure 14C). Thus, these results suggest that NEIL3 plays a role in activation of GABAergic interneurons in response to spatial training.

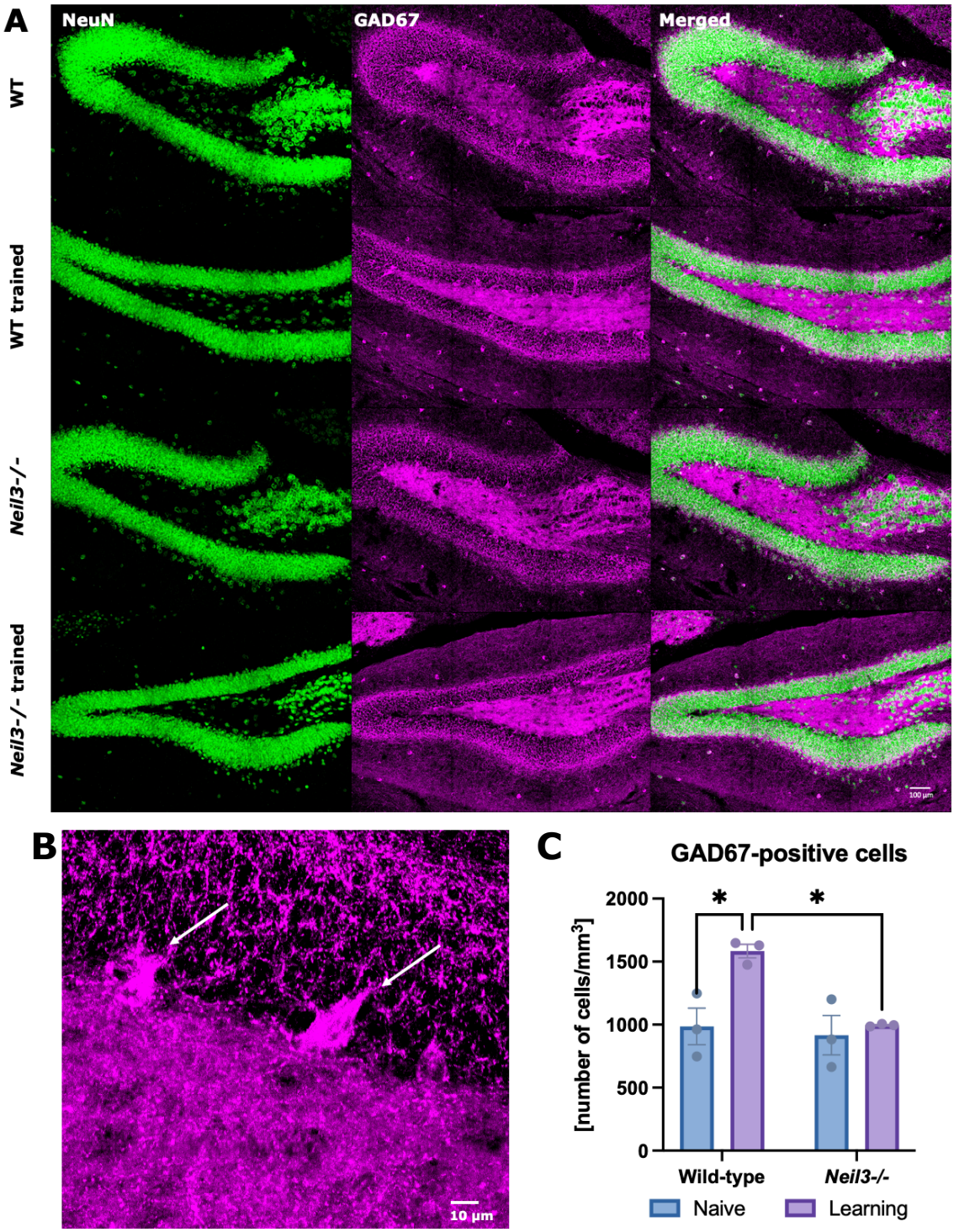

Figure 14: A. *Representative confocal images of immunostained DG samples from naïve WT (top), trained WT, naïve Neil3-/- and trained Neil3-/- (bottom). Each image is represented from left to right: NeuN (green), GAD67 (magenta) and both channels merged together. The samples were scanned with Zeiss LSM880 using a Plan-Achromat 40x/NA 1.3 oil immersion objective (Z stack (28), tile (2x3)). Each image is further processed with ImageJ (Fiji v1.53) to obtain a maximum intensity z-stack projection (n(z stacks) = 25). Scale bar 100 µm.* ***B.*** *A representative image of GAD67+ cells counted with Imaris 9.4. The image is obtained similar as described above. Scale bar 10 µm.* ***C.*** *Number GAD67+ cells/mm^3 in the granular zone of the DG in naïve WT, trained WT, naïve Neil3-/- and trained Neil3-/- mice. The data was statistically analyzed in GraphPad Prism 9.3.1 using a two-way ANOVA (Tukey) (n(naïve WT/Neil3-/-) = 3, n(trained WT/Neil3-/-) = 3). The error bars indicate SEM and a p-value below p = 0.05 was considered as significant.*

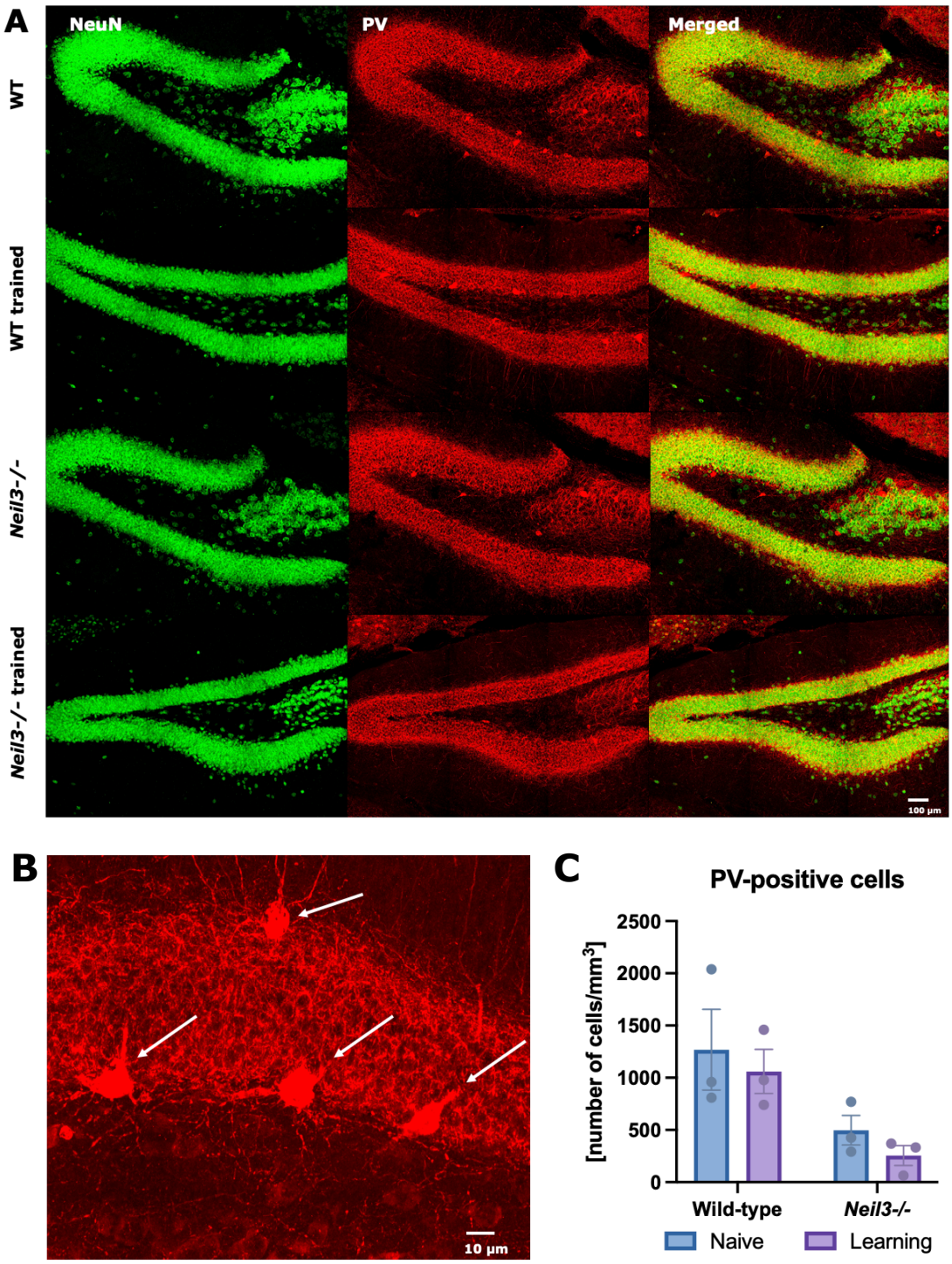

Figure 15: A. *Representative confocal images of immunostained DG samples from naïve WT (top), trained WT, naïve Neil3-/- and trained Neil3-/- (bottom). Each image is represented from left to right: NeuN (green), PV (red) and both channels merged together. The samples were scanned with Zeiss LSM880 using a Plan-Achromat 40x/NA 1.3 oil immersion objective (Z stack (28), tile (2x3)). Each image is further processed with ImageJ (Fiji v1.53) to obtain a maximum intensity z-stack projection (n(z stacks) = 25). Scale bar 100 µm.* ***B.*** *A representative image of PV+ cells counted with Imaris 9.4. The image is obtained similar as described above. Scale bar 10 µm.* ***C.*** *Number PV+ cells/mm^3 in the granular zone of the DG in naïve WT, trained WT, naïve Neil3-/- and trained Neil3-/- mice. The data was statistically analyzed in GraphPad Prism 9.3.1 using a two-way ANOVA (Tukey) (n(naïve WT/Neil3-/-) = 3, n(trained WT/Neil3-/-) = 3). The error bars indicate SEM and a p-value below p = 0.05 was considered as significant.*

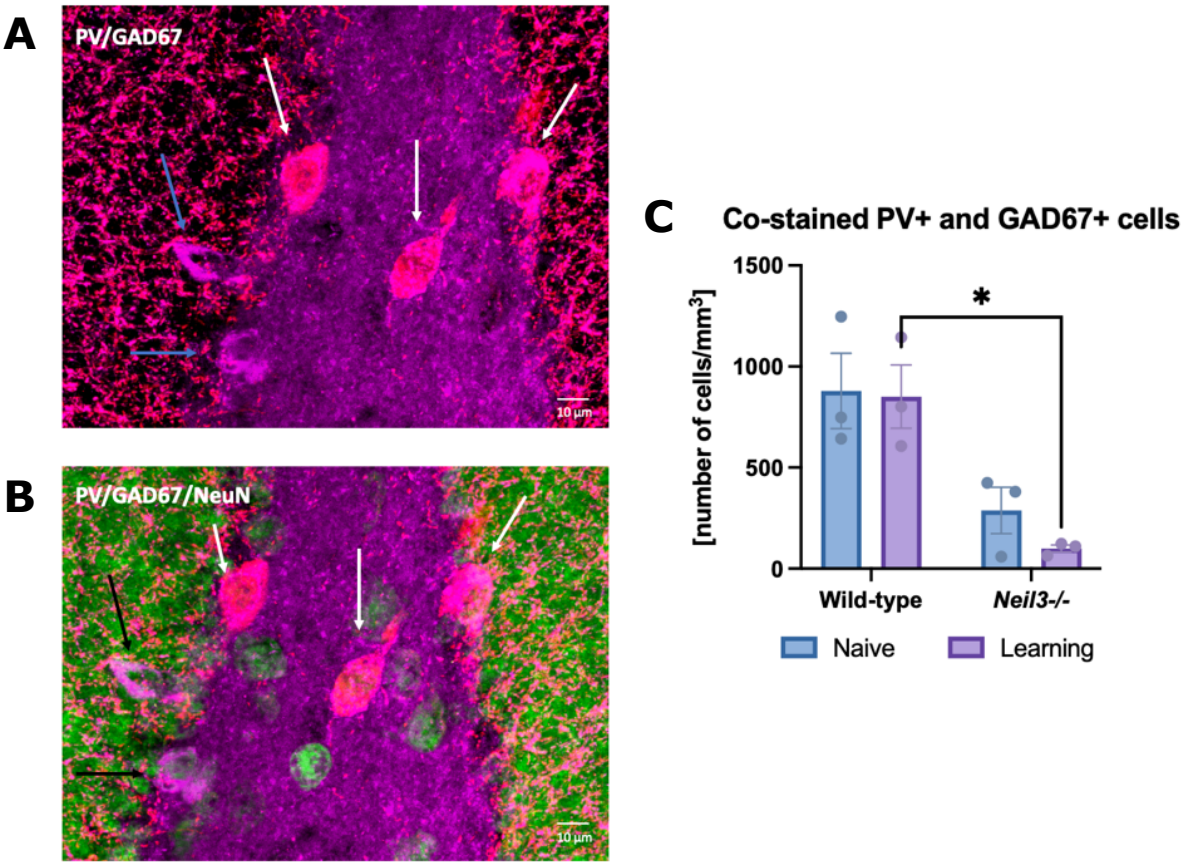

Figure 16: *Representative confocal images of co-stained PV-positive cells and GAD67-positive cells. Scale bar 10 µm. The samples were scanned with Zeiss LSM880 using a Plan-Achromat 40x/NA 1.3 oil immersion objective (Z stack (28), tile (2x3)). Each image is further processed with ImageJ (Fiji v1.53) to obtain a maximum intensity z-stack projection (n(z stacks) = 25).* ***A.*** *A representative image of co-stained PV+ cells (red) and GAD67+ cells (magenta). Co-stained cells are marked with white arrows and single GAD67+ cells are marked with blue arrows.* ***B.*** *A representative image of co-stained PV+ cells (red) and GAD67+ cells (magenta) with NeuN (green). Co-stained cells are marked with white arrows and single GAD67+ cells are marked with black arrows.* ***C.*** *Number of co-stained cells/mm^3 in the granular zone and hilus of the DG in naïve WT, trained WT, naïve Neil3-/- and trained Neil3-/- mice. The data was statistically analyzed in GraphPad Prism 9.3.1 using a two-way ANOVA (Tukey) (n(naïve WT/Neil3-/-) = 3, n(trained WT/Neil3-/-) = 3). The error bars indicate SEM and a p-value below p = 0.05 was considered as significant.*

PV-positive cells were found in the DG granular zone and in the hilus (Figure 15A-B). In WT mice, no difference was observed in the number of PV-positive cells after spatial training (n(naïve WT) = 1268 cells/mm^3, n(trained WT) = 1060 cells/mm^3; p = 0.9217; two-way ANOVA, Tukey; n(naïve WT) = 3 , n(trained WT) = 3) (Figure 15C). The same was detected for NEIL3 deficient mice, with no difference of PV-positive cells after spatial training (n(naïve *Neil3-/-*) = 497 cells/mm^3, n(trained *Neil3-/-*) = 255 cells/mm^3; p = 0.8854; wo-way ANOVA, Tukey; n(naïve *Neil3-/-*) = 3 , n(trained *Neil3-/-*) = 3) (Figure 15C). Further, no significant difference between the genotypes (naïve mice, p = 0.1755; mice after spatial learning p = 0.1532; two-way ANOVA (Tukey)) was detected (Figure 15C). However, a tendency of reduced number of PV-positive cells in mice lacking NEIL3 was detected, compared to the WT.

To analyze the group of PV-positive GABAergic interneurons, I counted the number of PV cells that co-stained with the GABA-synthesizing marker GAD67. As expected, 22.3 % (lower percentage) of PV-positive cells co-stained with GAD67-positive cells when comparing genotypes (Figure 16A-B). In WT, no difference in number of co-stained cells was detected after spatial training (n(naïve WT) = 879 cells/mm^3), n(trained WT) = 851 cells/mm^3; p = 0.9987, two-way ANOVA (Tukey); n(naïve WT) = 3 , n(trained WT) = 3) (Figure 16C). However, NEIL3-deficient mice displayed an insignificant tendency of decreased number of co-stained cells after learning (n(naïve *Neil3-/-*) = 288 cells/mm^3, n(trained *Neil3-/-*) = 99 cells/mm^3; p = 0.7605, two-way ANOVA (Tukey); n(naïve *Neil3-/-*) = 3 , n(trained *Neil3-/-*) = 3) (Figure 16C). Interestingly, a significant difference was observed between WT and NEIL3-depleted mice after spatial training (p = 0.0182, two-way ANOVA (Tukey)) (Figure 16C). No significant difference between the naïve genotypes (p = 0.0581, two-way ANOVA (Tukey) was detected. In general, a reduced number of co-stained cells (PV-positive and GAD67-positive) is found in the NEIL3-depleted DG.

In summary, these results demonstrate that NEIL3-deficient DG contains a reduced number of GAD67-positive/PV-positive interneurons, and the detected spatial-training induced activation of GABAergic neurons is not detected in the group of PV neurons. Taken together, these results suggest that NEIL3 may impact the activation of GABAergic interneurons and the regulation of PV-positive cells in the DG network.

4.4 Assessing possible spatial experience induced synaptic changes in *Neil3-/-* mice

4.4.1 Measuring the size of the infrapyramidal mossy fiber bundle

Mossy fibers are, as earlier mentioned (section 1.3.1), the synaptic connections between the DG and the CA3.[124] The mossy fiber bundle are separated in two tracts named the infrapyramidal mossy fiber (IMF) tract and the suprapyramidal mossy fiber (SMF) tract. The IMF tract is located below the pyramidal cell layer, while the SMF tract lies above the pyramidal cell layer.[47] New born granule cell axons preferentially contribute to the IMF tract and IMF chances dynamically in response to extrinsic and intrinsic stimuli.[125] On the other hand, the SMFs are larger and more stable than the IMFs.[125]

Several behavioral studies have revealed that the size of the IMF tract correlates positively with performance in spatial learning tasks.[125-127] I aimed to explore whether NEIL3 affects the size of the IMF bundle after spatial learning. To achieve this, I performed IHC with antibodies against calbindin to visualize the IMF bundle and its volume is measured by 3D-image analysis.

Calbindin is expressed in axons and dendritic spines, and can be used as a marker to visualize the mossy fiber bundle.[128] Frozen brain sections of WT and *Neil3-/-* mice (3-months-old) with and without spatial training was analyzed by IHC using antibodies against calbindin. The hippocampal CA3 was imaged by confocal fluorescence microscopy (Zeiss LSM880, Z-stack (25), tile (3x3)) and the volume of the IMF bundle were measured using the 3D-image analysis software Imaris 9.4. The definition of the IMF can be found in section 3.11, Figure 8.

Calbindin stained positive on the mossy fiber bundle as expected (Figure 17A). In WT mice, no difference in the IMF volume was detected after spatial learning (IMF volume as % of CA3 volume; naïve WT = 11.9 %, trained WT = 11.7 %; p = 0.9999; two-way ANOVA, Tukey; n(naïve WT) = 3, n(trained WT) = 5) (IMF volume as % of MF volume; naïve WT = 34.2 %, trained WT = 35.6 %; p = 0.9778; two-way ANOVA, Tukey; n(naïve WT) = 3, n(trained WT) = 5) (Figure 17B, 17D). This was also observed for the total mossy fiber (MF) volume (MF volume as % of CA3 volume; naïve WT = 34.3 %, trained WT = 32.9 %; p = 0.9855; two-way ANOVA, Tukey; n(naïve WT) = 3 , n(trained WT) = 5) (Figure 17C). The same observations were done for NEIL3 deficient mice, with no difference in IMF volume (IMF volume as % of CA3 volume; naïve *Neil3-/-* = 12.8 %, trained *Neil3-/-* = 12.6 %; p = 0.9991; wo-way ANOVA, Tukey; n(naïve *Neil3-/-*) = 3 , n(trained *Neil3-/-*) = 5) (IMF volume as % of MF volume; naïve *Neil3-/-* = 39.3 %, trained *Neil3-/-* = 36.8 %; p = 0.8912; wo-way ANOVA, Tukey; n(naïve *Neil3-/-*) = 3 , n(trained *Neil3-/-*) = 5) (Figure 17B, 17D) and total MF volume (MF volume as % of CA3 volume; naïve *Neil3-/-* = 32.6 %, trained *Neil3-/-* = 34.5 %; p = 0.9656; two-way ANOVA, Tukey; n(naïve *Neil3-/-*) = 3, n(trained *Neil3-/-*) = 5) (Figure 17C). No significant difference between the genotypes was detected in the IMF volume compared to CA3 volume (naïve mice, p = 0.9564; mice after spatial learning p = 0.9364; two-way ANOVA (Tukey)) or IMF volume compared to MF volume (naïve mice, p = 0.5829; mice after spatial learning p = 0.9784; two-way ANOVA (Tukey)) (Figure 17B, 17D). Following, total MF volume showed no difference between the genotypes (naïve mice, p = 0.9795; mice after spatial learning p = 0.9666;

two-way ANOVA (Tukey)) (Figure 17C). To summarize, these results suggest that NEIL3 have no effect on the regulation of the IMF volume after spatial learning.

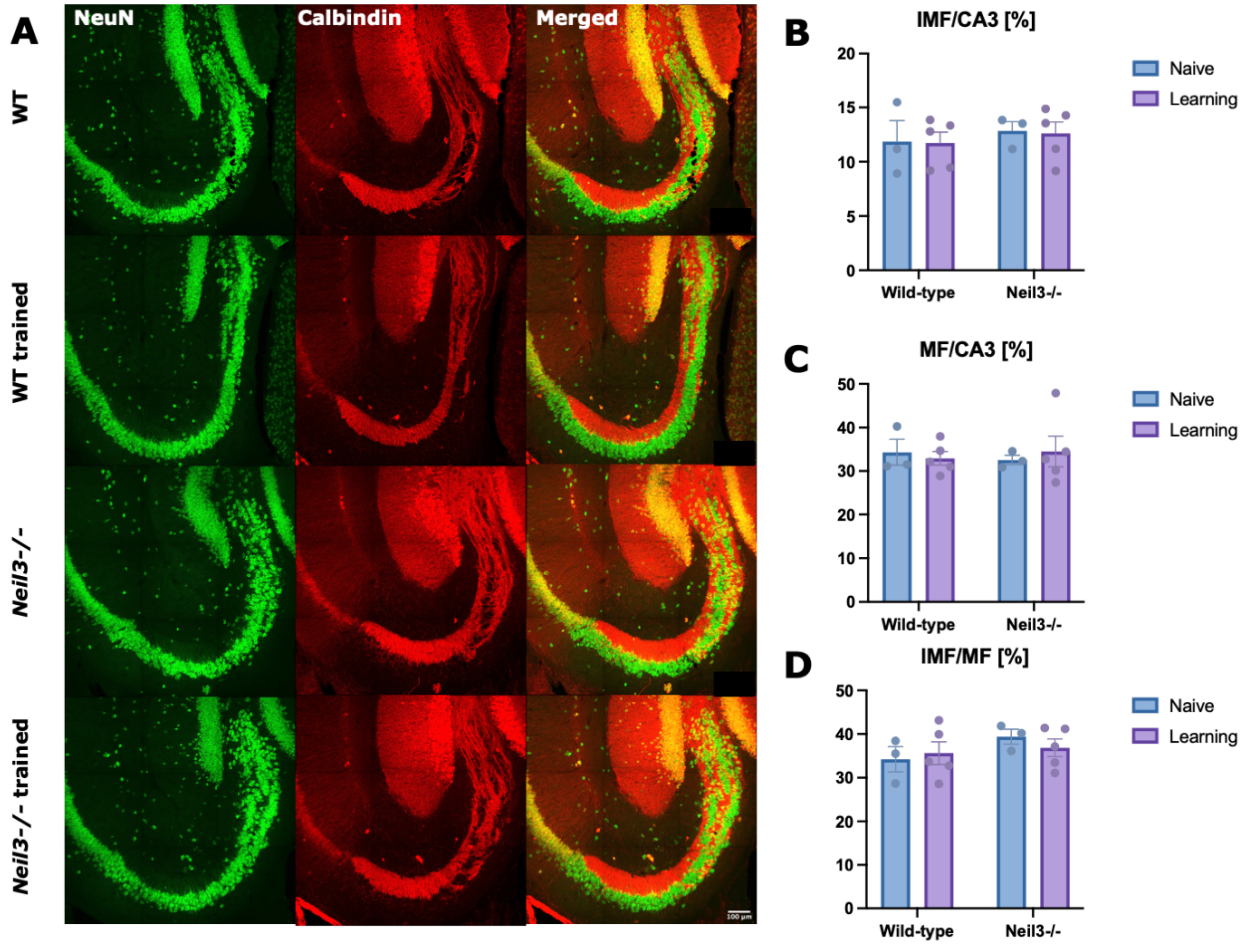

Figure 17: A. *Representative confocal images of immunostained CA3 samples from naïve WT (top), trained WT, naïve Neil3-/- and trained Neil3-/- (bottom). Each image is represented from left to right: NeuN (green), Calbindin (red) and both channels merged together. The samples were scanned with Zeiss LSM880 using a Plan-Achromat 40x/NA 1.3 oil immersion objective (Z stack (25), tile (3x3)). Each image is further processed with ImageJ (Fiji v1.53). to obtain a maximum intensity z-stack projection (n(z stacks) = 25). Scale bar 100 μm.* ***B.*** *The volume of infrapyramidal mossy fibers given as a percentage of the total CA3 volume in naïve WT, trained WT, naïve Neil3-/- and trained Neil3-/- mice.* ***C.*** *The volume of both infrapyramidal and suprapyramidal mossy fibers given as a percentage of the total CA3 volume in naïve WT, trained WT, naïve Neil3-/- and trained Neil3-/- mice.* ***D.*** *The volume of infrapyramidal mossy fibers given as a percentage of the total mossy fiber volume (infrapyramidal + suprapyramidal) in naïve WT, trained WT, naïve Neil3-/- and trained Neil3-/- mice. The data for figure B, C and D was statistically analyzed in GraphPad Prism 9.3.1 using a two-way ANOVA (Tukey) (n(naïve WT/Neil3-/-) = 3, n(trained WT/Neil3-/-) = 5). The error bars indicate SEM and a p-value below p = 0.05 was considered as significant.*

4.5 Exploring the impact of NEIL3 in embryonic hippocampal development

4.5.1 Genotyping

A heterozygous breeding of *Neil3+/-* mice was established to obtain WT and *Neil3-/-* mice from the same parents. The embryos were successfully collected at different timepoints, E13.5 and E18.5, and postnatal brains at P2. Embryonic brains were extracted and fixed in PFA (4 %) and the tail samples were collected for genotyping (see method section 3.5). The PCR results (Figure 18) show that the samples with a DNA amplification at 160bp are *Neil3-/-* mice, the ones with a DNA amplification at 260bp are WT mice, and the ones that contain both bands are heterozygous mice (*Neil3+/-*). These results show that WT and *Neil3-/-* mice was successfully obtained from the same parents with exactly same birth date.

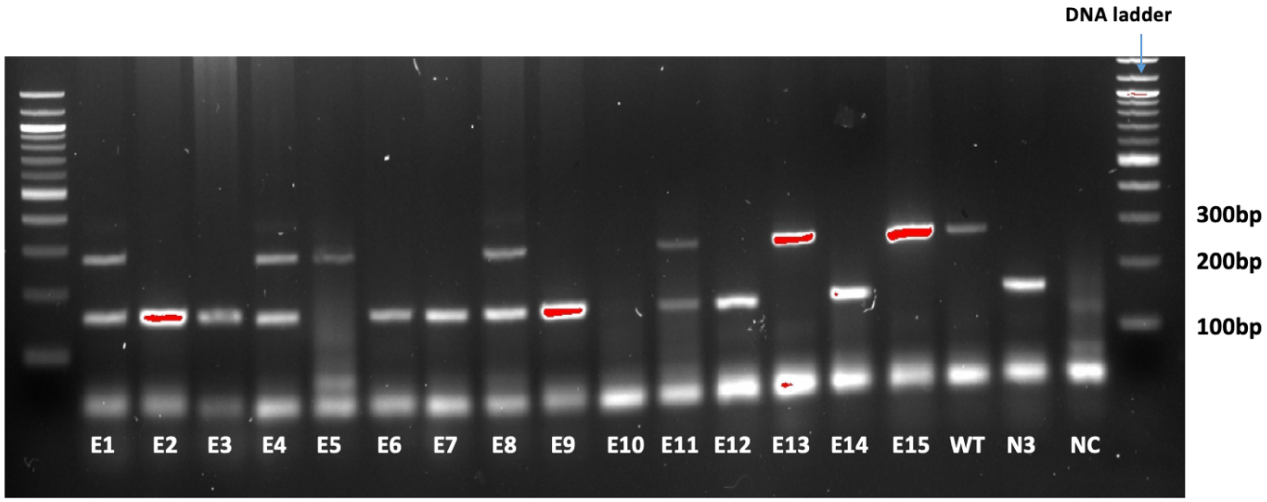

Figure 18: *Image of an agarose gel with PCR samples from different E18.5 mouse embryonic DNA samples.* The amplification with primer pair (section 3.5, table 3.5) gives *a specific band at 160bp for Neil3-/- samples and a specific band at 260bp for WT samples. The samples that show bands at both 160bp and 260bp are the heterozygous ones Neil3-/+. From left: 1, DNA ladder; E1-E15 PCR samples from different embryonic DNA samples; N3, Neil3-/- standard; WT, WT standard; NC, negative control (water with primers).*

4.5.2 Impact of NEIL3 in embryonic hippocampal development

Studies have revealed that there is a discrete expression pattern of NEIL3 in the SGZ and the SVZ in mice during embryonic development[28], suggesting that NEIL3 is present in NSPCs and a has role in embryonic neurogenesis.[29] Following, NEIL3 is found to be highly expressed at the same time neurogenesis is initiated in mice, which strengthen the evidence that NEIL3 is important for hippocampal development.[31] I aimed to investigate the role of NEIL3 in hippocampal development in mice by collecting embryos at different developmental stages and performing IHC with different cellular markers. Unfortunately, only a trial experiment to test the methodology was performed due to limited time.

The genotype was determined as described (section 3.5) and the brain was extracted from the embryo under a microscope. Further, the brain was embedded in paraffin and sectioned at the Histology Core. The paraffin embedded brain sections were analyzed with IHC using antibodies against Ki67, Sox2 and NeuN. Finally, one of the embryonic brains was imaged with Axioscan by María Cámara Quílez.

Sox2 is a marker for NSCs, and expressed in neuroepithelial cells and embryonic stem cells during development.[129] Therefore, it can be used as a marker for embryonic stem cells. Ki67 is a marker for proliferating cells as described in section 4.1.1. Co-staining of Ki67 and Sox2 often occurs, and is a measure of proliferating NSCs.[129] Further, NeuN is a neuron and nervous-system specific nuclear protein expressed in mature neurons.[130] Thus, NeuN is widely used as a marker for mature neurons.

The staining of the paraffin-embedded brain sections with different cellular markers was successful and Axioscan clearly visualized the embryonic brain (Figure 19A). The structure correlated well with the example image obtained from the Allen Brain Atlas (Figure 19B). As expected[74], embryonic stem cells were positively labeled for Sox2 in the ventricular zone (Figure 19-21). Ki67-positive proliferating NSCs were detected in the ventricular zone, but also in the developing CA region, which is according to the literature.[72](Figure 20-21) Further, only a few mature neurons were found to be located around the CA region. A strong staining of Sox2-positive cells were observed around the developing DG. However, the staining for Ki67 was weaker in this region.(Figure 20-21) It was expected to not see the characteristic DG structure at this time, because the granular cell layer of the DG starts to form at P0.[83] In DG development, the NSCs migrate from the VZ to the hippocampal fissure and forms a pool of NSCs, called the tertiary matrix.[72] This correlates well with these results (Figure 20).

In summary, I obtained WT and Neil3-/- embryonic (E13.5 and E18.5) and P2 brain samples from a heterozygous breeder. Immunohistochemistry with paraffin embedded brain sections is tested in a pilot experiment. Further studies using samples from *Neil3-/-* and WT mice should be continued to investigate the role of NEIL3 in hippocampal development from embryonic to postnatal stages.

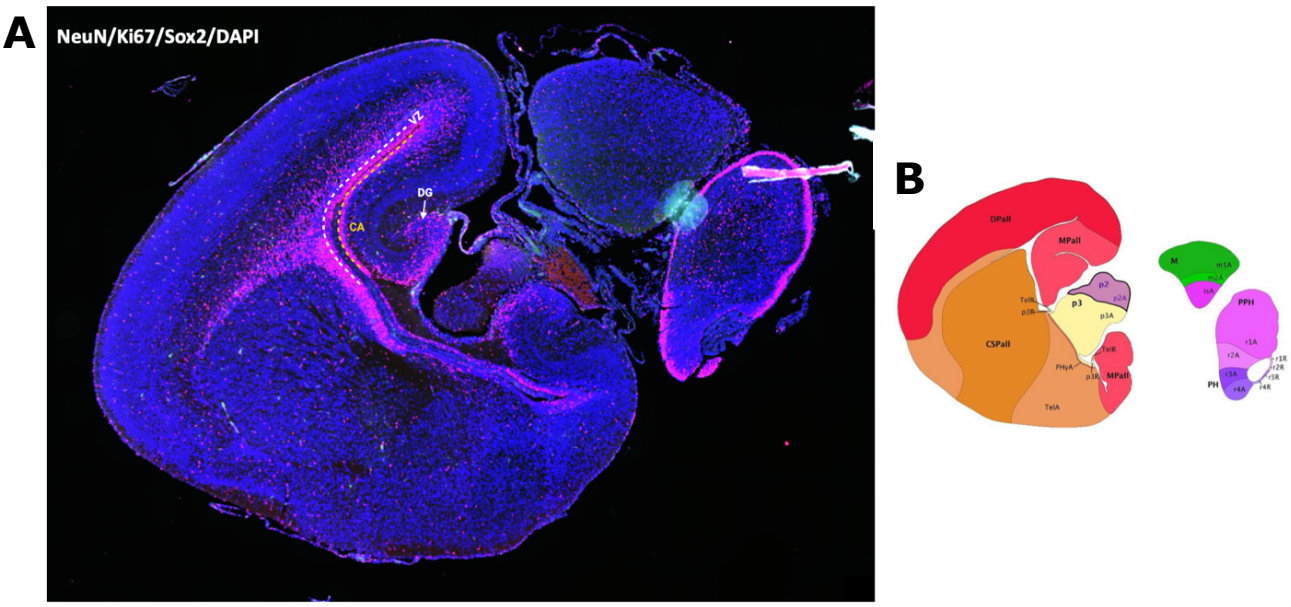

Figure 19: A. *Representative image of the developing mouse brain at E18.5. The ventricular zone, developing CA region and developing DG is marked in the figure. The image is obtained with Axioscan Z1 (Carl Zeiss, Jena, Germany) by María Cámara Quílez.* ***B.*** *Representative image of the developing mouse brain at E18.5 obtained from Allen Brain Atlas. Mpall = Medial Pallium, VZ = Ventricular Zone, DG = Dentate Gyrus.*

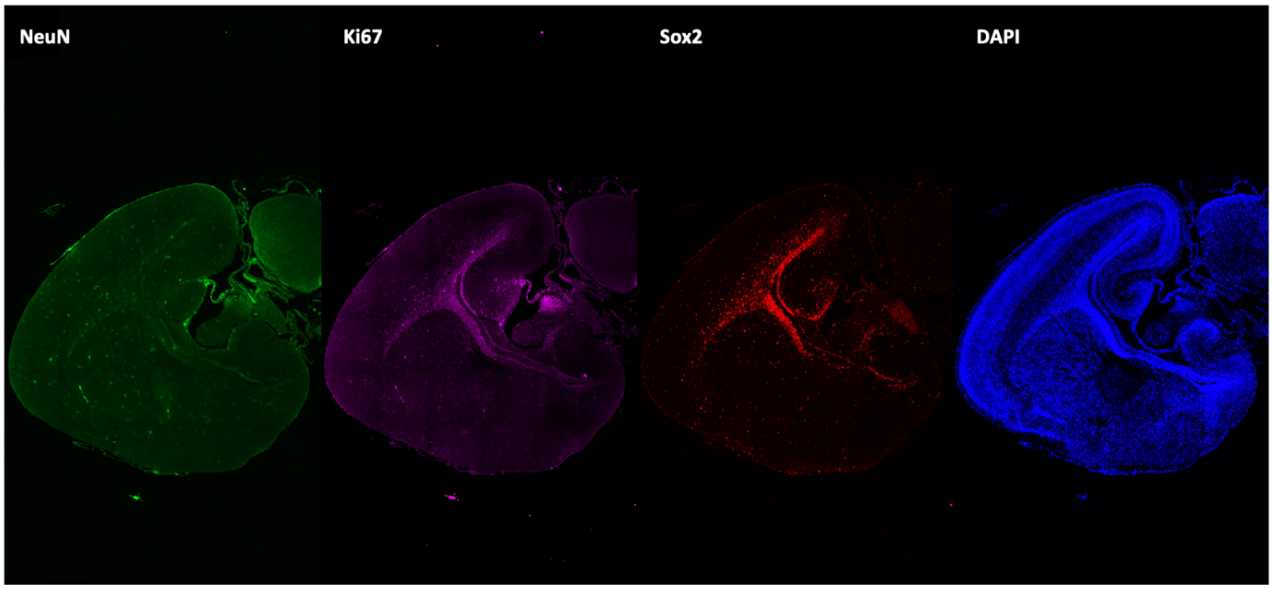

Figure 20: *Representative images of the developing brain in E18.5 mouse. Each image is represented from left to right: NeuN (green), Ki67 (magenta), Sox2 (red) and DAPI (blue). The image is obtained with Axioscan Z1 (Carl Zeiss, Jena, Germany) by María Cámara Quílez.*

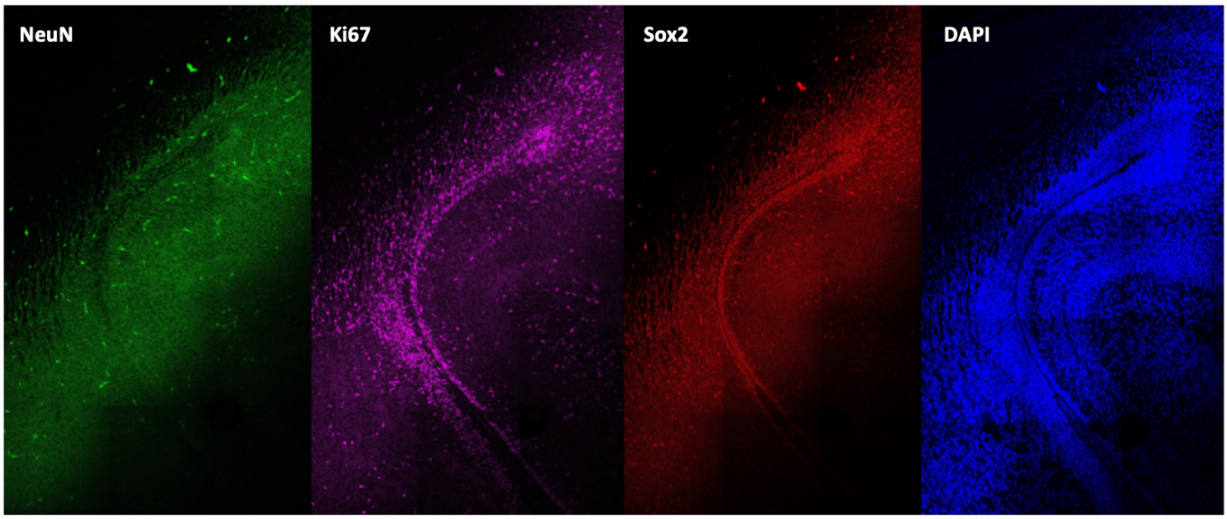

Figure 21: *Representative confocal images of the ventricular zone and developing CA region in E18.5 mouse. Each image is represented from left to right: NeuN (green), Ki67 (magenta), Sox2 (red) and DAPI (blue). The samples were scanned with Zeiss LSM880 using a Plan-Achromat 40x/NA 1.3 oil immersion objective (Z stack (30), tile (4x5)).*

5 Discussion

5.1 Main findings

As stated in the abstract, this project aimed to investigate the functional role of NEIL3 associated with hippocampal-dependent spatial learning and memory, with a special focus on the dentate gyrus. This was achieved by investigating the role of NEIL3 in learning-induced adult neurogenesis, expression of immediate early genes, activation of inhibitory interneurons and the volume changes in infrapyramidal mossy fiber bundles. Immunohistochemistry studies with detection of different cellular markers were performed using sagittal brain sections from naïve wildtype (WT) and *Neil3-/-* mice as well as the ones after spatial training. The samples were visualized with confocal imaging and analyzed in the 3D software Imaris. In addition, mouse embryos at different developmental stages were collected to study the function of NEIL3 in embryonic hippocampal development. However, due to limited time, only a trial experiment to test the methodology was performed.

The main finding in this project are: (1) Spatial experience-associated adult neurogenesis is increased in wildtype mice but displays a tendency to be impaired in mice lacking NEIL3. (2) Spatial experience-induced expression of immediate early genes in the hippocampal DG is impaired in NEIL3-deficient mice. (3) Inhibitory GABAergic interneurons are activated in response to spatial training in WT mice, but such activation is impaired in NEIL3-depleted mice. (4) NEIL3 has no effect on regulation of the infrapyramidal mossy fiber volume after spatial training. (5) I obtained WT and *Neil3-/-* embryos (E13.5 and E18.5) from a heterozygous breeder and immunohistochemistry with paraffin embedded brain sections is tested in a pilot experiment.

In summary, my results indicate that NEIL3 plays an important role in functions in the dentate gyrus associated with spatial learning and memory.

5.2 Methodological considerations

The main concern regarding this study is the low sample size (n(WT) = 3, n(*Neil3-/-*) = 3-5). Some of the samples had to be excluded due to bad quality, however each analysis included at least three animals. A small sample size gives a lower statistical power and might lead to invalid conclusions. In addition, a high SEM was observed in some of the analyses, especially for PV-positive cells. Therefore, the results should be interpreted with caution. In the future, a larger sample size should be used to see whether the trends observed in this project gain statistical significance with a larger sample size, and if the statistically significant results obtained here give similar outcome with a larger sample size.

There are however some other limitations of this study. Some of the samples, especially from c-fos and Arc stainings, had a high background signal and weak staining of the desired cells. In addition, the spots tool was found to quite often detect artifacts and the analysis had to be checked manually by counting each positive cell. Therefore, the analysis was highly subjective. Although the analysis was checked by another member of the research group to minimize bias, the risk of counting artifacts or missing cells cannot be excluded. Further, a limitation could have been different perfusion qualities and different exposure times in fixative agent, which could have affected the staining quality and the latter may have affected the binding of the antibodies.

5.3 Spatial experience-induced adult neurogenesis displays a tendency to be impaired in NEIL3-depleted DG

Adult neurogenesis is known to play an important role in spatial learning and memory[93, 96, 131], and inhibition of it is shown to impair hippocampal memory and learning.[35] During adult neurogenesis, NSCs proliferate and become immature neurons that migrate from the SGZ to the GCL where they differentiate and mature into granule neurons (section 1.4.2). NEIL3 is shown to play a role in adult neurogenesis.[20, 28], and found to be expressed in neurogenic niches in juvenile mice.[28] Further, NEIL3-deficient mice show impaired performance in the MWM.[20]

I aimed to see if NEIL3 has a role in adult neurogenesis associated with spatial learning and memory. This was done by investigating whether NEIL3 affected neuronal proliferation after spatial learning by quantifying the number of Ki67-positive proliferating neurons. Further, immature neurons express DCX, and the DCX expression level was quantified, where a higher expression level is associated with a higher number of immature neurons. I hypothesized that if NEIL3 have a role in adult neurogenesis associated with spatial training, the results would reflect a lower number of proliferating neurons and reduced DCX expression in the DG in the NEIL3-depleted animals compared to the controls after training.

5.3.1 Ki67-positive proliferating cells

As expected, the number of proliferating neurons in the DG showed a tendency to increase in WT mice after spatial training, which is according to the literature.[132] However, no difference was observed in NEIL3-depleted mice, indicating a tendency of impaired spatial experience-induced adult neurogenesis in the DG. Contrary to my assumptions, no statistically significant difference was seen between the genotypes neither in naïve or trained animals, although there is a tendency of a lower number of proliferating cells in the NEIL3-deficient DG compared to the WT after training. Regnell et al.[20] observed impaired proliferation of NSPCs derived from adult SVZ *Neil3-/-* mice brains compared to WT, indicating a lower number for adult-born DG granular neurons. Thus, a bold assumption would be to expect that the number of proliferating cells should be lower in naïve NEIL3-depleted animals compared to the naïve controls. NEIL3-deficient mice are shown to have impaired performance in spatial learning tasks. If this is due to impaired adult neurogenesis, a larger difference between the genotypes after training would be expected. However, the absent increase in proliferating neurons in NEIL3-depleted mice after training indicates that spatial experience-induced adult neurogenesis is impaired.

One possible explanation for the insignificant differences between the genotypes in both naïve and learned animals could be that the use of Ki67 as a proliferating neuron marker have masked the differences between the genotypes. Ki67 is a protein marker, expressed in all steps in the cell cycle except G0,[105] which only labels cells positive for that protein. Thus, it is impossible to determine whether the Ki67-positive proliferating NSCs are actually actively proliferating or in cell cycle arrest, which may have caused staining of inactive cells. A suggestion is to further investigate this by using another marker, like BrdU, which incorporates into newly synthesized DNA and actively replicating cells can be detected.[133] Recently obtained data from our groups' collaborators[134] show that NEIL3-deficiency causes reduced cell proliferation. Interestingly, they used BrdU labelling, suggesting that the differences may could be seen by using another marker like BrdU.

Another explanation could be that the time between training and termination of the animals is too long. The animals were sacrificed 24 hours after ended training. This may be enough time for the learning-induced proliferating cells to differentiate into immature/mature neurons, which no longer express Ki67. Then the number of these proliferating neurons would be lower than it was right after training in WT, but the number of the same cells in NEIL3-depleted mice would stay the same if the cell proliferation was impaired without NEIL3. Gould et al.[93] reported that number of proliferating cells in the DG did not change after spatial training in the MWM when BrdU was injected during training and the animals were killed 24 hours post-training. However, they observed a significant increase in immature and mature neurons in the DG after training when the injection was done 1 week prior to the learning procedure, indicating enhanced adult neurogenesis associated with spatial learning. This also indicates that the time the animals are sacrificed may affect the result. Dupret et al.[135] reported significantly higher number of Ki67-positive cells in MWM-trained animals compared to control animals. Interestingly, these animals were sacrificed 3 hours post-training. However, it is important to mention that Gould et al. and Dupret et al. used rats, and comparison should be done with caution due to species-specific features.[136] Nonetheless, a suggestion would be to further investigate this potential time-dependent factor by modifying the protocol with a smaller window between training and sacrificing, to see whether the differences are more pronounced.

In summary, these results indicate that there is a tendency of impaired spatial experience-induced adult neurogenesis in the NEIL3-depleted DG. However, there are some limitations in this study related to the methodology (section 5.2) which may have affected the results. Therefore, the results should be interpreted with caution.

5.3.2 DCX expression level in immature neurons

Contrary to my assumptions, a tendency of lower DCX expression level in immature neurons in the DG was observed in WT mice after spatial training. This is in conflict with previous studies that observed increased expression of markers for immature neurons after spatial exploration.[93] However, this study used BrdU and TOAD64 as a markers and counted cells individually, which may be a more precise method for assessing immature neurons. Subsequently, no difference was observed between naïve and trained NEIL3-deficient mice, suggesting that the levels of DCX-expressing immature neurons is the same after training as before. This would indicate that spatial experience-induced adult neurogenesis may be impaired. However, the DCX-expression level in the control animals was not as expected, and the results should be interpreted with caution. Further, there was a statistically significant difference between the genotypes after training, with a notably lower DCX-expression in the WT compared to NEIL3-depleted animals. This indicates a higher level of DCX-expressing immature neurons in trained NEIL-deficient animals compared to the trained WT animals.

One explanation of the results could be a delayed maturation of neurons in *Neil3-/-* DG. Interestingly, a delayed maturation of CA1 neurons in NEIL3-deficient brains was recently observed by Kunath et al.[27] This may also be the case for the DG. A slower maturation rate in NEIL3-depleted DG would cause a higher expression of DCX in the DG immature neurons following a spatial experience, compared to WT. This would also explain the decrease in DCX expression in WT after spatial training, because the immature neurons have already started to become mature neurons. Mature neurons do not express DCX[137], which would cause a lower number of DCX-expressing neurons in WT.

Subsequently, higher hippocampal network activity is associated with a higher maturation rate.[138] Therefore, the significant higher levels of DCX-expression in NEIL3-deficient animals could may be explained by impaired DG network activity, which also correlates well with the observed impaired spatial performance in NEIL3-deficient mice.[20] However, this is highly suggestive and should be further investigated.

In the Imaris image-analysis, images of the samples obtained with confocal fluorescence microscopy showed that both genotypes had dendrites stretching from the GCL to the MCL both before and after spatial learning, indicating a later maturation stage of the immature neurons.[137] However, the expression level was lower and the signal was more absent in WT dendrites, which might suggest that these cells no longer express DCX. This would further support the abovementioned theory about a slower maturation rate in NEIL3-depleted animals.

However, the main concern regarding the study of DCX-expression levels is the method of analysis. The DCX signal was very strong in the SGZ in all samples and appeared as clusters more than separate cells. This made an individual cell counting impossible due to the difficulties of separating them. Therefore, the DCX signal had to be calculated as a voxel

ratio representing the expression level instead of the number of positive cells. The 3.5xmean intensity threshold for detecting DCX signal was determined based on a subjective analysis, which could have affected the result. In addition, the changing cell morphology was not considered. DCX-expressing cells are shown to change morphology as they mature. First, they form large clusters both with and without defined processes.[137] When they begin to mature, they begin to develop dendrites stretching from the GCL to the MCL. The dendrites in all samples displayed a weaker staining intensity than the cell bodies, and the 3.5xmean intensity threshold used for detecting DCX signal may not have included the DCX signal in the dendrites. Further, dendrites in the MCL were not included in the analysis. These factors could have a negative effect on the results because they are volume-based and represented as a voxel ratio.

5.3.3 Ki67 and DCX

In summary, the number of Ki67-expressing proliferating cells and level of DCX-expression correlate well in NEIL3-deficient mice between naïve and learning. No difference is observed, suggesting a tendency of impaired spatial experience-induced neurogenesis. However, this is not the case for the WT mice. As expected, an increase in number of proliferating cells was observed after learning in WT mice, but an insignificant decrease in DCX-expression level was observed in the same mice. This indicates an increase in adult neurogenesis following a spatial experience, but a reduced DCX-expression from immature neurons. However, this may be explained by a rapid maturation of the neurons, but this is only suggestive and the results obtained from the DCX analysis should be interpreted with caution.

Further, a significant decrease in DCX expression level was observed between the genotypes after training, while an insignificant higher number of proliferating cells were detected between them after training. In WT, this indicates increased proliferation following spatial training, but a lower number of DCX-expressing immature neurons after training. This may indicate that in WT, some of the cells have already matured into neurons, which further may indicate a slower maturation rate in NEIL3-depleted animals. The higher levels of Ki67-expressing proliferating cells detected in WT compared to NEIL3-deficent mice after training, suggest a tendency of impaired spatial experience induced adult neurogenesis.

Taken together, the suggestion that NEIL3 plays a role in adult neurogenesis associated with spatial training cannot be excluded, but neither confirmed. Although there is a tendency of impaired adult neurogenesis in NEIL3-depleted mice after spatial training, further investigations with improved method of analysis for DCX-expression and a larger sample size should be done before any conclusions can be made. One interesting approach for further studies could be to look more into the impact on NEIL3 on the neuronal maturation in the DG, as my results may indicate a slower maturation rate in NEIL3-depleted animals. In addition, another suggestion could be to shorten the time window between learning and termination of the animals, and use another marker like BrdU, to see whether the differences in cell proliferation is more pronounced.

5.4 NEIL3 modulates spatial experience induced expression of IEGs in DG granular neurons

As earlier established, learning and behavioral experiences is associated with upregulated expression of IEGs, such as *c-fos*[97] and *Arc*[98], and play a critical role in regulating synaptic plasticity and formation of long term memory.[98, 111-113] Upregulation of IEGs following a spatial experience is also shown particularly for the DG.[97, 98] Further, IEGs have been identified as cellular representations in neuronal ensembles of the memory trace/engram.[139]

I hypothesized that if NEIL3 modulates expression of IEGs, a lower expression would be detected in NEIL3-depleted mice after spatial training. By using IHC with IEG protein markers Arc and c-fos before performing a 3D image analysis, I found that spatial experience induced expression of Arc and c-fos was increased in WT DG, which is according to literature.[97, 98] Strikingly, this spatial experience-induced IEG expression was significantly impaired in the NEIL3-depleted DG. Although there is no statistically significant difference between the genotypes in number of Arc-positive cells after spatial training, there is a strong tendency of lower Arc-expressing cells in the NEIL3-deficient mice. These results are similar to previous findings, where the same was seen in hippocampal CA1 neurons in NEIL3-depleted mice.[27] IEGs are as earlier mentioned expressed during spatial experience-induced neuronal activity. These results indicate that NEIL3-depleted mice display impaired neuronal activity in the DG after a spatial experience compared to WT mice, because the spatial experience-induced expression of IEGs is impaired in the NEIL3-depleted DG. Further, recent studies have shown that IEG-expressing neurons encode and store information required for memory recall, indicating that they may be involved in memory trace formation.[139] With this considered, my results would implicate that NEIL3 may plays a role in spatial experience-induced expression of IEGs and maintenance of IEG-dependent neuronal ensembles for long-term memory.

Several studies have reported a high IEG response in the DG right after animals have been exposed to a spatial experience.[98, 140] Moreover, all of them have observed a notably decrease in the hours following the experience, which is rather striking given that the expression of IEGs in my animals was still found to be of statistical significance even after 24 hours, suggesting that there is an additional wave of IEG expression in these animals.

However, Kunath et al. found a highly statistically significant difference between WT and NEIL3-depleted mice, with a massive increase in spatial experience-induced IEG-expression in the WT CA1 neurons, but this increase was found to be absent in NEIL3-depleted CA1 neurons. These animals were sacrificed 40 minutes after training. A suggestion for further studies of the role of NEIL3 in spatial experience-induced IEG expression could be to shorten the time between training and termination of the animals, to see whether the differences between WT and NEIL3-deficient mice are even more pronounced.

There are, however, some limitations with this study. The cell counting in the 3D software Imaris is a highly subjective analysis. In addition, there was a high background staining that complicated the cell counting. Further, several artifacts were detected in these images, and it is possible that some of them are included unintendedly affecting the result.

However, the main concern is the low sample size, and the results should therefore be interpreted with caution.

In summary, these results strongly suggest that NEIL3 has a role in regulating spatial experience induced expression of IEGs. However, due to small sample size and methodological issues, the results should be interpreted with caution. A suggestion for future studies could be to increase the sample size and shorten the window between learning termination of animals to investigate the immediate response of spatial-experience induced expression in the DG of IEGs in NEIL3-depleted mice.

5.5 Spatial experience-induced GABAergic interneuron activation displays a tendency to be impaired in NEIL3-deficient DG

The excitation-inhibition balance in the neural circuitry in the hippocampus is thought to be essential for normal functioning of memory and learning and inhibition of GABAergic interneuron activity have been related to impairments spatial learning and memory.[99] Learning is associated with increased GABA content of inhibitory synapses and enhanced synaptic inhibition in mice.[99] Accordingly, it would be interesting to see whether NEIL3 affects this GABA content and activation of GABAergic interneurons associated with spatial training.

The increase of GAD67 levels supports replenishing GABA released after stimulation.[123] The study with GAD67 revealed a higher number of GAD67-positive cells after training compared to naïve in WT animals, indicating a higher spatial experience-induced inhibitory interneuron activation compared to naïve animals.[121] However, the elevated GABAergic interneuron activation in response to spatial learning was not observed in NEIL3-depleted mice. Strikingly, there was a significant difference between the genotypes after spatial training, suggesting that NEIL3 may impact the activation of GABAergic interneurons in response to a spatial experience.

Interestingly, studies have shown that induction of GAD positively correlates with expression of the IEG-marker, c-fos, in response to stress.[123] This is in accordance with my results, where a significant higher spatial-experience induced expression of c-fos and GAD67 was observed. Therefore, it is tempting to speculate that spatial experience-induced stimulation could also increase expression of GAD67 and c-fos. This increased expression was not observed in NEIL3-depleted animals, and this would further strengthen the evidence that NEIL3 plays a role in regulating expression of IEGs and activation of GABAergic interneurons in response to a spatial training.

GAD67 is a widely used marker for GABAergic interneurons[122] and was chosen for this project due to experiences with better staining quality. However, GAD enzyme exist as two isotypes, namely GAD67 and GAD65.[141] Studies have shown that GAD65 knockouts have normal levels of GABA in the brain, suggesting that GAD67 is more abundant and may be sufficient for synthesizing GABA for neurotransmission.[141] However, although DISH-studies have shown that GAD67 and GAD65 are mostly colocalized in the rat DG[141], the same study revealed that GAD65 had a higher expression in the hilus compared to other regions.[141] The same is observed by Houser et al.[142]. A suggestion

for further investigation could be to use GAD65 as a marker for GABAergic interneurons in the mouse granular zone and in the hilus, to see whether the differences are more pronounced.

Subsequently, a balance between glutamatergic and GABAergic synthesis/excitatory and inhibitory activity is necessary for maintaining brain homeostasis and proper functioning of the neural network.[143] Further, inhibition of GABAergic interneurons is shown to impair spatial memory and learning.[99] An interesting approach for further studies would be to investigate this balance between glutamatergic and GABAergic activity to see whether there are any disruptions in the NEIL3-deficient DG.

A high number of different interneurons exists in the mammalian hippocampus, with 21 different subtypes of GABAergic interneurons.[144] It is estimated that 20 % of the inhibitory interneurons in the DG are PV-expressing interneurons.[144] These interneurons seem to be important for hippocampus-dependent learning tasks in rodents.[145, 146] I aimed to see whether NEIL3 affects PV-interneurons specifically, by using IHC with PV as a marker. No difference in number of PV-expressing neurons was seen after spatial training in the genotypes, suggesting no spatial experience-induced activation of these cells specifically. However, there was a notably lower number of PV-expressing neurons in the NEIL3-depleted DG compared to the WT DG, both in naïve and spatial-trained animals, suggesting that NEIL3 may impact the correct functioning/regulation of PV-interneuron activity in the DG. A future approach could be to use a marker for another interneuron subtype, like somatostatin, which also are associated with spatial memory [147], to investigate the role of NEIL3 in activation of these in response to spatial training.

PV-interneurons are shown to be mainly GABAergic.[119] Co-stained cells (PV-positive and GAD67-positive) were quantified to investigate how many of the PV-expressing neurons that were GABAergic. A notably lower number of PV-positive cells expressed GAD67 in NEIL3-depleted mice compared to controls after spatial training. The number of PV-expressing cells in the NEIL3-depleted mice were also notably lower and are in line with the results obtained from the PV analysis. This would further implicate a relationship between NEIL3 and correct functioning of activation of GABAergic interneurons and the regulation of PV-positive cells in the DG network.

Interestingly, cell recordings targeted against PV neurons with GAD67-deficiency has revealed that reduced expression of GAD67 in PV neurons may has a crucial impact on synaptic transmission, and that GAD67 levels directly contribute to the strength of synaptic inhibition.[148] Thus, lack of GAD67 likely contribute to network dysfunction. This correlates well with the observation of impaired spatial performance in MWM in NEIL3-depleted mice.[20] My results reflect a significantly lower expression of GAD67 in PV-expressing cells as well as GAD67-positive cells alone in the NEIL3-depelted DG compared to the WT DG after spatial learning, which would indicate that NEIL3-deficient mice may display network dysfunction due to impaired inhibitory activity by reduced activation of GABAergic interneurons.

In conclusion, these results are particularly interesting and indicate that deficiency of NEIL3 in the DG may results in impaired activation of GABAergic interneurons in response to spatial training and impact the regulation of PV-positive cells in the DG network. I encourage further investigations to be done with a larger sample size in order to unravel the specific functions of NEIL3 related to interneuron activation in association with spatial memory and learning.

5.6 NEIL3 in regulation of the infrapyramidal mossy fiber volume

A larger IMF volume is associated with better performance in spatial learning tasks. [125-127, 149] As earlier mentioned, behavioral studies have shown that NEIL3-depleted mice show impaired performance in the MWM. Therefore, I investigated whether there were any differences in the IMF volume between the genotypes after spatial learning.

No difference was detected in volume of the infrapyramidal mossy fiber bundle in the control animals after learning. This was contrary to what I hypothesized, because neurogenic stimuli, such as enriched environment, have been shown to cause an increase in the IMF volume.[150] Similar, no difference was detected for NEIL3-deficient mice. Finally, no difference was observed between the genotypes neither in naïve nor trained animals. This is contradictory to current literature, where a larger mossy fiber volume is associated with better performance in spatial learning tasks. [125-127, 149] These results suggest that NEIL3 has no role in regulation of the infrapyramidal mossy fiber volume. However, the control did not behave as expected, and it is difficult to draw any conclusions based on these results.

One explanation for the absent difference between WT and NEIL3-deficient mice in IMF volume could be that the spatial experience is not strong enough to induce these changes. Crusio et al.[126] reported a positive correlation between IMF volume and performance in the spatial radial-maze task. Further, they used food rewards as task motivation. The motivation for the task may affect the speed of learning.[151] The training paradigm used on the mice for this thesis did not include any task motivation, which may could explain that the spatial experience is not strong enough to extend the IMF volume.

The infrapyramidal mossy fiber volume alone may be a too simplified approach to assess the connections between the DG and the CA3 region. The infrapyramidal mossy fibers have to be connected to the CA3 in order for them to be functional.[125] This is shown by Römer et al.[125], which labeled immature cells with PSA-NCAM and observed a number of IMF that contributed to the IMF bundle, but was not connected to the CA3. A large infrapyramidal mossy fiber volume is not a relevant measurement if the fibers are not connected to the CA3. This was not considered in this analysis and may have affected the result. For future investigations, a suggestion would be to assess whether the infrapyramidal mossy fibers are connected and exclude the ones that are not.

Evidence suggest that there is a link between increase in infrapyramidal mossy fiber volume and adult neurogenesis.[125] Newly generated neurons preferentially contribute to the infrapyramidal mossy fiber bundle. One explanation for the absent increase in infrapyramidal mossy fiber volume could be that the new neurons had not yet extended their axons towards the CA3. Römer et al.[125] found that seizures in mice induces adult neurogenesis and increases the size of the infrapyramidal mossy fiber bundle. Interestingly, they reported no increase in infrapyramidal mossy fiber volume 7 days after the seizure, but a significant increase after 14 days. Although this is a completely different experiment, one highly suggestive theory could be that this also could be the case for spatial trained animals, where adult neurogenesis also is shown to be enhanced.[93, 96] The animals used in this project were sacrificed 24 hours after spatial training. This may not be enough time for the axons to extend and for detection of any possible dynamical

changes in the mossy fiber bundle, and the potential differences between WT and NEIL3 would not be detectable. A suggestion could be to further investigate this by comparing the size of the infrapyramidal mossy fiber volume at different timepoints after a spatial experience, to see whether the infrapyramidal mossy fiber volume display an increase. Following, if the control display an increase as expected, the same could be done for NEIL3 deficient mice and the comparison would be more reliable.

In summary, based on these results, NEIL3 seems to have no role in regulating the infrapyramidal mossy fiber volume. However, the possibility of this cannot be excluded because the control did not show the expected increase. Further investigation with a larger sample size and improved experimental design is required for any conclusion to be made.

5.7 Exploring the impact of NEIL3 in embryonic hippocampal development

NEIL3 is found to have a discrete expression pattern in neurogenic niches such as the SGZ of the DG[28], and the expression is shown to be initiated as the same time as neurogenesis during hippocampal-development.[31] I aimed to investigate the impact of NEIL3 during hippocampal development by establishing NEIL3-deficient and WT mice by heterozygous breeding and further assess different neuronal populations by performing IHC. However, due to limited time, this part was not completed.

The genotyping results confirmed that WT and NEIL3-depleted animals were successfully obtained by at exactly same birth date from the same parents. The trial experiment using IHC with paraffin-embedded brain sections and Ki67, Sox2 and NeuN as cellular markers were successful. Imaging with Axioscan and confocal imaging showed that the brain was intact and the cellular markers clearly visualized the different cellular populations. This confirms that embryonic brain extraction followed by paraffin-embedding and IHC is a suited method for studying the developing hippocampus.

In summary, I successfully obtained wildtype and *Neil3-/-* embryonic (E13.5 and E18.5) and P2 brain samples from a heterozygous breeder and immunohistochemistry with paraffin embedded brain sections was tested in a trial experiment. Further studies using samples from *Neil3-/-* and WT mice should be continued to investigate the role of NEIL3 in hippocampal development from embryonic to postnatal stages.

6 Conclusion and future perspectives

The primary objective of the project was to unravel new knowledge about how NEIL3 impacts hippocampal development and function, with a special focus on the dentate gyrus. Using IHC and 3D image analysis in Imaris, I made several observations.

My results suggest that spatial experience-associated adult neurogenesis displays a tendency to be impaired in mice lacking NEIL3, suggesting that NEIL3 may plays a role in spatial experience-induced adult neurogenesis in the DG. However, a low sample size and methodological issues complicates the interpretation, and further research should be done. In future research, I suggest increasing the sample size and modify the time between learning and animal termination to see whether the tendencies observed in this project are more pronounced. Further, an interesting approach would be to investigate the impact of NEIL3 on neuronal maturation in the adult-born neurons in the DG, as my results may indicate a slower maturation rate in NEIL3-depleted animals. Finally, use of another marker such as BrdU could be a more suited method for studying cell proliferation, and should be tried for this study.

Subsequently, I found that spatial experience induced expression of immediate early genes in the hippocampal DG is impaired in NEIL3-deficient mice, suggesting that NEIL3 plays a role in spatial-experience induced expression of IEGs. A suggestion for future studies could be to increase the sample size and shorten the time window between learning termination of animals to investigate the immediate response of spatial-experience induced expression of IEGs in the DG in NEIL3-depleted mice. I addition, another future approach could be to study the potential role of NEIL3 in memory trace/engram formation.

Another fascinating finding was that NEIL3-depleted mice contained a reduced number of PV-positive and GAD67-positive interneurons in the DG. The spatial-training induced activation of GABAergic neurons was not detected in the NEIL3-deficient DG and the NEIL3-depleted DG displayed a lower number of PV neurons, suggesting that NEIL3 may impact the activation of GABAergic interneurons and the regulation of PV-positive cells in the DG network. In the future, further investigations should be done with a larger sample size in order to unravel the specific functions of NEIL3 related to interneuron activity in association with spatial memory and learning. A future approach could be to study the excitation/inhibition balance in the NEIL3-depleted DG. In addition, somatostatin, as marker for another interneuron-subtype, could be used to investigate the role of NEIL3 in activation of these in response to spatial training.

My results showed no differences in the IMF volume between the genotypes, suggesting that NEIL3 has no role in regulating the infrapyramidal mossy fiber bundle in response to a spatial training. However, the experimental design may be too simplified, and future research should investigate it further by using an improved method of analysis.

Finally, I aimed to investigate how NEIL3 impacts embryonic brain development. Due to limited time, this question was not answered. However, I obtained wildtype and *Neil3-/-* embryonic (E13.5 and E18.5) and P2 brain samples from a heterozygous breeder and immunohistochemistry with paraffin embedded brain sections was tested in a pilot experiment. Further studies using samples from *Neil3-/-* and WT mice should be continued to investigate the role of NEIL3 in hippocampal development from embryonic to postnatal stages.

In summary, these results provide evidence that indicates that NEIL3 may have novel functions in the DG in response to spatial memory and learning. I encourage further investigations to be done in order to unravel the specific functions of NEIL3 in association with spatial memory and learning.

7 References

1. Alberts, B., et al., *Molecular biology of the cell.* Scandinavian Journal of Rheumatology, 2003. **32**(2): p. 125-125.
2. Chatterjee, N. and G.C. Walker, *Mechanisms of DNA damage, repair, and mutagenesis.* Environmental and molecular mutagenesis, 2017. **58**(5): p. 235-263.
3. Bosshard, M., E. Markkanen, and B. Van Loon, *Base Excision Repair in Physiology and Pathology of the Central Nervous System.* International Journal of Molecular Sciences, 2012. **13**(12): p. 16172-16222.
4. Canugovi, C., et al., *The role of DNA repair in brain related disease pathology.* DNA Repair, 2013. **12**(8): p. 578-587.
5. Wilson, D.M. and D.R. McNeill, *Base excision repair and the central nervous system.* Neuroscience, 2007. **145**(4): p. 1187-1200.
6. Barnes, D.E. and T. Lindahl, *Repair and Genetic Consequences of Endogenous DNA Base Damage in Mammalian Cells.* Annual Review of Genetics, 2004. **38**(1): p. 445-476.
7. Fishel, M.L., M.R. Vasko, and M.R. Kelley, *DNA repair in neurons: So if they don't divide what's to repair?* Mutation Research/Fundamental and Molecular Mechanisms of Mutagenesis, 2007. **614**(1): p. 24-36.
8. Fan, J. and D.M. Wilson, *Protein–protein interactions and posttranslational modifications in mammalian base excision repair.* Free Radical Biology and Medicine, 2005. **38**(9): p. 1121-1138.
9. Zhao, C., W. Deng, and F.H. Gage, *Mechanisms and Functional Implications of Adult Neurogenesis.* Cell, 2008. **132**(4): p. 645-660.
10. Pan, L., J. Penney, and L.-H. Tsai, *Chromatin regulation of DNA damage repair and genome integrity in the central nervous system.* Journal of molecular biology, 2014. **426**(20): p. 3376-3388.
11. Fortini, P., et al., *The base excision repair: mechanisms and its relevance for cancer susceptibility.* Biochimie, 2003. **85**(11): p. 1053-1071.
12. Dianov, G.L. and U. Hübscher, *Mammalian Base Excision Repair: the Forgotten Archangel.* Nucleic Acids Research, 2013. **41**(6): p. 3483-3490.
13. Akbari, M., et al., *The role of DNA base excision repair in brain homeostasis and disease.* DNA Repair, 2015. **32**: p. 172-179.
14. Krokan, H.E. and M. Bjørås, *Base excision repair.* Cold Spring Harbor perspectives in biology, 2013. **5**(4): p. a012583.
15. Gavin, D.P., K.A. Chase, and R.P. Sharma, *Active DNA demethylation in post-mitotic neurons: a reason for optimism.* Neuropharmacology, 2013. **75**: p. 233-245.
16. Ma, D.K., et al., *Epigenetic choreographers of neurogenesis in the adult mammalian brain.* Nature Neuroscience, 2010. **13**(11): p. 1338-1344.
17. Wu, S.C. and Y. Zhang, *Active DNA demethylation: many roads lead to Rome.* Nature Reviews Molecular Cell Biology, 2010. **11**(9): p. 607-620.
18. Wu, X. and Y. Zhang, *TET-mediated active DNA demethylation: mechanism, function and beyond.* Nature Reviews Genetics, 2017. **18**(9): p. 517-534.
19. Zhu, J.-K., *Active DNA demethylation mediated by DNA glycosylases.* Annual review of genetics, 2009. **43**: p. 143-166.
20. Regnell, Christine E., et al., *Hippocampal Adult Neurogenesis Is Maintained by Neil3-Dependent Repair of Oxidative DNA Lesions in Neural Progenitor Cells.* Cell Reports, 2012. **2**(3): p. 503-510.

21. Liu, M., S. Doublié, and S.S. Wallace, *Neil3, the final frontier for the DNA glycosylases that recognize oxidative damage.* Mutation Research/Fundamental and Molecular Mechanisms of Mutagenesis, 2013. **743-744**: p. 4-11.
22. Liu, M., et al., *The mouse ortholog of NEIL3 is a functional DNA glycosylase in vitro and in vivo.* Proceedings of the National Academy of Sciences, 2010. **107**(11): p. 4925-4930.
23. Ha, A., Y. Lin, and S. Yan, *A non-canonical role for the DNA glycosylase NEIL3 in suppressing APE1 endonuclease-mediated ssDNA damage.* J Biol Chem, 2020. **295**(41): p. 14222-14235.
24. Krokeide, S.Z., et al., *Human NEIL3 is mainly a monofunctional DNA glycosylase removing spiroimindiohydantoin and guanidinohydantoin.* DNA repair, 2013. **12**(12): p. 1159-1164.
25. Liu, M., et al., *Structural characterization of a mouse ortholog of human NEIL3 with a marked preference for single-stranded DNA.* Structure, 2013. **21**(2): p. 247-256.
26. Schomacher, L., et al., *Neil DNA glycosylases promote substrate turnover by Tdg during DNA demethylation.* Nature Structural & Molecular Biology, 2016. **23**(2): p. 116-124.
27. Kunath, N., et al., *DNA repair enzyme NEIL3 enables a stable neural representation of space by shaping transcription in hippocampal neurons.* iScience, 2021. **24**(12): p. 103470.
28. Sejersted, Y., et al., *Endonuclease VIII-like 3 (Neil3) DNA glycosylase promotes neurogenesis induced by hypoxia-ischemia.* Proceedings of the National Academy of Sciences, 2011. **108**(46): p. 18802-18807.
29. Rolseth, V., et al., *Widespread distribution of DNA glycosylases removing oxidative DNA lesions in human and rodent brains.* DNA Repair, 2008. **7**(9): p. 1578-1588.
30. Takao, M., et al., *Human Nei-like protein NEIL3 has AP lyase activity specific for single-stranded DNA and confers oxidative stress resistance in Escherichia coli mutant.* Genes to Cells, 2009. **14**(2): p. 261-270.
31. Hildrestrand, G.A., et al., *Expression patterns of Neil3 during embryonic brain development and neoplasia.* BMC Neuroscience, 2009. **10**(1): p. 45.
32. Müller, U., et al., *TET-mediated oxidation of methylcytosine causes TDG or NEIL glycosylase dependent gene reactivation.* Nucleic Acids Research, 2014. **42**(13): p. 8592-8604.
33. Torisu, K., et al., *Hematopoietic Tissue–Specific Expression of Mouse Neil3 for Endonuclease VIII–Like Protein.* The Journal of Biochemistry, 2005. **138**(6): p. 763-772.
34. Rolseth, V., et al., *No cancer predisposition or increased spontaneous mutation frequencies in NEIL DNA glycosylases-deficient mice.* Scientific Reports, 2017. **7**(1): p. 1-12.
35. Imayoshi, I., et al., *Roles of continuous neurogenesis in the structural and functional integrity of the adult forebrain.* Nature neuroscience, 2008. **11**(10): p. 1153-1161.
36. Reis, A. and O. Hermanson, *The DNA glycosylases OGG1 and NEIL3 influence differentiation potential, proliferation, and senescence-associated signs in neural stem cells.* Biochemical and Biophysical Research Communications, 2012. **423**(4): p. 621-626.
37. Squire, L.R., C.E.L. Stark, and R.E. Clark, *THE MEDIAL TEMPORAL LOBE.* Annual Review of Neuroscience, 2004. **27**(1): p. 279-306.
38. Buzsáki, G. and E.I. Moser, *Memory, navigation and theta rhythm in the hippocampal-entorhinal system.* Nature neuroscience, 2013. **16**(2): p. 130-138.

39. O'keefe, J. and L. Nadel, *The hippocampus as a cognitive map*. 1978: Oxford university press.
40. Strange, B., et al., *Segregating the functions of human hippocampus.* Proceedings of the National Academy of Sciences, 1999. **96**(7): p. 4034-4039.
41. Broadbent, N.J., L.R. Squire, and R.E. Clark, *Spatial memory, recognition memory, and the hippocampus.* Proceedings of the National Academy of Sciences, 2004. **101**(40): p. 14515-14520.
42. van Strien, N.M., N.L.M. Cappaert, and M.P. Witter, *The anatomy of memory: an interactive overview of the parahippocampal–hippocampal network.* Nature Reviews Neuroscience, 2009. **10**(4): p. 272-282.
43. Witter, M., *Chapter 5 - Hippocampus*, in *The Mouse Nervous System*, C. Watson, G. Paxinos, and L. Puelles, Editors. 2012, Academic Press: San Diego. p. 112-139.
44. Medina, L., A. Abellan, and E. Desfilis, *Contribution of genoarchitecture to understanding hippocampal evolution and development.* Brain, Behavior and Evolution, 2017. **90**(1): p. 25-40.
45. Amaral, D.G. and M.P. Witter, *The three-dimensional organization of the hippocampal formation: A review of anatomical data.* Neuroscience, 1989. **31**(3): p. 571-591.
46. Zemla, R. and J. Basu, *Hippocampal function in rodents.* Current Opinion in Neurobiology, 2017. **43**: p. 187-197.
47. Andersen, P., et al., *The hippocampus book*. 2006: Oxford university press.
48. Hargreaves, E.L., et al., *Major dissociation between medial and lateral entorhinal input to dorsal hippocampus.* science, 2005. **308**(5729): p. 1792-1794.
49. Eichenbaum, H., *Remembering: Functional Organization of the Declarative Memory System.* Current Biology, 2006. **16**(16): p. R643-R645.
50. Sargolini, F., et al., *Conjunctive representation of position, direction, and velocity in entorhinal cortex.* Science, 2006. **312**(5774): p. 758-762.
51. Ahmed, O.J. and M.R. Mehta, *The hippocampal rate code: anatomy, physiology and theory.* Trends in neurosciences, 2009. **32**(6): p. 329-338.
52. Li, Y., et al., *A distinct entorhinal cortex to hippocampal CA1 direct circuit for olfactory associative learning.* Nature Neuroscience, 2017. **20**(4): p. 559-570.
53. Freund, T.F. and G. Buzsáki, *Interneurons of the hippocampus.* Hippocampus, 1996. **6**(4): p. 347-470.
54. Grieves, R.M., et al., *The place-cell representation of volumetric space in rats.* Nature Communications, 2020. **11**(1): p. 789.
55. Leuner, B. and E. Gould, *Structural Plasticity and Hippocampal Function.* Annual Review of Psychology, 2009. **61**(1): p. 111-140.
56. Hainmueller, T. and M. Bartos, *Dentate gyrus circuits for encoding, retrieval and discrimination of episodic memories.* Nature Reviews Neuroscience, 2020. **21**(3): p. 153-168.
57. Gonçalves, J.T., S.T. Schafer, and F.H. Gage, *Adult Neurogenesis in the Hippocampus: From Stem Cells to Behavior.* Cell, 2016. **167**(4): p. 897-914.
58. Baker, S., et al., *The human dentate gyrus plays a necessary role in discriminating new memories.* Current Biology, 2016. **26**(19): p. 2629-2634.
59. Madroñal, N., et al., *Rapid erasure of hippocampal memory following inhibition of dentate gyrus granule cells.* Nature Communications, 2016. **7**(1): p. 10923.
60. Rolls, E.T. and R.P. Kesner, *A computational theory of hippocampal function, and empirical tests of the theory.* Progress in Neurobiology, 2006. **79**(1): p. 1-48.
61. Kesner, R.P., *A behavioral analysis of dentate gyrus function*, in *Progress in Brain Research*, H.E. Scharfman, Editor. 2007, Elsevier. p. 567-576.

62. Sutherland, R.J., I.Q. Whishaw, and B. Kolb, *A behavioural analysis of spatial localization following electrolytic, kainate-or colchicine-induced damage to the hippocampal formation in the rat.* Behavioural brain research, 1983. **7**(2): p. 133-153.
63. Jeltsch, H., et al., *Cognitive performances and locomotor activity following dentate granule cell damage in rats: role of lesion extent and type of memory tested.* Neurobiology of learning and memory, 2001. **76**(1): p. 81-105.
64. Lee, I. and R.P. Kesner, *Encoding versus retrieval of spatial memory: double dissociation between the dentate gyrus and the perforant path inputs into CA3 in the dorsal hippocampus.* Hippocampus, 2004. **14**(1): p. 66-76.
65. Kesner, R.P., *An analysis of the dentate gyrus function.* Behavioural Brain Research, 2013. **254**: p. 1-7.
66. Leal, S.L. and M.A. Yassa, *Neurocognitive aging and the hippocampus across species.* Trends in neurosciences, 2015. **38**(12): p. 800-812.
67. Hyman, B., et al., *Perforant pathway changes and the memory impairment of Alzheimer's disease.* Annals of Neurology: Official Journal of the American Neurological Association and the Child Neurology Society, 1986. **20**(4): p. 472-481.
68. Rodríguez, J.J., et al., *Impaired adult neurogenesis in the dentate gyrus of a triple transgenic mouse model of Alzheimer's disease.* PloS one, 2008. **3**(8): p. e2935.
69. Toda, T., et al., *The role of adult hippocampal neurogenesis in brain health and disease.* Molecular psychiatry, 2019. **24**(1): p. 67-87.
70. Yassa, M.A., et al., *Age-related memory deficits linked to circuit-specific disruptions in the hippocampus.* Proceedings of the National Academy of Sciences, 2011. **108**(21): p. 8873-8878.
71. Burke, S.N. and C.A. Barnes, *Neural plasticity in the ageing brain.* Nature reviews neuroscience, 2006. **7**(1): p. 30-40.
72. Urbán, N. and F. Guillemot, *Neurogenesis in the embryonic and adult brain: same regulators, different roles.* Frontiers in cellular neuroscience, 2014. **8**: p. 396.
73. Hayashi, K., et al., *Cellular dynamics of neuronal migration in the hippocampus.* Frontiers in Neuroscience, 2015. **9**.
74. Nakahira, E. and S. Yuasa, *Neuronal generation, migration, and differentiation in the mouse hippocampal primoridium as revealed by enhanced green fluorescent protein gene transfer by means of in utero electroporation.* Journal of Comparative Neurology, 2005. **483**(3): p. 329-340.
75. Lagali, P., C. Corcoran, and D. Picketts, *Hippocampus development and function: role of epigenetic factors and implications for cognitive disease.* Clinical genetics, 2010. **78**(4): p. 321-333.
76. Soriano, E., A. Cobas, and A. Fairén, *Neurogenesis of glutamic acid decarboxylase immunoreactive cells in the hippocampus of the mouse. I: Regio superior and regio inferior.* Journal of Comparative Neurology, 1989. **281**(4): p. 586-602.
77. Soriano, E., A. Cobas, and A. Fairén, *Neurogenesis of glutamic acid decarboxylase immunoreactive cells in the hippocampus of the mouse. II: Area dentata.* Journal of Comparative Neurology, 1989. **281**(4): p. 603-611.
78. Danglot, L., A. Triller, and S. Marty, *The development of hippocampal interneurons in rodents.* Hippocampus, 2006. **16**(12): p. 1032-1060.
79. Angevine Jr, J.B., *Time of neuron origin in the hippocampal region: an autoradiographic study in the mouse.* Experimental Neurology, 1965.
80. Schröder, H., N. Moser, and S. Huggenberger, *The Mouse Hippocampus*, in *Neuroanatomy of the Mouse: An Introduction*, H. Schröder, N. Moser, and S. Huggenberger, Editors. 2020, Springer International Publishing: Cham. p. 267-288.

81. Caronia-Brown, G., et al., *The cortical hem regulates the size and patterning of neocortex.* Development, 2014. **141**(14): p. 2855-2865.
82. Fan, S.J., A.B. Sun, and L. Liu, *Epigenetic modulation during hippocampal development.* Biomedical Reports, 2018. **9**(6): p. 463-473.
83. Reznikov, K.Y., *Cell proliferation and cytogenesis in the mouse hippocampus*. Vol. 122. 2012: Springer Science & Business Media.
84. Altman, J. and S.A. Bayer, *Migration and distribution of two populations of hippocampal granule cell precursors during the perinatal and postnatal periods.* Journal of Comparative Neurology, 1990. **301**(3): p. 365-381.
85. Khalaf-Nazzal, R. and F. Francis, *Hippocampal development – Old and new findings.* Neuroscience, 2013. **248**: p. 225-242.
86. Berg, D.A., et al., *A Common Embryonic Origin of Stem Cells Drives Developmental and Adult Neurogenesis.* Cell, 2019. **177**(3): p. 654-668.e15.
87. Winner, B. and J. Winkler, *Adult neurogenesis in neurodegenerative diseases.* Cold Spring Harbor perspectives in biology, 2015. **7**(4): p. a021287.
88. Gage, F.H., *Adult neurogenesis in mammals.* Science, 2019. **364**(6443): p. 827-828.
89. Deng, W., J.B. Aimone, and F.H. Gage, *New neurons and new memories: how does adult hippocampal neurogenesis affect learning and memory?* Nature Reviews Neuroscience, 2010. **11**(5): p. 339-350.
90. Abbott, L.C. and F. Nigussie, *Adult neurogenesis in the mammalian dentate gyrus.* Anatomia, histologia, embryologia, 2020. **49**(1): p. 3-16.
91. Braun, S.M. and S. Jessberger, *Adult neurogenesis: mechanisms and functional significance.* Development, 2014. **141**(10): p. 1983-1986.
92. Lazarov, O. and C. Hollands, *Hippocampal neurogenesis: Learning to remember.* Progress in Neurobiology, 2016. **138-140**: p. 1-18.
93. Gould, E., et al., *Learning enhances adult neurogenesis in the hippocampal formation.* Nature Neuroscience, 1999. **2**(3): p. 260-265.
94. Toda, T. and F.H. Gage, *Adult neurogenesis contributes to hippocampal plasticity.* Cell and tissue research, 2018. **373**(3): p. 693-709.
95. Nicola, Z., K. Fabel, and G. Kempermann, *Development of the adult neurogenic niche in the hippocampus of mice.* Frontiers in neuroanatomy, 2015. **9**: p. 53.
96. Clelland, C., et al., *A functional role for adult hippocampal neurogenesis in spatial pattern separation.* Science, 2009. **325**(5937): p. 210-213.
97. Vann, S.D., et al., *Fos Imaging Reveals Differential Patterns of Hippocampal and Parahippocampal Subfield Activation in Rats in Response to Different Spatial Memory Tests.* The Journal of Neuroscience, 2000. **20**(7): p. 2711-2718.
98. Guzowski, J.F., et al., *Experience-dependent gene expression in the rat hippocampus after spatial learning: a comparison of the immediate-early genesArc, c-fos, and zif268.* Journal of Neuroscience, 2001. **21**(14): p. 5089-5098.
99. Andrews-Zwilling, Y., et al., *Hilar GABAergic interneuron activity controls spatial learning and memory retrieval.* PloS one, 2012. **7**(7): p. e40555.
100. Honigman, J., et al., *Distribution maps of D-dopachrome tautomerase in the mouse brain.* Neuroscience, 2012. **226**: p. 382-387.
101. Shi, S.-R., R.J. Cote, and C.R. Taylor, *Antigen retrieval techniques: current perspectives.* Journal of Histochemistry & Cytochemistry, 2001. **49**(8): p. 931-937.
102. Seibenhener, M.L. and M.C. Wooten, *Use of the open field maze to measure locomotor and anxiety-like behavior in mice.* JoVE (Journal of Visualized Experiments), 2015(96): p. e52434.

103. Denninger, J.K., B.M. Smith, and E.D. Kirby, *Novel object recognition and object location behavioral testing in mice on a budget.* JoVE (Journal of Visualized Experiments), 2018(141): p. e58593.
104. Sanderson, D.J., et al., *Enhanced long-term and impaired short-term spatial memory in GluA1 AMPA receptor subunit knockout mice: evidence for a dual-process memory model.* Learning & memory, 2009. **16**(6): p. 379-386.
105. Urruticoechea, A., I.E. Smith, and M. Dowsett, *Proliferation marker Ki-67 in early breast cancer.* Journal of clinical oncology, 2005. **23**(28): p. 7212-7220.
106. Gleeson, J.G., et al., *Doublecortin is a microtubule-associated protein and is expressed widely by migrating neurons.* Neuron, 1999. **23**(2): p. 257-271.
107. Rao, M.S. and A.K. Shetty, *Efficacy of doublecortin as a marker to analyse the absolute number anddendritic growth of newly generated neurons in the adult dentate gyrus.* European Journal of Neuroscience, 2004. **19**(2): p. 234-246.
108. Friocourt, G., et al., *Doublecortin functions at the extremities of growing neuronal processes.* Cerebral cortex, 2003. **13**(6): p. 620-626.
109. Rao, M.S., B. Hattiangady, and A.K. Shetty, *The window and mechanisms of major age-related decline in the production of new neurons within the dentate gyrus of the hippocampus.* Aging cell, 2006. **5**(6): p. 545-558.
110. Ayanlaja, A.A., et al., *Distinct features of doublecortin as a marker of neuronal migration and its implications in cancer cell mobility.* Frontiers in molecular neuroscience, 2017. **10**: p. 199.
111. Marrone, D.F., et al., *Immediate-early gene expression at rest recapitulates recent experience.* Journal of Neuroscience, 2008. **28**(5): p. 1030-1033.
112. Korb, E. and S. Finkbeiner, *Arc in synaptic plasticity: from gene to behavior.* Trends in Neurosciences, 2011. **34**(11): p. 591-598.
113. Dyrvig, M., et al., *Epigenetic regulation of Arc and c-Fos in the hippocampus after acute electroconvulsive stimulation in the rat.* Brain research bulletin, 2012. **88**(5): p. 507-513.
114. Kovács, K., *Measurement of immediate-early gene activation-c-fos and beyond.* Journal of neuroendocrinology, 2008. **20**(6): p. 665-672.
115. Lazarus, M.S., K. Krishnan, and Z.J. Huang, *GAD67 Deficiency in Parvalbumin Interneurons Produces Deficits in Inhibitory Transmission and Network Disinhibition in Mouse Prefrontal Cortex.* Cerebral Cortex, 2013. **25**(5): p. 1290-1296.
116. Nahar, L., B.M. Delacroix, and H.W. Nam, *The role of parvalbumin interneurons in neurotransmitter balance and neurological disease.* Frontiers in Psychiatry, 2021. **12**: p. 985.
117. Kelsom, C. and W. Lu, *Development and specification of GABAergic cortical interneurons.* Cell & bioscience, 2013. **3**(1): p. 1-19.
118. Boonstra, E., et al., *Neurotransmitters as food supplements: the effects of GABA on brain and behavior.* Frontiers in psychology, 2015. **6**: p. 1520.
119. Kosaka, T., et al., *GABAergic neurons containing the Ca2+-binding protein parvalbumin in the rat hippocampus and dentate gyrus.* Brain research, 1987. **419**(1-2): p. 119-130.
120. Houser, C.R., *Interneurons of the dentate gyrus: an overview of cell types, terminal fields and neurochemical identity.* Progress in brain research, 2007. **163**: p. 217-811.
121. Lau, C.G. and V.N. Murthy, *Activity-dependent regulation of inhibition via GAD67.* Journal of Neuroscience, 2012. **32**(25): p. 8521-8531.
122. Yamashiro, K., et al., *Deep Learning-Based Classification of GAD67-Positive Neurons Without the Immunosignal.* Frontiers in Neuroanatomy, 2021. **15**.

123. Bowers, G., W.E. Cullinan, and J.P. Herman, *Region-specific regulation of glutamic acid decarboxylase (GAD) mRNA expression in central stress circuits.* Journal of Neuroscience, 1998. **18**(15): p. 5938-5947.
124. Koyama, R. and Y. Ikegaya, *The molecular and cellular mechanisms of axon guidance in mossy fiber sprouting.* Frontiers in Neurology, 2018. **9**: p. 382.
125. Römer, B., et al., *Adult hippocampal neurogenesis and plasticity in the infrapyramidal bundle of the mossy fiber projection: I. Co-regulation by activity.* Frontiers in neuroscience, 2011. **5**: p. 107.
126. Crusio, W.E. and H. Schwegler, *Learning spatial orientation tasks in the radial-maze and structural variation in the hippocampus in inbred mice.* Behavioral and Brain Functions, 2005. **1**(1): p. 1-11.
127. Schwegler, H., et al., *Water-maze learning in the mouse correlates with variation in hippocampal morphology.* Behavior genetics, 1988. **18**(2): p. 153-165.
128. Ramírez-Rodríguez, G.B., et al., *Melatonin influences structural plasticity in the axons of granule cells in the dentate gyrus of Balb/C mice.* International journal of molecular sciences, 2018. **20**(1): p. 73.
129. Suh, H., et al., *In Vivo Fate Analysis Reveals the Multipotent and Self-Renewal Capacities of Sox2+ Neural Stem Cells in the Adult Hippocampus.* Cell Stem Cell, 2007. **1**(5): p. 515-528.
130. Mullen, R.J., C.R. Buck, and A.M. Smith, *NeuN, a neuronal specific nuclear protein in vertebrates.* Development, 1992. **116**(1): p. 201-211.
131. Trouche, S., et al., *Recruitment of adult-generated neurons into functional hippocampal networks contributes to updating and strengthening of spatial memory.* Proceedings of the National Academy of Sciences, 2009. **106**(14): p. 5919-5924.
132. Drapeau, E., et al., *Spatial memory performances of aged rats in the water maze predict levels of hippocampal neurogenesis.* Proceedings of the National Academy of Sciences, 2003. **100**(24): p. 14385-14390.
133. Gratzner, H.G., *Monoclonal antibody to 5-bromo-and 5-iododeoxyuridine: a new reagent for detection of DNA replication.* Science, 1982. **218**(4571): p. 474-475.
134. Egiazarian, M.A., et al., *Age-and sex-dependent effects of DNA glycosylase Neil3 on amyloid pathology, adult neurogenesis, and memory in a mouse model of Alzheimer' s disease.* bioRxiv, 2022.
135. Dupret, D., et al., *Spatial learning depends on both the addition and removal of new hippocampal neurons.* PLoS biology, 2007. **5**(8): p. e214.
136. Cavegn, N., et al., *Habitat-specific shaping of proliferation and neuronal differentiation in adult hippocampal neurogenesis of wild rodents.* Frontiers in neuroscience, 2013. **7**: p. 59.
137. Brown, J.P., et al., *Transient expression of doublecortin during adult neurogenesis.* Journal of Comparative Neurology, 2003. **467**(1): p. 1-10.
138. Piatti, V.C., et al., *The timing for neuronal maturation in the adult hippocampus is modulated by local network activity.* Journal of Neuroscience, 2011. **31**(21): p. 7715-7728.
139. Minatohara, K., M. Akiyoshi, and H. Okuno, *Role of immediate-early genes in synaptic plasticity and neuronal ensembles underlying the memory trace.* Frontiers in molecular neuroscience, 2016. **8**: p. 78.
140. Barry, D.N. and S. Commins, *Temporal dynamics of immediate early gene expression during cellular consolidation of spatial memory.* Behavioural Brain Research, 2017. **327**: p. 44-53.

141. Stone, D.J., J. Walsh, and F.M. Benes, *Localization of cells preferentially expressing GAD67 with negligible GAD65 transcripts in the rat hippocampus. A double in situ hybridization study.* Molecular Brain Research, 1999. **71**(2): p. 201-209.
142. Houser, C.R. and M. Esclapez, *Localization of mRNAs encoding two forms of glutamic acid decarboxylase in the rat hippocampal formation.* Hippocampus, 1994. **4**(5): p. 530-545.
143. Bannai, H., et al., *Bidirectional Control of Synaptic GABAAR Clustering by Glutamate and Calcium.* Cell Reports, 2015. **13**(12): p. 2768-2780.
144. Molgaard, S., et al., *Immunofluorescent visualization of mouse interneuron subtypes.* F1000Research, 2014. **3**: p. 242-242.
145. Kiljan, S., et al., *Enhanced GABAergic Immunoreactivity in Hippocampal Neurons and Astroglia of Multiple Sclerosis Patients.* Journal of Neuropathology & Experimental Neurology, 2019. **78**(6): p. 480-491.
146. Fuchs, E.C., et al., *Recruitment of parvalbumin-positive interneurons determines hippocampal function and associated behavior.* Neuron, 2007. **53**(4): p. 591-604.
147. Abbas, A.I., et al., *Somatostatin Interneurons Facilitate Hippocampal-Prefrontal Synchrony and Prefrontal Spatial Encoding.* Neuron, 2018. **100**(4): p. 926-939.e3.
148. Lazarus, M.S., K. Krishnan, and Z.J. Huang, *GAD67 deficiency in parvalbumin interneurons produces deficits in inhibitory transmission and network disinhibition in mouse prefrontal cortex.* Cerebral cortex, 2015. **25**(5): p. 1290-1296.
149. Laghmouch, A., J.-Y. Bertholet, and W.E. Crusio, *Hippocampal morphology and open-field behavior in Mus musculus domesticus and Mus spretus inbred mice.* Behavior genetics, 1997. **27**(1): p. 67-73.
150. Römer, B., et al., *Adult hippocampal neurogenesis and plasticity in the infrapyramidal bundle of the mossy fiber projection: I. Co-regulation by activity.* Frontiers in neuroscience, 2011. **5**: p. 107-107.
151. Hodges, H., *Maze procedures: the radial-arm and water maze compared.* Cognitive Brain Research, 1996. **3**(3): p. 167-181.

APPENDIX

Solutions

1. **1000ml of 1x PBS (ready-made tablets)**
   - For 1L of 1x PBS, 10 tablets of ready-made PBS (*OXOID PBS Dulbecco A, BR0014G,* common stock), was dissolved in 500ml ddH2O and filled up to 1000ml with ddH2O.
2. **0,1% PBS-T**
   - 1ml of Tween20 *(Sigma P1379-500ML/Lot# SLBZ5658*) was dissolved in 1000ml of 1x PBS.
3. **1000ml of 4% Paraformaldehyde (PFA)**
   - 500ml of 1xPBS was heated to around 60°C (don't boil)
   - 40g of PFA *(Merck, 1.04005.1000)* was added and filled up to 1000ml with 1xPBS
   - The solution was filtered with a 0,2µm-filter (optional) and aliquoted to 50ml tubes and stored at -20°C
4. **500ml of 10%BSA/10%BS (stock solution for making blocking buffer and dilution buffer)**
   - 50ml of 10x PBS was mixed with 300ml of Milllipore water
   - 50g of BSA and 50ml of GS *(use container available in common stock 4th floor, serial# subject to change)* was added and the solution was stirred until dissolved; and filled up with Millipore water to 500ml
   - The 10%BSA/10%GS was aliquoted to 50ml and freezed at -20°C
5. **Blocking buffer (100ml of 5% BSA/5% GS in 0,1% Triton/PBS)**
   - 1ml of PBS/Triton10% and 50ml of 10% BSA/10% GS was added
   - Filled up to 100ml with 1xPBS
6. **Dilution buffer (100ml of 1% BSA/1% GS in 0,1% Triton/PBS)**
   - 10ml of 10% BSA/10% GS and 1ml of PBS/Triton 10% was added
   - Filled up to 100ml with 1xPBS
7. **100ml of 100mM Trisodium-Citrate Buffer Stock for Antigen Retrieval**
   - A glass bottle was filled with 50ml of ddH2O
   - 3,57g of Trisodium-Citrate *(Trisodium citrate 5,5 hydrate, Merck-Millipore 1.06431.1000)* was added and stirred
   - pH was adjusted to 6 by adding droplets of 1M HCl using a Pasteur-Pipette and filled up to 100ml with ddH2O.
8. **TAE buffer**

   - 242g Tris Base
   - 57.1ml Glacial Acetic Acid
   - 100ml 0.5 M EDTA
   - 242 g Tris Base was dissolved in about 600ml ddH2O, 100mL 0.5M EDTA and 57.1 mL Acetic Acid was added. Final volume was filled to 1L with ddH2O.

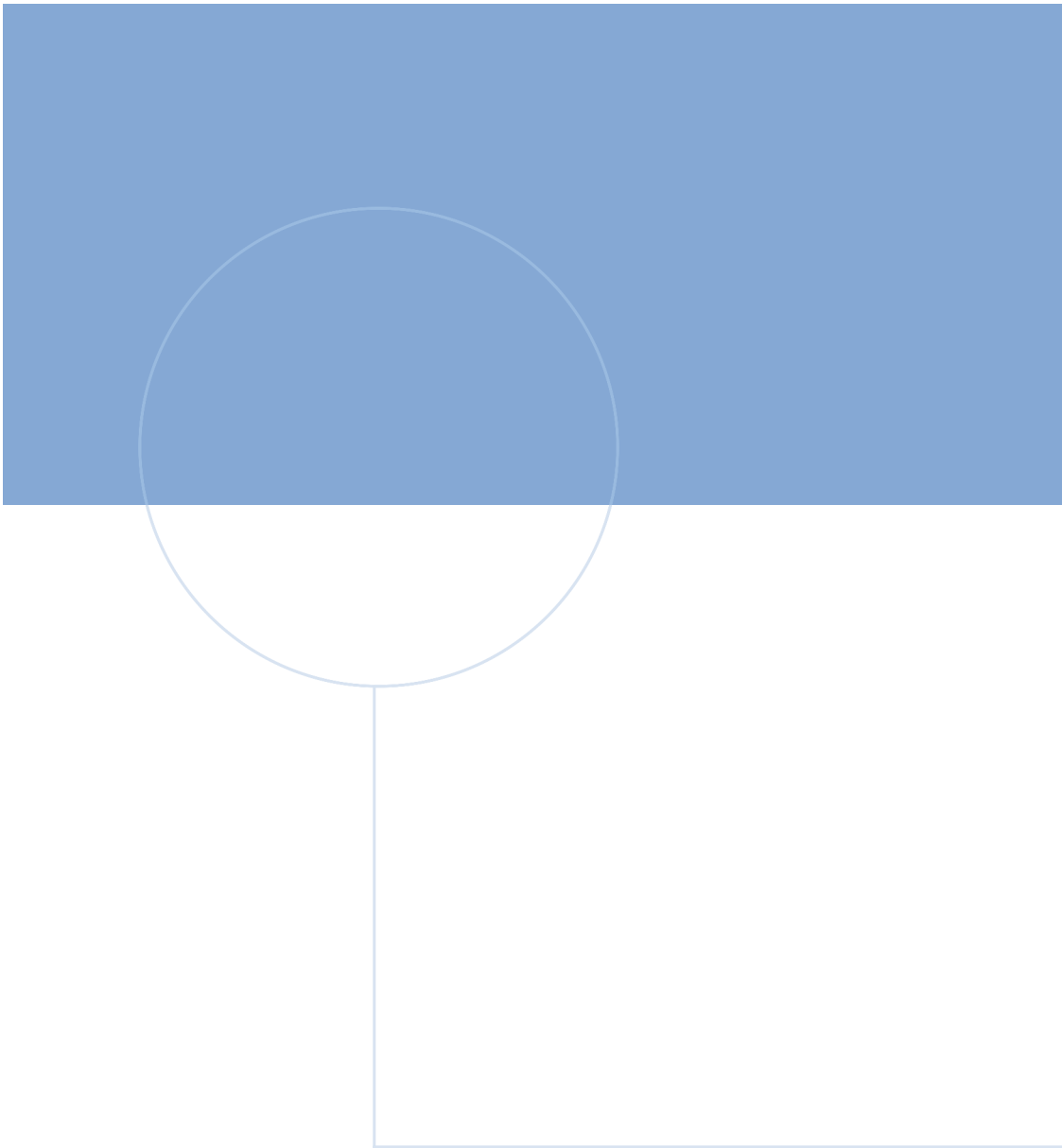

NTNU

Kunnskap for en bedre verden